

A New Approach to Seismic Base Isolation Using Air-bearing Solutions



MohammadHossein HarbiMonfared

Department of Engineering and Built Environment

Anglia Ruskin University

This dissertation is submitted for the degree of Doctor of Philosophy

December 2015

This work is dedicated to those who have lost their loved ones in an earthquake.

Acknowledgement

I would like to express my sincere appreciation to Prof. Hassan Shirvani, my supervisor for his insightful guidance, inspiring encouragement and the continuous support of my Ph.D. study and related research. My special thanks also goes to Dr. Ayoub Shirvani, my former supervisor whom without his precious support it would have not been possible to conduct this research. Besides, I would like to thank the rest of my supervisory team: Dr. Sunny Nwaubani and Dr. Ahad Ramezanpour for their valuable comments and encouragement.

My warm thanks goes to all my colleagues and friends at Anglia Ruskin University who helped me in this research project; Dr. Ehsan Eslamian for sharing his knowledge in fluid mechanics and Mr. Dan Jackson, for workshop preparation and laboratory tests.

I am also grateful to Mr. Reza Ghadimzadegan of GeoSIG for providing the measurement instruments used in experimental tests.

Last but not the least, I would like to express my heart-felt gratitude to my family for their love, patience and supports throughout my life.

Declaration

I certify that except where due acknowledgment is made in the text, the contents of this dissertation are genuine results of my own work and have not been submitted in any form for another degree or diploma.

Abstract

Earthquake, the natural phenomena, is conceived by the movement of the tectonic plates that induce shocks and impulse of devastating magnitude at ground level. Reducing losses during an earthquake has always been one of the most critical concerns of humans in earthquake prone areas. The main goal has been always to attenuate the shocks induced by ground motions on man-made structures. Two approaches have been conducted; increasing the earthquake resistant capacity of a structure, and reducing the seismic demands on a structure. With regard to the concept of reducing seismic demands on a structures, seismic base isolation is considered as an efficient method in mitigation of earthquake damages.

A proper base isolation framework offers a structure great dynamic performance and in this way, the structure will be able to remain in elastic mode during an earthquake. On the other hand, not all isolation systems can provide the target structure with efficient seismic performance. The majority of currently available isolation systems still have some practical limitations. These limitations affect the functionality of a structural system and impose some restrictions to its proper use and protection level, causing it not to achieve anticipated level of performances.

In this dissertation, an innovative seismic isolation system is proposed and investigated via laboratory tests and computer simulation to introduce a practical and effective seismic isolation system. The proposed system has aimed to modify some drawbacks of current seismic isolation system whilst at the same time keeping their advantages. The innovative isolation system in this study incorporates air-bearing benefits together with roller bearings and bungee cords in a complex system for horizontal base isolation.

An experimental study was carried out to test a scale structure model ($1/10^{\text{th}}$ in length) as a case study for this research, to observe the behaviour of the structure with and without isolation system and to extract the dynamic characteristics of the structure by measuring fundamental frequencies and damping through a free vibration test.

Computer simulation was conducted to simulate the dynamic behaviour of the structure when it is subjected to three different types of earthquakes; and with different base

configurations (fixed base and base isolated). The simulation was performed to gain an insight into the performance of the proposed isolation system under the given structure.

Results from computer simulation were compared and validated with findings from experimental tests. It was confirmed that the present isolation system offers a significant reduction in acceleration demand in the structure leading to the reduction of base shear and consequently the level of damage to the structure. Results revealed that the proposed isolation system is able to mitigate the seismic responses under different ground motion excitations while exhibiting robust performance for the given structure. Furthermore, the system can also be used to isolate sensitive equipment or hardware in buildings affected by seismic shocks.

Table of Contents

1	Introduction	27
1.1	Seismic isolation	27
1.2	Motivations for this study	29
1.3	Gap in knowledge	29
1.4	Aim and objectives of this research	30
1.5	Research methodology	31
1.5.1	Air-bearing device	31
1.5.2	Scaled structure model	32
1.6	Dissertation scope	33
1.7	Dissertation outline	33
2	Literature review	35
2.1	Introduction	35
2.2	Seismic base isolation from historical perspective	35
2.3	Seismic base-isolation efforts in the modern time	36
2.4	Recent progress in seismic-base isolation	38
2.5	Seismic base-isolation systems	40
2.5.1	Elastomeric-bearing isolation systems	41
2.5.2	Sliding base-isolation systems	45
2.5.3	Dampers used for seismic isolation	46
2.5.4	Soft first-story building	47
2.5.5	Artificial soil layers	47

2.5.6	Rolling base-isolation systems	48
2.5.7	Air-bearing for base isolation	48
2.5.8	Other isolation systems	49
2.5.9	Advantages and disadvantages of current seismic isolators	50
2.6	Air-bearing perspective	50
2.6.1	Applications	50
2.6.2	Technical research	52
2.7	Earthquake Early Warning systems	53
2.8	Summary	54
3	New base isolation system	55
3.1	Introduction	55
3.2	Seismic base-isolation principals	56
3.2.1	Horizontal isolation	57
3.2.2	Damping	62
3.3	Innovative isolation system using air bearing	67
3.4	Case study	69
3.4.1	Scaling procedure	70
3.5	Scaled model strucutre	72
3.5.1	Mechanical characteristics of the scaled model	74
3.5.2	Isolation system for scaled model	76
3.6	Analytical model of the scaled structure	79
3.6.1	Modal analysis	80
3.6.2	Modal analysis for scaled model	83

3.7	Conclusion	90
4	Air-bearing device design and development	91
4.1	Introduction	91
4.2	Air bearing design	91
4.3	Simulation methods	94
4.3.1	Governing equations	94
4.3.2	Turbulence modelling	97
4.4	Numerical solutions	100
4.4.1	Geometry	100
4.4.2	Discretisation	101
4.4.3	Mesh generation	103
4.4.4	Numerical setting	103
4.4.5	Numerical results	105
4.5	Experimental study	109
4.5.1	Air-bearing device	110
4.5.2	Tests	112
4.5.3	Experimental results	113
4.6	Validation	117
4.6.1	Numerical study and experiments	117
4.6.2	Numerical validations	117
4.7	Conclusion	118
5	Experimental study on the model structure	120
5.1	Introduction	120

5.1.1	Experimental study (general argument)	120
5.1.2	Experimental study for this research	122
5.2	Test rig	124
5.3	Dynamic test	124
5.4	Tests' procedure	126
5.4.1	Fixed base	127
5.4.2	Base isolated	127
5.5	Measurement devices	128
5.5.1	Data acquisition	128
5.5.2	Sensors	128
5.5.3	Data communication software	129
5.6	Data analysis and results	129
5.6.1	Absolute acceleration on top of the structure	130
5.6.2	Natural frequencies and periods	134
5.6.3	Story drifts	137
5.6.4	Damping	141
5.7	Conclusion	146
6	Computer simulation of the structure	148
6.1	Introduction	148
6.2	Physical model	150
6.3	Mathematical model	151
6.4	Simulation	152
6.4.1	Earthquakes	152

6.5	Program settings	155
6.5.1	Mass	155
6.5.2	Stiffness	156
6.5.3	Time history input	157
6.6	Results	160
6.6.1	Frequencies and periods	160
6.6.2	Accelerations	160
6.6.3	Displacements	162
6.6.4	Base-shear	165
6.6.5	Earthquake input energy	166
6.7	Conclusion	170
7	Conclusion and future works	171
7.1	Conclusion	171
7.2	Contributions	173
7.3	Future works	173
8	References	175
	Appendices	183
A.1	Research flowchart	183
A.2	BI projects around the world	184
A.3	Roller bearing specifications	189
A.4	Modal analysis (fixed-base model)	191
A.5	Modal analysis (base isolated)	194

A.6 Air pump specifications	198
A.7 GMSplus specifications and calibration	200
A.8 Accelerometer specifications and calibration	204
A.9 FFT algorithm and implementation	208

List of figures

Figure 2-1 Rubber bearing schematic view	41
Figure 2-2 Laminated rubber bearing also known as Low damping rubber bearing (Buchanan, et al., 2011)	42
Figure 2-3 Lead rubber bearing section (Saiful-Islam, et al., 2011)	44
Figure 2-4 High damping rubber bearing (Saiful-Islam, et al., 2011)	44
Figure 2-5 Spherical sliding system schematic view (Buchanan, et al., 2011).....	46
Figure 2-6 An air-bearing schematic view	51
Figure 2-7 An Air float bearing schematic view (HOVAIR, 2013)	51
Figure 2-8 Comparison of coefficient of friction for three types of bearing (Newway, 2006)	52
Figure 3-1 Elastic design spectrum, (ξ denotes damping) (Chopra, 2007).....	56
Figure 3-2 Behavior of building structure with base-isolation system	57
Figure 3-3 (a) fixed base and (b) isolated structures.....	58
Figure 3-4 Idealized mass-spring model of 2DOFs structure	58
Figure 3-5 Effects of period shifting in acceleration mitigation	62
Figure 3-6 Mass-spring model with damping	63
Figure 3-7 Increase in period of vibration reduces the base shear (Symans, 2004).....	65
Figure 3-8 Increase in period increases displacement (Symans, 2004)	66
Figure 3-9 The proposed seismic isolation system works with earthquake early warning system.....	68
Figure 3-10 Schematic view of the case study in real scale.....	70
Figure 3-11 Scaled model structure built in the workshop	73
Figure 3-12 Scaled model dimensions (mm)	73
Figure 3-13 Lateral stiffness test diagram.....	74
Figure 3-14 Isolation system for scaled model	76
Figure 3-15 The air-bearing pallet to be installed underneath of the structure.....	77
Figure 3-16 Beneath view of the air-bearing pallet	77
Figure 3-17 Beneath view of ball-bearing pallet.....	77
Figure 3-18 Air bearings installed underneath of the scaled model.....	78
Figure 3-19 Air bearings and ball bearings installed underneath of the structure	78

Figure 3-20 Isolation system for scaled model using bungee cords for re-centring	79
Figure 3-21 analytical model of the structure (fixed-base conditions)	80
Figure 3-22 Mode shapes corresponding to the scaled structure	85
Figure 3-23 Mode shapes of isolated scaled structure	88
Figure 4-1 Air-bearing device chamber (dimensions in mm).....	92
Figure 4-2 Air-bearing seal with nozzles (dimensions in mm).....	92
Figure 4-3 Nozzle geometry used in air-bearing design	93
Figure 4-4 The effects of divergence in nozzle shape on flow parameters (Beychok, 2010)	94
Figure 4-5 CFD model volume (dimensions in mm).....	101
Figure 4-6 Geometry of flow domain	101
Figure 4-7 Mesh generation by ANSYS Mesh	103
Figure 4-8 Output results for Mach number (nozzle 2-3 side view).....	106
Figure 4-9 Output results for Mach number (nozzle 2-6 side view).....	106
Figure 4-10 Output results for Mach number (nozzle 2-12 side view).....	107
Figure 4-11 Mass flow rate through a nozzle at different pressure ratios (Tiwari, et al., 2013)	109
Figure 4-12 Three different types of nozzle used in numerical study and laboratory tests (dimensions in mm)	110
Figure 4-13 The bottom plate of air bearing device made in workshop	111
Figure 4-14 Air-bearing device components.....	111
Figure 4-15 The air-bearing device bottom plate dimensions and position of nozzles (dimensions in mm)	111
Figure 4-16 Air-bearing tests diagram	112
Figure 4-17 Air valve to adjust the pressure	112
Figure 4-18 Lift against Weight diagram and trend lines for three different nozzles.....	113
Figure 4-19 Lifts against weights for three different distribution of nozzles to the bottom plate	115
Figure 4-20 Different pressures on air bearing with one nozzle at the centre and 12 around.....	116
Figure 5-1 Schematic view of the snap-back test.....	125
Figure 5-2 Fixed-base configuration.....	126

Figure 5-3 Base-isolated configuration	127
Figure 5-4 Acceleration on top of the structure in horizontal direction due to 5kgf snap-back test (Fixed-base); maximum absolute value = 36.96 cm/s^2	131
Figure 5-5 Acceleration on top of the structure in horizontal direction due to 10kgf snap-back test (Fixed-base); maximum absolute value = 60.65 cm/s^2	131
Figure 5-6 Acceleration on top of the structure in horizontal direction due to 15kgf snap-back test (Fixed-base); maximum absolute value = 126.82 cm/s^2	131
Figure 5-7 The effects of applied load magnitudes in accelerations experienced on top of the structure (Fixed-base conditions)	132
Figure 5-8 Acceleration on top of the structure due to 5kgf in snap-back test; Fixed base (FB) and Base isolated (BI) conditions	133
Figure 5-9 Acceleration on top of the structure due to 10kgf in snap-back test; Fixed base (FB) and Base isolated (BI) conditions	133
Figure 5-10 Acceleration on top of the structure due to 15kgf in snap-back test; Fixed base (FB) and Base isolated (BI) conditions	133
Figure 5-11 The effect of isolation system in shifting the fundamental frequency of the structure to a lower one	136
Figure 5-12 Displacement values on top three levels of the structure in snap-back test (5kgf), in Fixed-base condition	137
Figure 5-13 Displacement values on top three levels of the structure in snap-back test (5kgf), in Base-isolated conditions	137
Figure 5-14 Displacement values on top three levels of the structure in snap-back test (10kgf), in Fixed-base condition	139
Figure 5-15 Displacement values on top three levels of the structure in snap-back test (10kgf), in Base-isolated conditions	139
Figure 5-16 Displacement values on top three levels of the structure in snap-back test (15kgf), in Fixed-base condition	140
Figure 5-17 Displacement values on top three levels of the structure in snap-back test (15kgf), in Base-isolated conditions	140
Figure 5-18 Effects of damping in response of the structures, where D denotes the response of the structure and β is the ratio of applied loading frequency to the natural free-vibration frequency (Clough & Penzien, 2003)	141

Figure 5-19 Impulse response of an oscillatory system (De Silva, 2007)	144
Figure 6-1 Physical model of the structure (dimensions in mm)	150
Figure 6-2 shear building model of the structure for dynamic analysis (direction of movement is shown)	150
Figure 6-3 El-Centro earthquake acceleration data.....	154
Figure 6-4 Kobe earthquake acceleration data.....	154
Figure 6-5 Manjil earthquake acceleration data.....	154
Figure 6-6 Assigning mass to the model in SAP2000	155
Figure 6-7 Defining lateral stiffness as Link in SAP2000	156
Figure 6-8 Definition of stiffness as Spring type Link in SAP2000.....	156
Figure 6-9 Definition of properties for spring links in SAP2000	157
Figure 6-10 A sample of *.txt file corresponds to the earthquake recorded data	158
Figure 6-11 Definition of Kobe earthquake acceleration records as a function of time in SAP2000	158
Figure 6-12 Load case data assignment to a time history function in SAP2000	159
Figure 6-13 Acceleration response on top of the structure due to El-Centro earthquake (FB: Fixed base and BI: Base isolated).....	161
Figure 6-14 Acceleration response on top of the structure due to Kobe earthquake (FB: Fixed base and BI: Base isolated)	161
Figure 6-15 Acceleration response on top of the structure due to Manjil earthquake (FB: Fixed base and BI: Base isolated)	161
Figure 6-16 Displacement response of the fixed-base structure due to El-Centro earthquake	163
Figure 6-17 Displacement response of the fixed-base structure due to Kobe earthquake	163
Figure 6-18 Displacement response of the fixed-base structure due to Manjil earthquake	163
Figure 6-19 Displacement response of the base-isolated structure due to El-Centro earthquake	164
Figure 6-20 Displacement response of the base-isolated structure due to Kobe earthquake	164

Figure 6-21 Displacement response of the base-isolated structure due to Manjil earthquake	164
Figure 6-22 Input energy trend over time due to El-Centro earthquake on fixed-base structure (N-m).....	167
Figure 6-23 Input energy trend over time due to Kobe earthquake on fixed-base structure (N-m).....	167
Figure 6-24 Input energy trend over time due to Manjil earthquake on fixed-base structure (N-m).....	168
Figure 6-25 Input energy trend over time due to El-Centro earthquake on base-isolated structure (N-m).....	168
Figure 6-26 Input energy trend over time due to Kobe earthquake on base-isolated structure (N-m).....	169
Figure 6-27 Input energy trend over time due to Manjil earthquake on base-isolated structure (N-m).....	169

List of tables

Table 3-1 Scaling relations in terms of geometric scaling factor.....	72
Table 3-2 Results of lateral stiffness test	75
Table 3-3 Prediction of scaled model mechanical characteristics based on scaling factors	75
Table 3-4 Story drifts	89
Table 4-1 Simulation cases definition.....	105
Table 4-2 Mass flow rate calculated for three different cases	109
Table 4-3 Lifting capacity of each nozzle type investigated by experiments	113
Table 4-4 Lifts corresponding to different loadings for air bearing with one nozzle at the centre	114
Table 4-5 Lifts corresponding to different loadings for air bearing with one nozzle at the centre and six nozzles far around	114
Table 4-6 Lifts corresponding to different loadings for air bearing with one nozzle at the centre and 12 nozzles around	115
Table 4-7 Comparison of mass flow rates (kg/s)	117
Table 5-1 Story drifts on top of the structure in Fixed-base (FB) and Base-isolated (BI) conditions in snap-back test with 5kgf.....	138
Table 5-2 Story drifts on top of the structure in Fixed-base (FB) and Base-isolated (BI) conditions in snap-back test with 10kgf.....	139
Table 5-3 Story drifts on top of the structure in Fixed-base (FB) and Base-isolated (BI) conditions in snap-back test with 15kgf.....	140
Table 5-4 Damping ratios extracting from displacement response of the structure ...	145
Table 6-1 Earthquakes used for simulation.....	153
Table 6-2 Comparison of fundamental frequencies and periods	160
Table 6-3 Peak acceleration at each level of the structure due to input ground motion (m/s^2)	162
Table 6-4 Displacements and story drifts due to El-Centro earthquake (mm)	165
Table 6-5 Displacements and story drifts due to Kobe earthquake (mm).....	165
Table 6-6 Displacements and story drifts due to Manjil earthquake (mm)	165
Table 6-7 Maximum base-shear force (N)	166

Table 6-8 Maximum input energy by different earthquakes (N-m).....	166
--	-----

Nomenclature

A	bearing horizontal cross sectional area of isolator
A	real acceleration
a	scaled acceleration
c	damping
c_e	equivalent damping
C_p	base-isolated natural period coefficient
D	real density
d	scaled density
e	total specific energy, solution error
e_k	kinetic energy
F	shear force
f_r	frictional force
g	acceleration of gravity
\mathbf{g}	body force
\mathbf{I}	unit tensor
k	stiffness
k_b	isolation system stiffness
k_s	story stiffnesss
L	real length
l	scaled length
M	Mach number (chapter 4)

M	real mass
m	scaled mass
m	mass and total mass of the structure
m_b	base mass
m_s	superstructure mass
N	number of identically performed experiments
P	pressure, point in the centre of the control volume
\mathbf{p}	position difference vector
p	kinematic pressure, order of accuracy
Q	volume energy source
Q_s	surface source
\mathbf{q}	heat flux
\mathbf{S}	outward-pointing face area vector
T	temperature, time-scale
T	period of vibration
T_b	period of vibration of isolated structure
T_s	period of vibration of fixed-base structure
T	real time
t	scaled time
t	time
\mathbf{U}	velocity vector
u	specific internal energy (chapter 4)

u	velocity of fluid (chapter 4)
u	displacement of the structure
u_g	ground displacement
\ddot{u}_g	ground acceleration during an excitation
u_{b0}	initial elongation of the fictitious spring in the current non-sliding phase
V	volume
V_M	material volume
\mathbf{x}	position vector
x_s	relative displacement of super-structure to ground
x_b	relative displacement of base-mass to ground
Γ_k	the effective diffusivity of k
Γ_ω	the effective diffusivity of ω
G_k	the generation of turbulence kinetic energy due to mean velocity gradients
G_ω	the generation of specific dissipation rate
S_k	user defined source term
S_ω	user defined source term
Y_k	the dissipation of k
Y_ω	the dissipation of ω
μ_t	the turbulent viscosity
ξ	damping ratio
ξ_b	damping ratio of the isolation system
σ_{v_b}	Root-mean-square (RMS) velocity of base mass

σ_k	the turbulent Prandtl number for k
σ_ω	the turbulent Prandtl number for ω
μ	dynamic viscosity (chapter four)
μ	coefficient of friction
γ	shear strain
λ	heat conductivity
λ	geometric scale factor
ν	kinematic viscosity
ρ	density
σ	stress tensor
τ	shear stress
φ	general scalar property
ω	frequency of vibration
ω_b	frequency of vibration of isolated structure
ω_s	frequency of vibration of fixed-base structure

Abbreviations

BI	Base Isolated
CAD	Computer Aided Design
CFD	Computational Fluid Dynamic
CNC	Computer Numerical Control
DNS	Direct Numerical Simulation
EEW	Earthquake Early Warning
FB	Fixed Base
FEMA	Federal Emergency Management Agency
FFT	Fast Fourier Transformation
FPS	Friction Pendulum System
HDRB	High Damping Rubber Bearing
IBC	International Building Code
ICBO	International Conference of Building Officials
LDRB	Low Damping Rubber Bearing
LES	Large Eddy Simulation
LRB	Lead Rubber Bearing
MDOF	Multiple Degree Of Freedom
MUSCL	Monotonic Upstream-Centered Scheme for Conservation Laws
NEHRP	National Earthquake Hazards Reduction Program
NMA	National Meteorological Agency

NRB	Natural Rubber Bearing
RANS	Reynolds-Averaged Navier-Stokes
RSM	Reynolds Stress Model
SDOF	Single Degree Of Freedom
SEAONC	Structural Engineers Association of Northern California
UBC	Uniform Building Code
USGS	United States Geological Survey
VAC	Volts of Alternate Current
VDC	Volts of Direct Current
PGA	Peak Ground Acceleration

1 Introduction

1.1 Seismic isolation

An earthquake is a devastating natural event which affects human lives, properties, lifelines and has a general impact on daily life. Mitigating earthquake hazards is necessary in order to provide safety and comfort for human beings. This is possible by undertaking comprehensive investigations on how a structure, soil and surrounding environment are affected by an earthquake. As the majority of lives lost during an earthquake have been caused by structural collapses, seismic design of a building has been considered by engineers and designers.

In order to reduce or mitigate earthquake damage, increasing the earthquake resistance capacity of a building structure is taken into account in conventional design methods. This is possible to do by strengthening structural components such as columns, beams and slabs to resist greater lateral loads. This method will increase the total mass of the structure and produce a greater acceleration during an earthquake. A laterally stiff building will transmit greater acceleration due to an earthquake which cause damage to the building and discomfort for occupants. On the other hand, a very flexible building will exhibit a high level of inter-story drift during an earthquake which could cause quick collapse as a result of large deformations and $P-\Delta$ effects. In addition, some

specific structures, which house valuables inside (e.g. museums and galleries) or important buildings (e.g. hospitals, police and fire stations), must not suffer such devastating shocks. Therefore, another concept was introduced in order to reduce the seismic demand instead of increasing the resistant capacity and it was Seismic Isolation.

Seismic isolation is a nonconventional approach to reduce or mitigate earthquake damage based on the concept of reducing the seismic demand of a structure. Seismic isolation offers better performance to a structure during an earthquake if it is applied properly. Seismic isolation has been used to rehabilitate existing buildings and in the construction of new buildings as a practical design strategy. This comes about by separating the ground motion from the building by means of installation of particular isolator devices between a building and its foundation. It can be also be applied to isolate important equipment in a structure protecting them from floor vibrations. The structure which is built on top of the isolation system is known as a *superstructure*.

Basically, the response of a superstructure is reduced by separation from devastating ground shocks thanks to a proper seismic isolation system. In general, seismic forces transmitted to a superstructure are limited due to the application of seismic isolation which lengthens the natural period of a structure as well as some amount of additional damping. The additional damping is inherent in almost all isolation systems but sometimes is provided by additional dampers known as energy dissipation devices. An ideal seismic isolation system will reduce the inter-story drifts and floor accelerations. Reduction of inter-story drifts in the superstructure protects structural components and elements and, therefore, mitigate the damage. Reduction of acceleration provides comfort for the occupants and protects non-structural components.

The other design approach to reduce the response of a structure and alleviate damage in the structure is to make use of energy dissipation devices widely known as dampers throughout the height of the structure (e.g. in line with or in place of diagonal braces). Energy dissipation devices increase the energy dissipation capacity of a structure and in some cases increase the stiffness. Although, increasing the energy dissipation capacity reduces the drift and therefore, reduces damages, increasing the stiffness results in more acceleration and therefore, more lateral force (base shear) exerted to the structure.

In contrast to conventional structural systems and supplementary energy dissipation systems, seismic base-isolation systems reduce inter-story drifts and floor accelerations simultaneously.

Current seismic isolation systems still have some practical limitations which do not allow the isolation system to exhibit satisfactory protection levels. Any proposed systems to date have their own restrictions and functional limitations.

1.2 Motivations for this study

It has been proven that seismic base isolation technology is an effective way of protecting buildings' structural and non-structural elements through a variety of isolation systems which are accepted in concept and, therefore, constructed. However, structural engineers' enthusiasm for proposing innovative systems and/or devices seems to be never-ending. There are a number of patents proposed every year regarding new ideas for seismic isolations. However, not all of them can attract investors in the industry.

1.3 Gap in knowledge

There are two world-widely used isolation systems namely, rubber bearing system and sliding based system. Rubber bearing system generally provides acceptable vertical stiffness and reasonable levels of damping, but damping is strain based and sometimes complex for analysis. Furthermore, the superstructure is susceptible to torsion during an earthquake when it is isolated by rubber bearings. Sliding based bearings or friction pendulum systems (FPS) offer great levels of isolation along with acceptable levels of damping. Additionally, they have a gravity based re-centring mechanism, but the changeable coefficient of friction has brought some difficulties in design and application.

A review of the literature and applications in seismic isolation systems shows that there are still some drawbacks in the functionality of each system. Hence, researchers around the world have been trying to improve the existing systems and overcome the difficulties

in design or concentrate their efforts in designing a new system and creating an innovative design for seismic isolation.

1.4 Aim and objectives of this research

The argument over ideal seismic isolation (complete separation of the structure from ground shocks with no negative effect) has not yet been settled. This study aims to develop an innovative system for seismic base isolation purposes which has the benefits of current systems whilst simultaneously resolving some of their drawbacks. The main advantages of the proposed isolation system in this study include, multi-directional isolation, self re-centring mechanism, variable levels of stiffness and damping, high level of horizontal isolation, and that it provides very small inter-story drifts and a low level of acceleration transmitted to the structure. The proposed isolation system - which works with the air-bearing to detach the structure from horizontal movements - is designed for practical use and its performance is tested via laboratory experiments. In addition, a numerical study was conducted to validate the results from experiments.

The objectives of this study are summarised as follows:

- To introduce an innovative isolation system highlighting the concepts of design, principal components, related devices, operation and functionality.
- To design and develop a 1/10th scaled model of an ordinary five-story building as a case study to highlight the ability of the proposed isolation system in lengthening the natural period of the structure and functionality of an air bearing mechanism.
- To design and develop the air-bearing device and conducting laboratory tests to determine its functionality and compare with numerical results for validation.
- To instal the proposed air-bearing device under the scaled model and testing its functionality under structural loadings.
- To conduct dynamic laboratory tests on the scaled model structure in order to determine the dynamic characteristics of the model in fixed-base and isolated conditions and compare with analytical results.

- To make use of data acquisition system along with high precision accelerometers in dynamic laboratory tests in order to gain an insight about the performance of structure in real world.
- To perform numerical study of the model using time history analysis in order to obtain the response of the structure during an earthquake in fixed-base and isolated conditions.
- To investigate the performance of the proposed system for application in seismic isolation of equipment inside the structure.

1.5 Research methodology

Experimental study and numerical modelling is the research methodology generally used in this study.

1.5.1 Air-bearing device

A numerical simulation was generated to facilitate the understanding of the behaviour of the fluid in the air bearing different parts. The performance of the nozzle highly depends on the fluid flow. The single phase flow modelling was considered for this purpose to investigate the phenomena such as shock waves, turbulence and viscosity. The commercial software, FLUENT, was used for single phase simulation of air inside the nozzle. Different Reynolds-Averaged Navier-Stokes (RANS) turbulence model, $k-\omega$, and Reynolds Stress Model (RSM) was used to accurately simulate the flow inside the nozzle. Advances in computer performances and speeds have made it possible to use Large Eddy Simulation (LES) and Direct Numerical Simulation (DNS) for this application.

Experimental study on the air bearing was also conducted in order to gain knowledge on its performance in real conditions and as a validation for numerical modelling. Experimental tests on the air-bearing device with different nozzle shapes were performed to discover the optimised shape. Tests on devices were designed to observe the performance of bearing unit in handling different size loads in two different input pressures based on the capabilities of the air pump in the workshop.

1.5.2 Scaled structure model

Since the main purpose of this research is to propose an innovative design for seismic base isolation, a scaled structure ($1/10^{\text{th}}$ scaled in dimensions) was considered for experimental tests and numerical modelling.

The methodology for scaling is based on defining a geometry scale factor as $1/10^{\text{th}}$ and subsequently working out the other physical parameters. In this methodology, acceleration and mass density are the same for the real and scaled model (Wu & Samali, 2002); meaning that the scaling factor for those two parameters is defined as 1.

Experimental tests were then conducted on the scaled structure in the workshop with the purpose of finding key dynamic characteristics of the structure. The dynamic tests were performed on the structure according to two conditions, Fixed Base (FB) and Base Isolated (BI). The snap-back test method was used to excite the structure with different loading to achieve structural fundamental frequencies of vibration.

Based on the time history response of the structure, the peak absolute accelerations were compared for two different base conditions (isolated and non-isolated) on top levels. Fast Fourier Transformation (FFT) was then employed to analyse the data in order to find structural natural frequencies.

One of the most important dynamic parameters which should be highlighted is *damping*. Damping is an empirical parameter which can be discovered by analysis of the results from a time history function of system behaviour. In this research, the method of Logarithmic Increments over the time history response of the structure was used to determine damping.

The numerical simulation of the scaled structure was generated to test the structural performance during different earthquakes with different characteristics. SAP 2000 was employed as the most reliable modelling software for time history analysis of structures and the assumption of Shear Building was applied for simulation. It should be noted that just one direction of horizontal movements of earthquakes was applied at a time with respect to the scope of this study.

1.6 Dissertation scope

The design and analysis in this research are based on considering the horizontal movements of an earthquake on structures located far from the epicentre of the earthquake. However, the effect of the proposed system for near field shocks was also investigated. The proposed isolation system in this study was investigated by considering a scaled model building as a case study built specifically for this purpose. The dimensional analysis used to determine the structural properties of the scaled model structure was based on geometry scaling and the model was analysed and designed in linear mode. The components of the isolation system were also analysed and designed in linear conditions. For dynamic laboratory tests, only one component of horizontal movement was measured at a time. In numerical simulation of the air bearing device, the fluid was considered as non-compressible. In numerical analysis of the structure, the effect of soil underneath the foundation was not considered. The response of the structure was obtained in terms of absolute accelerations, absolute and relative drifts, and subsequently, frequencies of vibration for fixed-base and isolated conditions were measured. The research path from proposal to the thesis is shown in appendix A.1 Research flowchart.

1.7 Dissertation outline

The present dissertation is structured as below:

Chapter 1 consists of an introduction to seismic isolation and motivations for this study along with aims and objectives of the present work.

Chapter 2 reviews the historical background of seismic isolation and further looks at recent progress in this area.

Chapter 3 explains the philosophy behind seismic base isolation and characteristics of the proposed system along with its principles of operation on a 1/10th scaled structure. Structural characteristics of the scaled model are also explained in this chapter.

Chapter 4 includes modelling of the air-bearing device, its design and development with respect to experimental results and numerical simulations.

Chapter 5 presents the dynamic characteristics of the structure with respect to the laboratory tests. Results from the experimental study are further compared with those from the analytical model of the structure presented in chapter 3.

Chapter 6 explains the numerical study of the proposed isolation system and its performance during different earthquakes.

Chapter 7 summarises the results from experimental and numerical studies and further discussions on the subject. This chapter sums up the dissertation with main research conclusion and recommendations for future works.

2 Literature review

2.1 Introduction

Isolation from the ground during a seismic excitation has been one of the challenging subjects for researchers for many years. From the audit of current approach to date, the general principles are for buildings or structures to be decoupled from the horizontal components of the earthquake ground motion by interposing a layer with low horizontal stiffness between the structure and the foundation. The harmonious movement of the structural basement will cause a significant reduction of fundamental frequency that is much lower than its fixed-base frequency and also much lower than the predominant frequencies of the ground motion (Monfared, et al., 2013). History tells us that many efforts were made to find out a best practical solution with respect to facilities and science progress of the specific era.

In this chapter, *seismic base isolation* technique is investigated from historical overview to the state-of-the-art practices.

2.2 Seismic base isolation from historical perspective

Historically, one of the big challenges for researchers has been to design structures that could provide an assurance of safety to its occupants at times of natural disasters such as Earthquake. Many efforts have been made to find out the best solutions in resisting against this catastrophic event.

First evidences shall be found in historical buildings in some seismically active regions of the world, where utilizing multi-layer stones as a construction method had been considered. The surfaces of these large stones are smoothed and flat. It seems that they have been made to have less friction during an earthquake excitation and able to move back and forth over the lower foundation without damage. Sensible examples shall be found in some monuments of Pasargadae the capital city of ancient Persia which date back to at least 2500 years ago and have lasted without seismic damages to date. The other example of this kind shall be found in Dry-stone walls of Machu Picchu Temple of the Sun, in Peru (dates back to the 15th century) (Wright & Zegarra, 2000). In Europe, understanding the concept of seismic isolation, dates back many hundreds of years. For instance, the Roman historian Gaius Plinius Secundus wrote in the first century AD about an example of Greek magnificence, worthy of true wonder, which is the temple of Diana that stands in Ephesus and took the 120 years to build. It was erected in a marshy area so that there would be no fear of earthquakes or cracks in the soil, and to avoid founding such an imposing monument on slippery and unstable soil, a layer of coal chippings and a layer of wool fleeces were laid underneath (Forni & Martelli, 1998). Other kind of earliest protecting system was using a crisscross pattern of circular cross-section timbers under the structure and above its base for light buildings. The concepts of this method come from rolling of a layer of circular cross-section timbers which are parallel together in longitudinal direction and perpendicular to the lower layer. In Japan, a five story temple which dates back to the 12th century is claimed to be adopting a passive control system because of possessing long natural period as a result of friction damping in its wooden frames and dispersion of natural period due to the central column (Izumi, 1988). Former emperor palace in Beijing, China, is the other example which has been built on a kind of base isolation system, because its foundation is built on boiled glutinous rice and lime, so the artificial ground has high viscosity and damping (Izumi, 1988).

2.3 Seismic base-isolation efforts in the modern time

Continuing and longstanding attempt to limit the effects of large earthquakes in uniquely different manners, such as decoupling the structure from its base, was led to some

activities in late 19th century. One of the earliest in this regard is the patent by Jules Touaillon of San Francisco filed in the US Patent Office in February 1870 (Buckle, 2000). It describes an 'earthquake proof building' which is seated on steel balls which roll inside shallow dishes. As far as can be determined, few if any of these early proposals were built, most probably due to their impracticality and a lack of enthusiasm from the building officials of the day (Buckle, 2000). Twenty years later in 1891, a base-isolated structure was proposed by Kawai after the Nobi Earthquake on *Journal of Architecture and Building Science* (Izumi, 1988). His structure has rollers at its foundation mat of logs put on several steps by lengthwise and crosswise mutually. In early 20th century, a similar proposal was made in Italy in 1909 by the Commission that was given the task of making suggestions for rebuilding the area destroyed by the Messina earthquake of 1908. This proposal was for the interposition of rolls of material or sand beds between the base of the structure and the ground (Forni & Martelli, 1998). In the same year a seismic isolation system was proposed by Dr. Johannes Calantarientis, an English medical doctor (Naeim & Kelly, 1999). He proposed separation of building from its foundation by a layer of talc which would isolate the main structure from seismic shock (Saiful-Islam, et al., 2011). His idea was utilised in construction of Imperial Hotel in Tokyo in 1921 and the building survived the devastating 1923 Tokyo earthquake which was believed to have registered around 8.3 on the Richter scale (Ismail, et al., 2010). After the 1923 Great Kanto earthquake, numbers of patents in Japan were submitted. For instance, the proposal of double column with damper was proposed by Nakamura (Izumi, 1988). In 1927, Nakamura proposed a system which consisted of several columns under the ground floor slab with around 15 meters length to the depth of the soil under the structure and utilizing dampers at the joint points of ground floor slab and these columns. He named his design, Double Column and Dampers. One year later, in 1928, Oka proposed and designed a special kind of isolation for Fudo Bank buildings in Japan (Izumi, 1988). However, some of base-isolated models had bigger response than ordinary structures in artificial earthquake tests. In 1930s the idea of flexible first-story column proposed by Martel in 1929, Green in 1935 and Jacobsen in 1938 had gained popularity (Iqbal, 2006). The idea seemed to be impractical as a result of columns yielding which vastly reduces buckling load. A real example was Olive View hospital in California which was damaged just one year after

construction during San Fernando earthquake in 1971 (FEMA 451B, 2007) . During world war two and some years after that no progress in the idea of base isolation had been reported. In 1968 a building in Macedonia was built on hard rubber blocks (Ismail, et al., 2010). Soon after that, in 1969 a primary school in Yugoslavia was built on rubber bearings as a base isolation system for strong earthquake (Izumi, 1988). Steel rubber-laminated bearing was developed at the same time in Japan. During that era, the concept of Base Isolation with utilizing rubber bearing was becoming more and more a practical issue for engineers and constructors. Progressive research led to invention of a new kind of bearing named Lead Rubber Bearing (LRB) in 1970s. LRB overcame the lack of re-centring and damping in rubber bearing mechanism, but not completely. These kind of bearings were stiff under vertical loads and very flexible under lateral loads. In the early 1980s developments in rubber technology lead to new rubber compounds which were termed High Damping Rubber (HDR) (Ismail, et al., 2010). Friction Pendulum System (FPS) introduced by Zayas in 1986, is another kind of base-isolating system which uses friction principles for shifting the fundamental period of the structure to a greater one and away from the destructive period range of ground motion. It is made up of dense Chrome material over Steel concave surface in contact with an articulated friction slider and free to slide during lateral displacements (Kravchuk, et al., 2008).

2.4 Recent progress in seismic-base isolation

The use of LRB, HDR and FPS systems as the most popular techniques for base isolating has been increased for the past 2 decades. The concept of Base Isolation has been an increasing interest for many companies and they have worked along with researchers and engineers to develop this idea as a passive seismic-response control.

In 1986 a simple regulation named Tentative Seismic Isolation Design Requirements was published by a subcommittee of the Structural Engineers Association of Northern California (SEAONC), and it was known also as the Yellow Book (Naeim & Kelly, 1999). Provisions in this book, along with subsequent revised and expanded provisions in the SEAOC Blue Book (SEAOC 1990, 1996), the Uniform Building Code (ICBO 1991, 1994, 1997) and NEHRP (National Earthquake Hazards Reduction Program)

provisions (NEHRP 1995, 1997) paved the way for implementation of seismic isolation in the United States. Nowadays, the comprehensive regulations in the subject of seismic Base Isolation, is available for engineers and scientists in IBC (International Building Code) 2012 as well as the latest version of NEHRP provisions published by FEMA (Federal Emergency Management Agency).

Normally, important structures such as historical buildings, museums, hospitals and also official buildings in the U.S.A are more likely to be designed and built or retrofitted by means of base isolation techniques in seismic areas.

In Europe, Eurocode 8 has mentioned some regulations in a chapter named “Design of structure for earthquake resistance”. This specific chapter deals with the design of seismically isolated structures. The “EUROPEAN COMMITTEE FOR STANDARDIZATION” has published code number 15129:2009 in 2009 namely “Anti-seismic devices. This code works alongside other Euro codes with several references which provides the user with some difficulties if other Euro codes are not available. The most notable country of Europe with major earthquake is Italy. During 1982-1992 more than a hundred highway bridges (new constructions and retrofitted existent structures) were equipped with seismic-isolation systems in Italy (Parducci, 2010). In 1998 the Italian Ministry of Works issued the first official recommendations for the design of seismic isolated structures, in which particular attention was paid to the use of rubber bearings. This is a significant step that allows and popularises the use of seismic isolation in Italy (Parducci, 2010). The last Italian code is called “Nuove Norme Tecniche per le Costruzioni” , (Ministerial Decree of 14 January 2008), and moves closer to European Code.

Japan has been known as one of the most seismically susceptible areas in the world which is located next to the intersection borders of three major tectonic plates named Pacific Plate, Eurasian Plate and Philippine Plate. The islands of Japan are primarily the result of several large oceanic movements occurring over hundreds of millions of years. Destructive earthquakes, often resulting in tsunamis, occur several times a century. Tectonic and volcanic activities have made a long history of earthquake for this country. Japan has a very colourful building regulation history over the last 100 years. The

Japanese Seismic Design Code (BSL) was revised in 2000 (Nakashima & Chusilp, 2003). Seismic provisions in the building code were significantly revised in 2000 from prescriptive to performance based to enlarge choices of structural design, particularly the application of newly developed materials, structural elements, structural systems, and construction (Kuramoto, 2006). The number of base-isolated structure in Japan continues to increase as well as other seismic retrofitting systems, particularly after the 1995 Kobe earthquake.

One of the pioneering countries in Seismic Base-Isolation system design is New Zealand. The first New Zealand seismic design code, NZSS 95 published in 1935 and the first Lead Rubber Bearing in the world had been installed into the William Clayton building in Wellington, New Zealand in 1981. This building was also the first base-isolated building in New Zealand.

In China, the widespread use of base isolation for housing has only been employed since 1990, with the first code addressing this technology published in 2000. In Chapter 12 of Chinese Code for Seismic Design of Buildings (2010 version), regulations for design of seismically isolated and energy-dissipated buildings are mentioned.

2.5 Seismic base-isolation systems

Every base-isolation (BI) system must have three major capabilities to be considered as a practical one. First of all is an acceptable level of horizontal flexibility which helps the structure to be decoupled from ground underneath to be isolated completely or partially from ground horizontal movements. Secondly, each BI system needs a kind of damping properties to dissipate parts of the energy entered the structure; and finally a type of re-centring mechanism is essential to re-locate the super-structure to its initial position.

There have been so many BI devices proposed so far. Some were successful in practice and have been improved during the time and some were just remain in proposal phase as they were not practical or worthwhile to be developed. In this section a number of notable devices are discussed in popularity order and mechanism.

2.5.1 Elastomeric-bearing isolation systems

The most common system of base isolation is using elastomeric bearings such as, natural rubber bearings (NRB), lead rubber bearings (LRB) and high damping rubber bearings (HDRB). Rubber Bearings are spring-like isolation bearings and mainly made up of horizontal layers of natural (or synthetic) rubber in thin layers bonded between steel plates with strong cohesive (Saiful-Islam, et al., 2011); and this mechanism with pre-determined lateral flexibility results in reducing the earthquake forces by shifting the structure's fundamental frequency to a smaller one and avoid resonance with the predominant frequency contents of the earthquakes.

These bearings are strong and stiff under vertical loads, yet very flexible under lateral forces. The formulation of mechanical characteristics of elastomeric bearings can be simply worked out by predictions based on elastic theory which has verified by laboratory testing and finite element analysis.

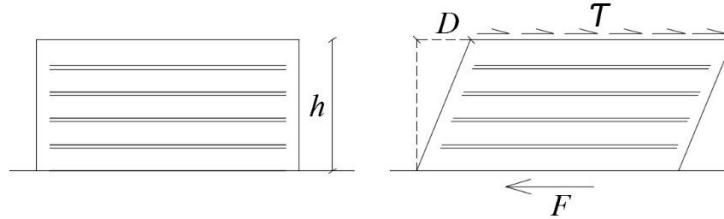


Figure 2-1 Rubber bearing schematic view

In Figure 2-1, F is the shear force and defined as below:

$$F = \tau A \quad (2.1)$$

A is the bearing horizontal cross sectional area and τ represents the shear stress. The shear strain, γ , of the bearing is defined as follow:

$$\gamma = \frac{D}{h} \quad (2.2)$$

D and h are shown in Figure 2-1.

It is show by (Naeim & Kelly, 1999) that the material is nonlinear at shear strain less than 20% and is characterised by higher stiffness and damping, which tends to minimize

response under wind load and low level seismic loads. Between the range 20% and 120% shear strain, the shear modulus is low and constant. The modulus will increase at large strains as a result of a strain crystallization process in the rubber, which is going along with an increase in the level of dissipated energy (Naeim & Kelly, 1999). Two general shapes are known for elastomeric bearings: conventional *round* type and *square*. Changes in shapes could be advantageous in terms of economy concern. By reduction in size, stability and capacity for large deformations could be varied, yet their basic function remains the same. There are three main groups of elastomeric bearings namely, Low Damping Rubber Bearings (LDRB), Lead Rubber Bearings (LRB) and High Damping Rubber Bearings (HDRB).

2.5.1.1 Low damping rubber bearings

This type of isolators has been adopted most widely in recent years and are also known as *Laminated rubber bearings*. The elastomer is made of either Natural rubber or Neoprene. Using low damping rubber bearings, the structure is decoupled from the horizontal components of the earthquake ground motion by interposing a layer with low horizontal stiffness between the super-structure and the foundation (Buchanan, et al., 2011). A typical *laminated rubber bearing* is shown in Figure 2-2.

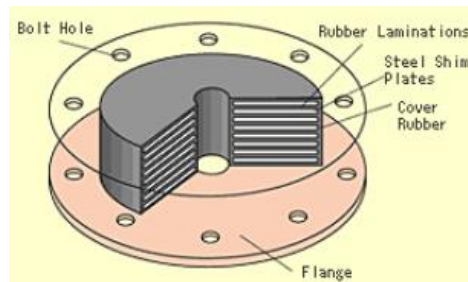


**Figure 2-2 Laminated rubber bearing also known as Low damping rubber bearing
(Buchanan, et al., 2011)**

In order to provide vertical rigidity along with lateral flexibility, low damping rubber bearings are made of steel plates bonded together with thin rubber layers. These type of bearings are usually used in bridge construction. The device is fitted with strong steel plates to the top and bottom in order for attachment to the super-structure and foundation. Vertical rigidity assures the isolator will support the weight of the super-

structure, while horizontal flexibility converts devastating horizontal shocks into gentle movement.

Laminated rubber bearings have a disadvantage of *low damping* properties. Thus, sometimes they are called ***Low Damping Rubber Bearings***. For overcoming this problem, Lead Rubber Bearings were developed.

2.5.1.2 Lead rubber bearings

A slightly modified form of laminated rubber bearing with a solid lead ‘plug’ in the middle to absorb energy and add damping is called a lead-rubber bearing which has been widely used in seismic isolation of buildings. This kind of elastomeric bearings is made up of *thin layers of low damping natural rubber* and *steel plates* formed in alternate layers and a *lead cylinder plug* firmly fitted in a designated hole at its centre to deform in pure shear as shown in Figure 2-3. Invented in New Zealand in 1975, LRB has been widely used also in Japan and United States. The steel plates ensure the vertical rigidity as well as forcing the lead plug to deform in shear (Naeim & Kelly, 1999). This type of bearings provides an elastic restoring force and simultaneously produces a required level of damping by selection of the appropriate size of lead plug. Seismic performance of LRB is maintained during frequent strong motions, with appropriate durability and proper reliability (Saiful-Islam, et al., 2011). The basic functions of LRB include:

Load supporting: Due to a multilayer construction of the bearing rather than single layer rubber pads, better vertical rigidity is provided.

Horizontal elasticity: By means of LRB, earthquake shocks are converted into gentle motions. As a result of the low horizontal stiffness of bearing, strong vibrations are lightened and the period of the vibration of the isolated structure is lengthened.

Restoration: Because of LRB’s inherent horizontal elastic characteristics, the isolated structure will be back to its original position after shocks. These elastic properties are mainly produced from restoring force of the rubber layers.

Damping: The lead plug provides required amount of damping.

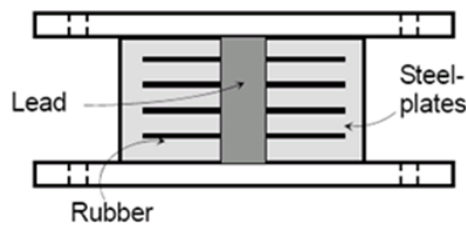


Figure 2-3 Lead rubber bearing section (Saiful-Islam, et al., 2011)

2.5.1.3 High damping rubber bearings

HDRB is another type of elastomeric bearings. These type of bearings are also made up of thin layers of rubber and steel plates built in alternate layers as shown in Figure 2-4. The rubber layers used in HDRB possess high damping properties. The damping in the bearing is increased by adding extra-fine carbon black, oils or resins and other proprietary fillers (this is the main different between LDRB and HDRB). The dominant features of HDRB system are the parallel action of linear spring and viscous damping. The damping in the isolator is neither viscous nor hysteretic, but somewhat in between. The vertical stiffness of the bearing is much higher than the horizontal stiffness due to the presence of internal steel plates. Steel plates also prevent bulging of rubber.

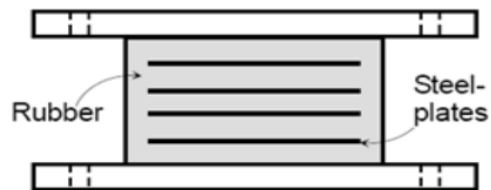


Figure 2-4 High damping rubber bearing (Saiful-Islam, et al., 2011)

The basic functions of HDRB include:

Vertical load bearing: Rubber layers are reinforced with steel plates, therefore, a stable rigid vertical support is provided for super-structure.

Horizontal elasticity: HDRB, like the other types of elastomeric bearings, converts the devastating shocks of earthquake into gentle motion due to the low horizontal stiffness of the multi-layer rubber bearing which lengthens the period of vibration to a greater one.

Restoration: Again, very similar to other types of elastomeric bearings, horizontal elasticity of HDRB returns the isolated structure to its original position after shocks.

Damping: Higher values of damping is provided thanks to the additional materials used in production of rubber for HDRB isolators.

2.5.2 Sliding base-isolation systems

The second major type of seismic base isolation system is characterised by the sliding mechanism which works by limiting the transfer of shear across the isolation interface (Buchanan, et al., 2011). Numbers of sliding system have been proposed over the past decades, yet just some have been practical. Sliding bearing system is simple in concept; where a layer with a defined and very low coefficient of friction, so the forces transmitted to the structure will be limited to the coefficient of friction multiplied by weight. One commonly used sliding system called, spherical sliding bearing (SSB). In this system, the structure is mounted on bearing pads that have a curved surface with a low coefficient of friction. The structure, then, is free to slide on the bearings during an earthquake. Since the bearings have a curved surface, the building slides both horizontally and vertically (Buchanan, et al., 2011). The limit on the horizontal or lateral forces are determined by the forces needed to move the huge weight of the structure slightly upwards. The advantages of this system are summarised in their ability to provide vibration isolation for light loads as well as large-scale loading conditions; large deformation performance; providing protection against a wide range of tremors from small vibrations to major earthquakes; and the ability of being used in conjunction with other isolation systems such as elastomeric bearings (Saiful-Islam, et al., 2011).

2.5.2.1 Friction pendulum bearings

Friction Pendulum Bearing (FPB) or Friction Pendulum System (FPS) is very similar to SSB in functionality. The concept is based on three features: an articulated friction slider, a spherical concave sliding surface, and an enclosing cylinder for lateral displacement restraint (Buchanan, et al., 2011). FPS is known as a type of isolation system suitable for small to large-scale structures. It combines a sliding action and a restoring force by geometry (Naeim & Kelly, 1999) (Figure 2-5).

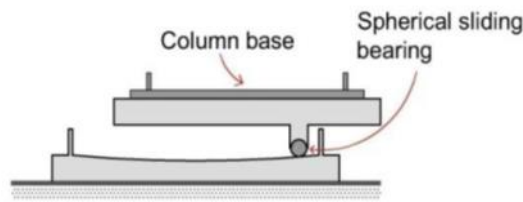


Figure 2-5 Spherical sliding system schematic view (Buchanan, et al., 2011)

However, as mentioned before, the sliding-type bearings have limited restoring capability. To overcome this drawback, the FPB was developed by introducing a spherical sliding interface to provide restoring stiffness, while the friction between the sliding interfaces helps in dissipating energy (Buckle, 2000). The FPB, as a result, is functionally equivalent to elastomeric bearings in lengthening structure's fundamental period. The additional advantageous features of FPB over elastomeric bearings such as period-invariance, torsion-resistance, temperature-insensitivity and durability (Buckle, 2000). The FPB has recently found increasing applications whereas, the elastomeric bearings have been extensively adopted for seismic isolation.

2.5.3 Dampers used for seismic isolation

Dampers provide sufficient resistance with reducing the effects of displacement and acceleration imposed to the structure during an excitation. The effect of damping on dynamic response is very important and beneficial. In general, any structural system exhibits various degrees of damping. It is assumed that, structural damping is viscous by nature (Saiful-Islam, et al., 2011). In physics, damping coefficient relates force to velocity. It is viable to restrain the oscillatory motion when damping coefficient is sufficiently large. In structural engineering, the damping value that completely suppress the vibration is termed as critical damping. In frequency and period calculations, damping is usually neglected unless it exceeds about 20% of critical. In structural analysis, it is customary to use two types of damping as follows:

Elementary damping: All isolators have some levels of pure damping with respect to their component materials. Some of them such as HDRB and LRB are used in low weight structure in order to absorb vibrations. In this case they act as pure damper devices rather than isolators. The level of elementary damping in analysis are defined

as a percentage of critical damping (usually around 10% of critical) and considered as viscous damping.

Supplementary damping: Some types of isolators such as LDRB are able to provide flexibility but they do not provide significant damping. In such cases, in order to strengthen the damping phenomena, supplementary devices are included with general Isolators (Saiful-Islam, et al., 2011). There are a number of supplemental damping devices able to absorb energy and add damping to buildings, in order to reduce seismic responses. These devices can be combined with base isolation system of the building, or placed elsewhere up the height of the building, often in diagonal braces, or they can be used as part of damage-resistant designs (Buchanan, et al., 2011). Dampers in buildings do resist service loads; they just provide damping in vibrations.

Supplemental damping devices are especially suitable for tall buildings which cannot be effectively base-isolated (Buchanan, et al., 2011). Tall buildings are very flexible compared to low-rise buildings, therefore, it is necessary to control their horizontal displacement to some extent. This is usually achieved by the use of damping devices, which are able to absorb a reasonable part of the energy and subsequently making the displacement tolerable.

2.5.4 Soft first-story building

In 1930s the idea of flexible first-story column was proposed by Martel 1929, Green 1935, Jacobsen 1938. This idea for several reasons seemed to be impractical as a result of columns yielding which vastly reduces buckling load. A real example was Olive View hospital in California which was damaged just one year after construction during San Fernando earthquake in 1971.

2.5.5 Artificial soil layers

In 1910 a seismic isolation system was proposed by Dr. Johannes Calantarients, an English medical doctor (Naeim & Kelly, 1999). His diagrams in his patent show a building separated from its foundation by a layer of talc which would isolate the main structure from seismic shock (Saiful-Islam, et al., 2011). His idea was utilised in construction of Imperial Hotel in Tokyo in 1921. The building was founded on an 8 ft

(2.44 m) thick layer of firm soil under which there is a 60-70 ft (18.29-21.34 m) thick layer of mud. The soft mud acted as isolation system and the building survived the devastating 1923 Tokyo earthquake which was believed to have registered around 8.3 on the Richter scale (Ismail, et al., 2010). Another same ideas were considered in designs and constructions but they never became a reliable method for seismic isolation purposes as there are many conceptual and practical barriers to prove this system for practice.

2.5.6 Rolling base-isolation systems

First evidences of rolling base-isolation system were found in Japan as it has discussed in previous section. The most recent progress in rolling isolation system has been proposed recently by M Ismail at Technical University of Catalonia in 2009 (Ismail, et al., 2010). His new innovative device is called *Roll-n-cage isolation bearing*. His proposed idea is an innovative rolling-based seismic isolation which is benefited from the principals of elliptical shape of rollers to ensure a gravity-based re-centring mechanism. Roll-n-cage system provides engineers with acceptable numerical results but it is too complicated to design as it has so many components relating to the proposed device. On the other hand this system does not have adequate flexibility in terms of maximum deflection in large magnitude earthquakes.

2.5.7 Air-bearing for base isolation

Recently in Japan a research paper proposed an isolation system consisting of isolation devices using air bearings, and an isolation activation judgment device using EEW (Earthquake Early Warning) by Satoshi Fujita in 2011 (Fujita, et al., 2011). Their isolation system is able to float by air bearings with the system needing to know whether an earthquake is going to occur. In this isolation system, EEW provides earthquake information, and the system determines activation by using information from EEW. Although this isolation system has adequate isolation performance, the system is complicated and has many components. On the other hand their proposed system has the lack of re-centring and also damping properties. The proposed system by Fujita is just suitable for isolating stuffs like computer servers or storages with no more than 500

kg of weight and further more works are needed to comply with isolating of a structure like a residential building.

2.5.8 Other isolation systems

There are some other types of isolator, which have been rarely used in isolating buildings or structures. Rollers, springs, and sleeved piles are some examples of such isolators. A brief description of those is presented here.

Roller Isolators: Cylindrical rollers and ball races are amongst well-known roller type isolators. Depends on the structure and material of the roller or ball bearing the resistance to movement may be sufficient to resist service loads and may generate damping to some degrees. They have been commonly used for machinery isolation. Roller bearings are attractive in theory as a simple means of providing flexibility, however, they have functionality drawbacks in practice. Solid metal ball and roller bearings made up of steel or alloys usually have the problem of flattening of the contact surface under time when they are under the weight of huge structures and high compressive stress which restrict their use. In addition, they are not able to provide either damping or resistance to service loads; therefore, they should be used in parallel with other devices such as springs or dampers (Kelly, 2001).

Spring Isolators: There are some devices work based on steel springs which are rarely used and their most likely application is for machinery isolation. The main drawback with spring isolators is that they are almost flexible in both the *vertical* and the *lateral* directions (Kelly, 2001). The vertical flexibility in seismic base isolation is not desirable as it could cause damages in some structural elements. As springs alone can provide just a little damping and would move disproportionately under service loads, the main disadvantages of this kind is lack of sufficient damping properties.

Sleeved Piles Isolators: The system comprising piles inside a sleeve can provide flexibility which allows movement in the structure. Sleeved piles are able to provide flexibility yet no any degrees of damping (Saiful-Islam, et al., 2011). It is necessary to use dampers in parallel to the system of sleeved piles for seismic isolation.

2.5.9 Advantages and disadvantages of current seismic isolators

As discussed above, some factors may not be recognised as the disadvantages of the device on its own but may be a design disadvantage in the construction projects. As an example, the high damping rubber bearings could produce primary and secondary (P- Δ) moments which are distributed equally to the top and bottom of the bearing and therefore, these moments must be designed for in both the foundation and super-structure above the isolators (Kelly, 2001). For sliding bearing systems, static friction is known as a disadvantage in general, but for certain construction projects, the manufacture of devices such as the FPS may attempt to produce sliding surfaces reducing this friction as much as possible. Dampers can be used almost anywhere in a structure to control the displacements but can add force to the system and cannot be used individually for isolation. However, depending on the project needs, some characteristics may be found more important than others.

A list of significant base isolation projects around the world are given in appendix A.2 BI projects around the world.

2.6 Air-bearing perspective

2.6.1 Applications

Nowadays, the industrial factories benefit from cutting-edge technologies for handling heavy loads by interposing a fluid layer with low horizontal stiffness between the load panel and the ground. One of the most well-known technologies is the Air Bearing system, which produces a thin layer of pressurized air between the load base plane and the surface of the ground giving an advantage of a near zero friction. The fluid film of the bearing is achieved by supplying a flow of air through the bearing face and into the bearing gap. This is typically accomplished through an orifice to provide the flow of air into the gap (Percision, 2003).

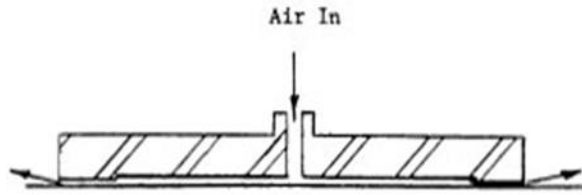


Figure 2-6 An air-bearing schematic view

Very similar to an air hockey table, air bearings support even heavy loads on a cushion of air. Therefore, there is an essential need for a sufficient air pump for practical works. This kind of air bearings is known as *Flat Air Bearing* or *Rigid Air Bearing* (typical flat air bearing shown in Figure 2-6). Utilising flat air bearings for very heavy loads needs fairly smooth surfaces as the gap between two surfaces is less than 1 millimetre. The other kind of air-bearing systems for moving heavy loads is *Air Float Bearing*. This type works as similar as hovercrafts. Air float uses a flexible diaphragm beneath the load support surface. Air is pumped into the diaphragm and passes freely through the diaphragm holes and into the plenum beneath, raising the platform off the ground.

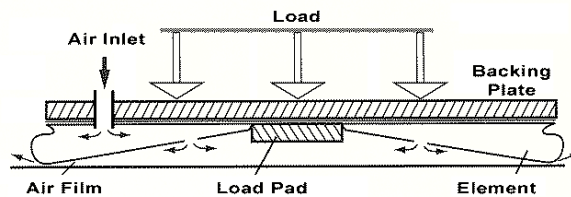


Figure 2-7 An Air float bearing schematic view (HOVAIR, 2013)

The advantages of air bearing system are identified as follow:

Zero Friction: there is a large difference in the level of friction manifested in an air bearing system in comparison to the other methods. In air bearing system there is no difference between static and dynamic coefficient of friction. Friction in air bearings is a function of air shear from motion.

Silent and smooth operation: rollers or balls create noise at the event of vibration and become loaded and unloaded whereas an air bearing system does not produce any notable noise at the time of operation.

Higher damping: Being fluid film bearings, air bearings have a squeeze film damping effect resulting in higher dynamic stiffness and better controllability.

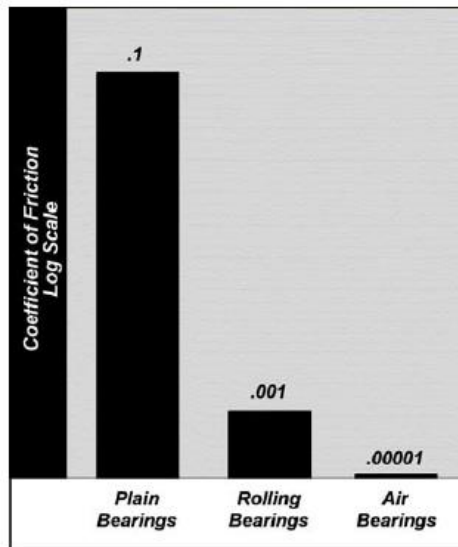


Figure 2-8 Comparison of coefficient of friction for three types of bearing (Newway, 2006)

Air-bearing technology has been utilised in various industries for handling and moving heavy loads such as diesel engines, machineries, train wagons and also military tanks of approximately 60 tonnes and higher.

2.6.2 Technical research

The air-bearing solutions have been used for handling heavy weights and also in precision manufacturing for the past three decades. Nowadays, several companies all around the world take the advantages of pressurized air for taking heavy loads in industry and in factories. Companies provide air-bearing solution devices have their own design procedure and manufacturing. As the choices for design and manufacturing of a device for a particular purpose of bearing solution could be endless, there are not organised rules or regulations for the design of air-bearing unit in a specific project. Beside, manufacturers tend to keep their own research and design unpublished for a while for competitive purposes. One of the pioneer researchers in this area is John William Powell who published a book namely “Design of Aerostatic Bearings” in 1970 (Powell, 1970). He introduced basic equations, which are commonly used in the modelling of the mass flow-rate of gas through an orifice-type restrictor in aerostatic bearings. In 2004, Renn and Hsiao (Renn & Hsiao, 2004) proposed a CFD simulation focussing on the mass flow-rate characteristic of gas through orifice, based on using empirical equations for estimation of controlling coefficients which results in some

limitations in application of the method. In 2006, Mukai investigated the dynamic properties of a manufacturer made air-bearing units (Mukai, 2006). In that report the effects of shape and geometry of the orifice or nozzle is not presented, whereas the shape of the nozzle can play a significant role in changing the capacity of air bearing. Another research by (Wei & Gang, 2010) shows the effect of entrance on load capacity of nozzle. In their study the density of fluid is assumed as constant which may not lead to accurate results in turbulence and high Mach numbers.

2.7 Earthquake Early Warning systems

The EEW (Earthquake Early Warning) system can estimate intensity and arrival time of an earthquake before its principal motion arrives. This is a prevention and warning system mostly used to control trains, elevators, and medical institution or to warn the residents of condominium. The principle of the operation and flow of EEW is as follows: Firstly, seismometers installed near an earthquake focus detect a primary wave, and then this information is transmitted to the National Meteorological Agency (NMA). Next, earthquake intensity and estimated time of arrival at a particular place are analysed using the information of the seismometers. Finally EEW is transmitted from the NMA to medical institutions, medias, facilities, or residence in order to warn everyone about the earthquake arrival and thus avoid secondary disaster. Fortunately, EEW systems are operated and used in many earthquake prone areas of the world. These systems can provide a few tens of seconds warning prior to damaging ground motions. The amount of time for early warning depends on the distance from the epicentre of the earthquake. For example, a study of warning times for the city of San Francisco shows that it is likely that the city would receive more than 20 sec for the most damaging earthquakes (Elarms, 2012). Having had the initial alarm, the system could rapidly detect the initiation of an earthquake, then determine the magnitude and location of the event, consequently predict the peak ground motion expected in the region around the event, and at last issue a warning to people in locations that may expect significant ground motion. The algorithms use data from regional broadband seismic networks. There are other kinds of similar systems for early warning in other parts of the world like Japan.

Therefore, much of the damage and deaths caused by earthquakes will be prevented if early warning given of a destructive earthquake is used appropriately and effectively.

2.8 Summary

In this chapter Seismic Isolation Systems were investigated from ancient seismic protection technics to the state-of-the-art practices. It was concluded that not all proposed techniques were practical. The efficiency of any seismic isolation system should be measured with respect to the three important aspects: reasonable level of isolation; adequate level of damping; and re-centring mechanism. Some isolator devices such as HDRB (High Damping Rubber Bearings) can provide moderate to high level of damping yet because of strain dependent stiffness properties, they are very complex in analysis and providing a structure with torsion and P- Δ moments on top and bottom during an earthquake. Sliding systems, in general, provide a structure with high level of isolation and moderate damping, but the problem of changeable coefficient of friction (sometimes leads to sticking) and high level of structural acceleration when using these types of isolators are yet to resolved. In the lack of a perfect and flawless system, scientists and researchers have been always looking for overcoming these drawbacks and difficulties in design. Therefore, there have been ongoing research on the subject of Seismic Base Isolation either in improving the existing systems or introducing a new system. The present research introduces a new innovative Seismic Isolation system in which the requirements of Seismic Base Isolation are satisfied and at the same time, it overcomes some drawbacks of the current systems.

3 New base isolation system

3.1 Introduction

The new seismic base-isolation system proposed in this study is categorized as Semi-active systems which triggers with alarms of Earthquake Early Warning (EEW) systems. The main feature of the new isolation system is taking the advantages of air bearings. Air bearings provides a thin layer of air between the bottom of device and contacting surface which enables the unit to handle heavy loads with minimum possible friction and hence minimum energy. Utilizing air bearings underneath of a structure in designated points helps in reducing contacts of structure with its base (seismic isolation) at the time of earthquake and therefore, reducing the damage. This needs an appropriate design and simulations before applying on real scale structure.

In this chapter, the principals of seismic isolation is explained and the proposed system is introduced. For better understanding of the performance of the new system, a scaled structure is designed and tested as a case study. The scaled model is designed based on a real scale five-story building and the structural characteristics of the scaled model is based on dimensional analysis and scaling principals. Analytical model of the scaled structure is then presented based on the assumption of “shear building” and the results of “dynamic modal analysis” for fixed base and isolated conditions are discussed at the end.

3.2 Seismic base-isolation principals

In general, base isolation techniques follow two basic approaches. Firstly, the isolation system introduces a layer of low lateral stiffness between a structure and its foundation underneath. This Isolation layer provides the structure with a natural period which is much longer than its fixed-base natural period (Chopra, 2007).

$$\omega = \sqrt{\frac{k}{m}} \quad (3.1)$$

$$T = \frac{2\pi}{\omega} \quad (3.2)$$

Here, ω represents the frequency of vibration, m and k denote mass and lateral stiffness of a structure respectively. The natural period of a structure T , increases by a reduction of lateral stiffness. As shown by the elastic design spectrum of Figure 3-1, this lengthening of period can reduce the acceleration and hence the earthquake-induced forces in a structure, but the deformation is increased. This deformation is concentrated in the isolation system, however, accompanied by only small deformations in the structure (Chopra, 2007).

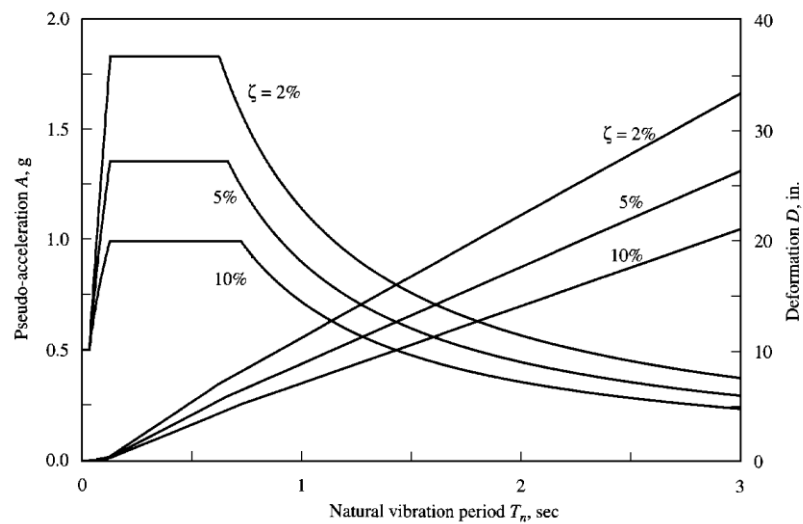


Figure 3-1 Elastic design spectrum, (ξ denotes damping) (Chopra, 2007)

Secondly, damping is beneficial for reducing the effects of accelerations and forces in a structure due to an earthquake. A suitable seismic isolation system can produce a level of acceptable damping.

As a result of reduction in horizontal stiffness of a building at its base in base-isolated structure and increasing the natural damping, the super-structure will remain undamaged or slightly damaged after earth shakes. This is schematically presented in Figure 3-2.

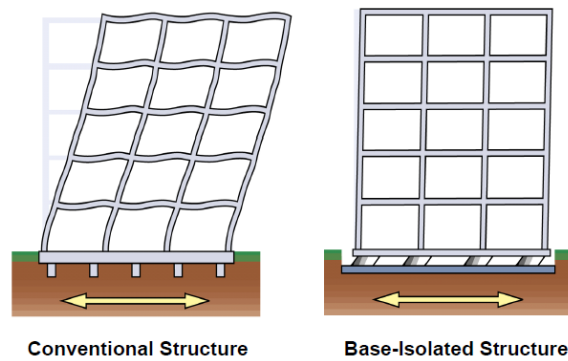


Figure 3-2 Behavior of building structure with base-isolation system

An ideal base-isolation condition is when the ground under a structure is moving and these movements are not transmitted to the structure. If a structure is completely fixed to ground, it means that stiffness k is infinity; hence, fraction k/m has a great value. It means that ω (fundamental circular frequency) is very large (see equations 3.1 and 3.2); therefore fundamental period is near zero. Accordingly, the acceleration induced in the structure as a result of ground movements is equal to the ground acceleration, and likewise relative displacement between the structure and ground underneath is zero.

On the other hand, for an ideal seismically-isolated structure, relative horizontal stiffness is near zero; therefore, fundamental period is infinity; thus, no acceleration induced in the structure and also relative displacement has some values generally less than peak ground displacement.

3.2.1 Horizontal isolation

For investigating seismic base-isolation principal, a single degree of freedom structure is considered (see Figure 3-3); the equation of motion is as follow:

$$m\ddot{u} + c\dot{u} + ku = -m\ddot{u}_g \quad (3.3)$$

Where, m is indicating the mass of the structure, c and k representing damping ratio and stiffness respectively. u is representing the displacement of the structure and u_g is the displacement of the ground, consequently \ddot{u}_g is the ground acceleration during an excitation. This single story building which is not benefited from any additional damping system (c equals zero) is isolated from the ground underneath by means of a set of flexible rubber bearings as it is shown in Figure 3-3.

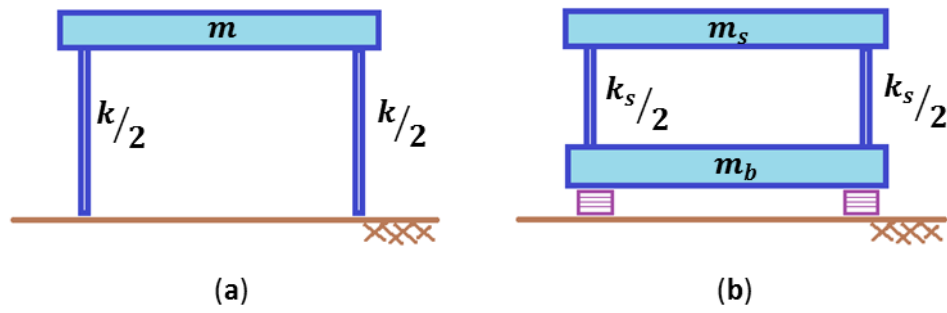


Figure 3-3 (a) fixed base and (b) isolated structures

A rigid diaphragm of mass m_b is added to connect bearings. Each bearing has the horizontal stiffness of $k_b/2$. The idealized two degrees of freedom (2DOFs) mass-spring model can be drawn as Figure 3-4. Therefore the governing equation of motion changes as equations (3.4) (Chopra, 2007).

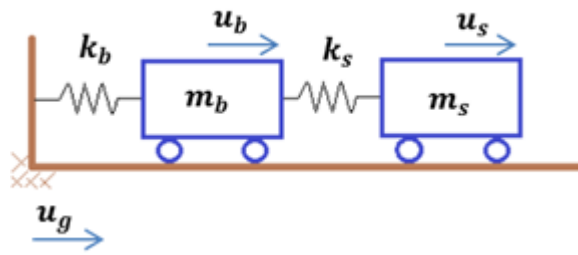


Figure 3-4 Idealized mass-spring model of 2DOFs structure

$$\begin{bmatrix} m_b & 0 \\ 0 & m_s \end{bmatrix} \begin{bmatrix} \ddot{u}_b \\ \ddot{u}_s \end{bmatrix} + \begin{bmatrix} k_b + k_s & -k_s \\ -k_s & k_s \end{bmatrix} \begin{bmatrix} u_b \\ u_s \end{bmatrix} = \begin{bmatrix} m_b & 0 \\ 0 & m_s \end{bmatrix} \begin{bmatrix} 1 \\ 0 \end{bmatrix} \ddot{u}_g \quad (3.4a)$$

$$\begin{bmatrix} m_b & 0 \\ 0 & m_s \end{bmatrix} \begin{bmatrix} \ddot{u}_b \\ \ddot{u}_s \end{bmatrix} + \begin{bmatrix} k_b + k_s & -k_s \\ -k_s & k_s \end{bmatrix} \begin{bmatrix} u_b \\ u_s \end{bmatrix} = \begin{bmatrix} k_b u_g \\ 0 \end{bmatrix} \quad (3.4b)$$

Where u_b and u_s are representing displacement of base-mass (m_b) and mass of the structure (m_s) respectively. Equation (3.4b) represents the equation of motion with respect to ground displacement (u_g). The total mass of the structure m is defined as follow:

$$m = m_b + m_s \quad (3.5)$$

Therefore, nominal frequencies are defined as (3.6).

$$\omega_b = \sqrt{\frac{k_b}{m_b + m_s}} \quad , \quad \omega_s = \sqrt{\frac{k_s}{m_s}} \quad (3.6)$$

Expanding the first line of equation of motion (3.4b) gives:

$$m_b \ddot{u}_b + (k_b + k_s)u_b - k_s u_s = k_b u_g \quad (3.7a)$$

$$m_b \ddot{u}_b + k_b u_b + k_s(u_b - u_s) = k_b u_g \quad (3.7b)$$

Definition of x_b and x_s as relative displacement of base-mass and super-structure respectively:

$$x_b = u_b - u_g \quad (3.8a)$$

$$x_s = u_s - u_g \quad (3.8b)$$

and replacing in equation (3.7b), changes the first line of equation of motion as (3.9)

$$m_b \ddot{u}_b + k_b(x_b + u_g) + k_s(x_b - x_s) = k_b u_g \quad (3.9)$$

which is simplified to (3.10)

$$m_b \ddot{u}_b + k_b x_b + k_s x_b - k_s x_s = 0 \quad (3.10)$$

Considering the special case when m_b is very small (near zero), equation (3.10) can be written as (3.11) (Ismail, 2009).

$$k_b x_b + k_s x_b - k_s x_s = 0 \quad (3.11)$$

Solving for x_b in terms of x_s gives

$$x_b = \frac{k_s}{k_s + k_b} x_s \quad (3.12)$$

It is obvious from (3.12) that for a perfect isolated system, where k_b is near zero, x_s and x_b will have the same value and this means that the structural system acts as a rigid body.

The second line of matrix equation (3.4b) is expanded as follow:

$$m_s \ddot{u}_s - k_s u_b + k_s u_s = 0 \quad (3.13)$$

Expanding with respect to equations (3.8):

$$m_s (\ddot{x}_s + \ddot{u}_g) - k_s u_b + k_s (x_s + u_g) = 0 \quad (3.14a)$$

$$m_s \ddot{x}_s + k_s x_s + k_s (u_g - u_b) = -m_s \ddot{u}_g \quad (3.14b)$$

$$m_s \ddot{x}_s + k_s x_s - k_s x_b = -m_s \ddot{u}_g \quad (3.14c)$$

It then follows from substituting (3.12) into (3.14c) that

$$m_s \ddot{x}_s + k_s x_s - k_s \frac{k_s}{k_s + k_b} x_s = -m_s \ddot{u}_g \quad (3.15a)$$

$$m_s \ddot{x}_s + k_s x_s \left(1 - \frac{k_s}{k_s + k_b}\right) = -m_s \ddot{u}_g \quad (3.15b)$$

Thus, the natural frequency of vibration for isolated structure is defined as (3.16):

$$\omega_b = \sqrt{\left(1 - \frac{k_s}{k_s + k_b}\right) \frac{k_s}{m_s}} \quad (3.16)$$

Where $\sqrt{\frac{k_s}{m_s}}$ is representing the natural frequency of fixed-base structure. Now the concepts of period shifting could be understood. The natural period of vibration can be defined as (3.17):

$$T_b = \frac{2\pi}{\omega_b} \quad (3.17a)$$

$$T_b = \frac{2\pi}{\sqrt{\left(1 - \frac{k_s}{k_s + k_b}\right) \frac{k_s}{m_s}}} \quad (3.17b)$$

Where, T_b is the natural period of vibration of the isolated structure. The natural period of vibration of fixed-base structure is defined by

$$T_s = \frac{2\pi}{\omega_s} = \frac{2\pi}{\sqrt{\frac{k_s}{m_s}}} \quad (3.18)$$

Therefore, T_b can be defined as a multiple of T_s :

$$T_b = \frac{2\pi}{\sqrt{\left(1 - \frac{k_s}{k_s + k_b}\right) \frac{k_s}{m_s}}} = \frac{1}{\sqrt{\left(1 - \frac{k_s}{k_s + k_b}\right) \frac{k_s}{m_s}}} \frac{2\pi}{\sqrt{\frac{k_s}{m_s}}} \quad (3.19a)$$

$$T_b = \frac{1}{\sqrt{\left(1 - \frac{k_s}{k_s + k_b}\right)}} T_s = C_p T_s \quad (3.19b)$$

Where C_p defined as *base isolated natural period coefficient*.

For a perfectly fixed-base condition k_b is infinity so, T_b equals T_s . When k_b is much greater than k_s , then again T_b approaches the natural period of fixed-base condition. In a perfectly base-isolated structure, it is assumed that k_b is near zero, so T_b is a large multiple of T_s ; it means that the structure will not experience any shocks from ground underneath and the structure acts as a rigid body (no inter-story drifts). For base-isolation purposes, designers tend to reduce the ratio of horizontal stiffness of isolators over stiffness of super-structure, hence, the natural period of the structure will be shifted to a much greater one in practice. This will benefits the structure in terms of reducing the acceleration transmitted to the structure and also damage alleviations. Effects of period shifting in reducing the acceleration experienced by the structure is shown in Figure 3-5.

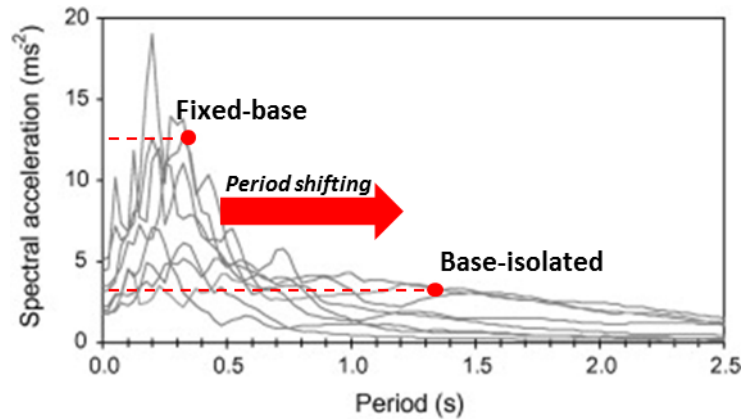


Figure 3-5 Effects of period shifting in acceleration mitigation

When the fundamental period (also known as natural period of vibration) of a structure is shifted to a greater one far from the fundamental period of possible shocks, the structure is highly likely rescued from resonance phenomenon. The frequency in which resonance happens is also known as resonance frequency. If the structure is driven by a kind of external dynamic force such as earthquake with a frequency near to its natural frequency of vibration, resonance happens. In small damping resonance frequency and natural frequency are approximately the same and equal to a frequency of unforced vibrations. In practice, resonating vibrations can cause terrific stress and rapid failure of structural members (Hibbeler, 2002). Thus, it is important to design a structure with a fundamental frequency far from the frequency of possible shocks. Seismic base isolation can provide a reasonable gap between the fundamental frequency of isolated structure and possible earthquake frequencies.

3.2.2 Damping

Damping is beneficial in reducing the effects of earthquakes on a structure. An appropriate base isolation system is the one which offers reasonable levels of damping. Considering mass-spring model of Figure 3-4 with damping properties, the effect of damping on an isolated structure is determined.

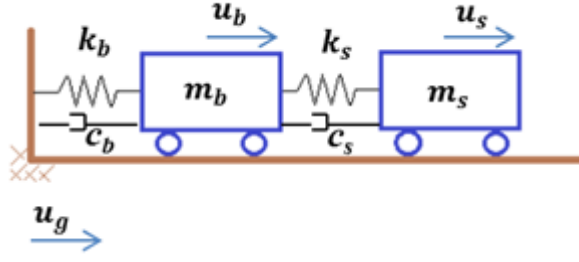


Figure 3-6 Mass-spring model with damping

Recalling the general equation of motion (3.3) and add damping terms into matrices form of equation of motion (3.4a), this equation with respect to damping is rewritten as follow:

$$\begin{bmatrix} m_b & 0 \\ 0 & m_s \end{bmatrix} \begin{bmatrix} \ddot{u}_b \\ \ddot{u}_s \end{bmatrix} + \begin{bmatrix} c_b + c_s & -c_s \\ -c_s & c_s \end{bmatrix} \begin{bmatrix} \dot{u}_b \\ \dot{u}_s \end{bmatrix} + \begin{bmatrix} k_b + k_s & -k_s \\ -k_s & k_s \end{bmatrix} \begin{bmatrix} u_b \\ u_s \end{bmatrix} = \begin{bmatrix} m_b & 0 \\ 0 & m_s \end{bmatrix} \begin{bmatrix} 1 \\ 0 \end{bmatrix} \ddot{u}_g \quad (3.12)$$

Where, \dot{u}_b and \dot{u}_s corresponds to the velocity of the base-mass and mass of the structure, respectively. c_b and c_s are viscous damping of the isolation system and super structure, respectively.

At this stage it is necessary to define the nature of isolation system. For example if sliding isolation system is considered, the following assumptions are applied (De Silva, 2007):

$$f_r = k_b(u_b - u_{b0}) \quad \text{non - sliding phase} \quad (3.13a)$$

$$f_r = \pm \mu(m_b + m_s)g \quad \text{sliding phase} \quad (3.13b)$$

Where,

f_r is frictional force,

k_b is isolation system stiffness,

u_{b0} is initial elongation of the fictitious spring in the current non-sliding phase,

μ is the coefficient of friction,

g is the acceleration of gravity.

This will add a new term relating to friction force to equation 3.12 as

$$\begin{aligned} \begin{bmatrix} m_b & 0 \\ 0 & m_s \end{bmatrix} \begin{bmatrix} \ddot{u}_b \\ \ddot{u}_s \end{bmatrix} + \begin{bmatrix} c_b + c_s & -c_s \\ -c_s & c_s \end{bmatrix} \begin{bmatrix} \dot{u}_b \\ \dot{u}_s \end{bmatrix} + \begin{bmatrix} k_b + k_s & -k_s \\ -k_s & k_s \end{bmatrix} \begin{bmatrix} u_b \\ u_s \end{bmatrix} + \begin{bmatrix} f_r \\ 0 \end{bmatrix} \\ = \begin{bmatrix} m_b & 0 \\ 0 & m_s \end{bmatrix} \begin{bmatrix} 1 \\ 0 \end{bmatrix} \ddot{u}_g \end{aligned} \quad (3.14)$$

Applying equation 3.13b in 3.14, the equation of motion of base mass is derived as follow:

$$m_b \ddot{u}_b + c_b \dot{u}_b + k_b u_b + \mu(m_b + m_s)g \cdot \text{sgn}(\dot{u}_b) + c_s \dot{u}_s + k_s u_s = m_b \ddot{u}_g \quad (3.15)$$

Basically, the damping properties of a superstructure (c_s) is not known explicitly. It can be constructed by assumptions in modal damping for each mode of vibration. However, viscous damping of an isolation system is defined as below (Jangid, 1996):

$$c_b = 2\xi_b M \omega_b \quad (3.16)$$

Where,

ξ_b is damping ratio of the isolation system,

ω_b is base isolation frequency.

Equation 3.15 which governs the motion of base mass is non-linear due to the presence of friction term. The equivalent linear equation obtained by utilizing the time-dependent equivalent linearization technique (Jangid, 1996) is

$$m_b \ddot{u}_b + c_e \dot{u}_b + k_b u_b + c_s \dot{u}_s + k_s u_s = m_b \ddot{u}_g \quad (3.17)$$

Where,

c_e is equivalent damping and defined as

$$c_e = c_b + \frac{\sqrt{\frac{2}{\pi}} \mu M g}{\sigma_{v_b}} \quad (3.18)$$

σ_{v_b} is the Root-mean-square (RMS) velocity of base mass.

More information about optimum level of damping for an isolation system could be found in (Jangid, 1996).

Having known the equation of motions (3.12 and 3.14) it is possible to construct the response spectra with respect to damping for a specific earthquake (Figure 3-1). By keeping the period of vibration, T , constant and changing the damping ratio, ξ ; and again repeat the procedure by keeping the damping ratio, ξ , constant and changing the period of vibration, T , *displacement response spectra* and *pseudo-acceleration response spectra* under a given earthquake are constructed. Acceleration response spectra correspond to the base shear; the more the base shear the more damage is expected in the structure at the time of earthquake. These are schematically presented in Figure 3-7 and Figure 3-8.

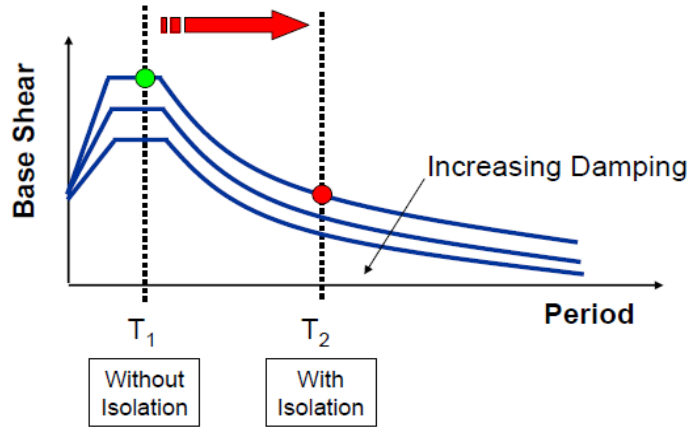


Figure 3-7 Increase in period of vibration reduces the base shear (Symans, 2004)

Figure 3-7 shows a typical acceleration design response spectra for different damping levels. Increase in natural period of the structure reduces the acceleration and thus base shear (force demand) on the structure.

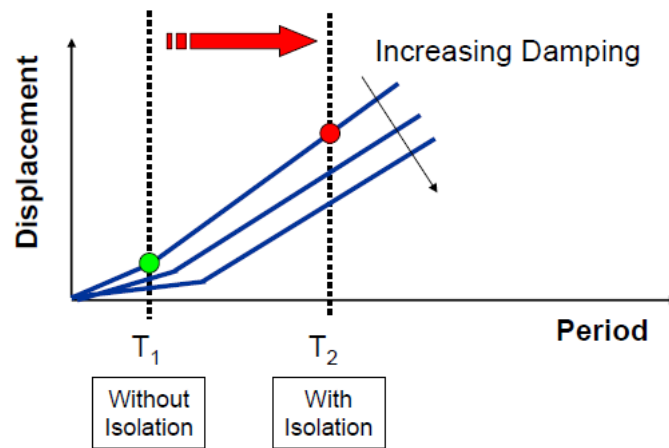


Figure 3-8 Increase in period increases displacement (Symans, 2004)

Figure 3-8 corresponds to the typical displacement design response spectra for different damping levels. As it is shown, an increase in natural period increases the displacement demand in a structure. Although, the displacement demand will be partially removed from a super structure to an isolation system. The isolation system will reflect the input energy away from the super structure. The input energy which is transmitted to the structure will be dissipated by means of energy dissipation mechanism of the isolation system. Therefore, when the isolation system has a reasonable level of damping, it reduces the displacement demand in the structure. It is clear from Figure 3-8 that a structure with a longer natural period has more displacement response when subject to an earthquake. In order to reduce the effect of shifting the natural period to a greater one it is necessary to produce a higher level of damping by the isolation system. By increasing the total damping ratio of the structure, not just the displacement response is reduced significantly (Figure 3-8), the acceleration response is also reduced to a lower level (Figure 3-7).

To sum up, the main responsibility of an isolation system is to shift the natural period of a structure away from the dominant frequency range of expected earthquake and to input more level of damping to the structure.

3.3 Innovative isolation system using air bearing

So far there has not been an ideal isolation system to separate the structure from its base at the time of earthquake with no negative effects. As it was discussed before, the perfect isolation system is the one which isolates a structure from ground shocks completely which, however, is almost impossible with respect to the weight of a structure and uncertainty in the position of the structure after earthquake shocks. The main idea behind the design of an innovative system in this research is to separate the structure from horizontal movements of the ground at the time of earthquake with help of air-bearing solutions. Commercial use of air-bearing technology shows that it is possible to handle loads up to around 5000 metric tons thanks to the modular design of air caster system (Aerogo, 2015) (Airfloat, 2015) (Solving, 2015); whereas a typical weight for building in total is around 1000 kg per meter square including super imposed load (Monfared, et al., 2013). Therefore, it is possible to handle a five story building with 100 meter square area of each floor with existing technology. Indeed, the application of air-bearing technology is underneath of selected columns with less vertical load to carry, as the newly proposed isolation system is not going to handle the whole weight of a building. This innovative isolation system is a combination of air-bearing devices with a re-centring mechanism which can add some additional damping. The re-centring mechanism can be provided by one of the existing technologies such as sliding system in real scale. In this research a simplified method of adding ball bearings and bungee cords are employed for providing the structure with re-centring mechanism.

The air-bearing devices become active just before the main shocks of earthquake arrive. And after the main earthquake shocks have gone and the building returns to its original position the air bearings go off and the building rests. The *earthquake early warning system* (EEW) will notify the building sensors if the main shocks seems to be greater than the designated limit and hence air bearings start to work and isolate the building from horizontal movements of the ground. Otherwise, for example in reaction to small shocks or winds the air bearings are inactive. This limit is set in the design prior to construction and with respect to the importance of the building, seismic performance constraint and structural conditions (Figure 3-9).

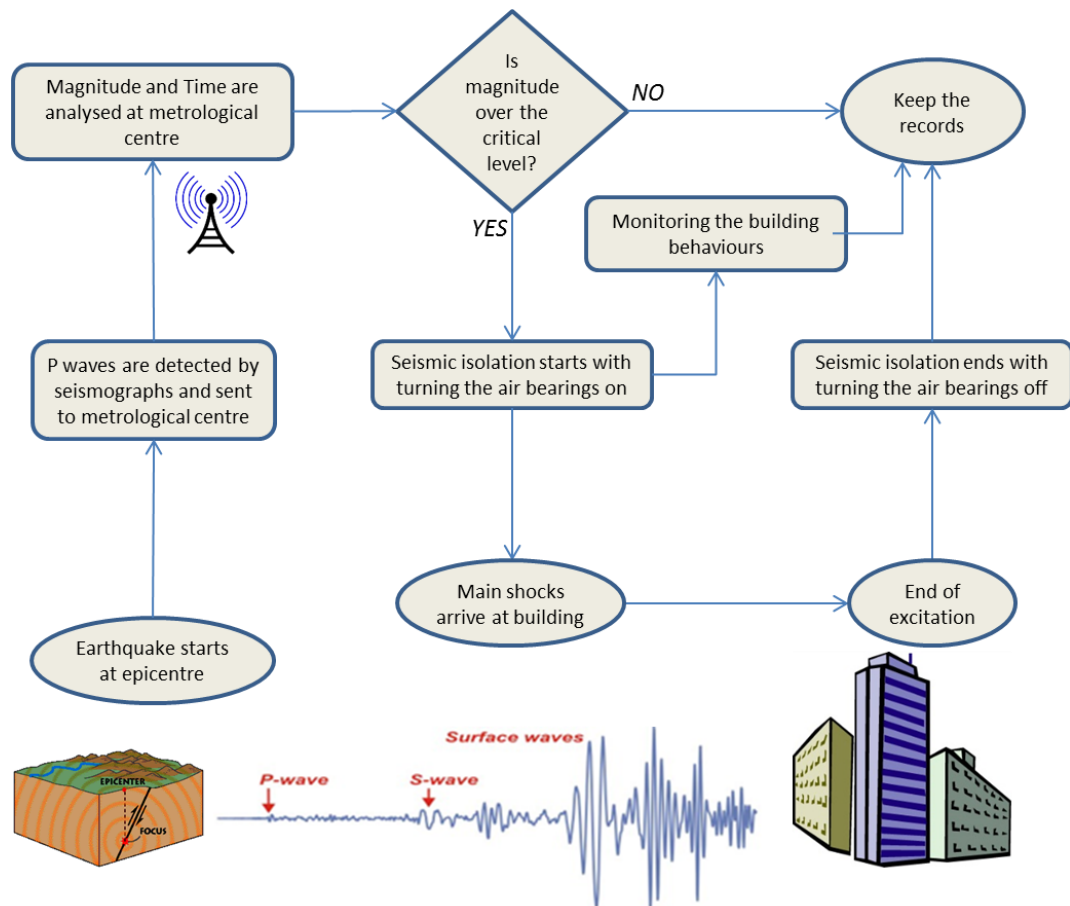


Figure 3-9 The proposed seismic isolation system works with earthquake early warning system

Firstly, seismographs detect primary waves, and then this information is transmitted to the National Meteorological Agency (NMA). At metrological centre earthquake likely intensity and estimated time of arrival at a particular place are analysed using the information of the seismographs (by detecting P wave energy). Finally EEW is transmitted from the NMA to a particular building with proposed seismic isolation system. In the building the magnitude and time of arrival of the main shocks are analysed by computer programme and it is decided if the building needs to be isolated. If it is needed, the air bearings start to work, otherwise (if the magnitude is small or there is not enough time for proper operation) the air bearings do not start working. Fortunately, EEW systems are operated and used in many earthquake prone areas of the world (e.g. Japan and California). These systems can provide a few tens of seconds warning prior to damaging ground motions. The amount of time for early warning depends on the distance from the epicentre of the earthquake which could take seconds to minutes. The warning message can be transmitted instantly, while the shaking waves from the

earthquake focus travel through the shallow layers of the Earth at speeds of one to a few kilometers per second (USGS, 2015). This time is long enough for air bearings to operate as the existing technology needs a few seconds for full operation (Aerogo, 2015).

3.4 Case study

In order to investigate the new system for seismic isolation, a five-story ordinary building made up of steel structure with 48 m² area for each story is considered as a case study (Figure 3-10). For better understanding of how the new isolation system works, a 1/10th scaled model of case study was designed based on scaling principals and dimensional analysis. The building was designed based on real sizes and then the parameters were scaled accordingly.

After determining the dimensions of real scale building, scaling relations in terms of geometric scaling factor (λ) need to be worked out. In this case the scaling factor equals to 1/10. This scaling factor is chosen with respect to the purpose of the study and facilities available.

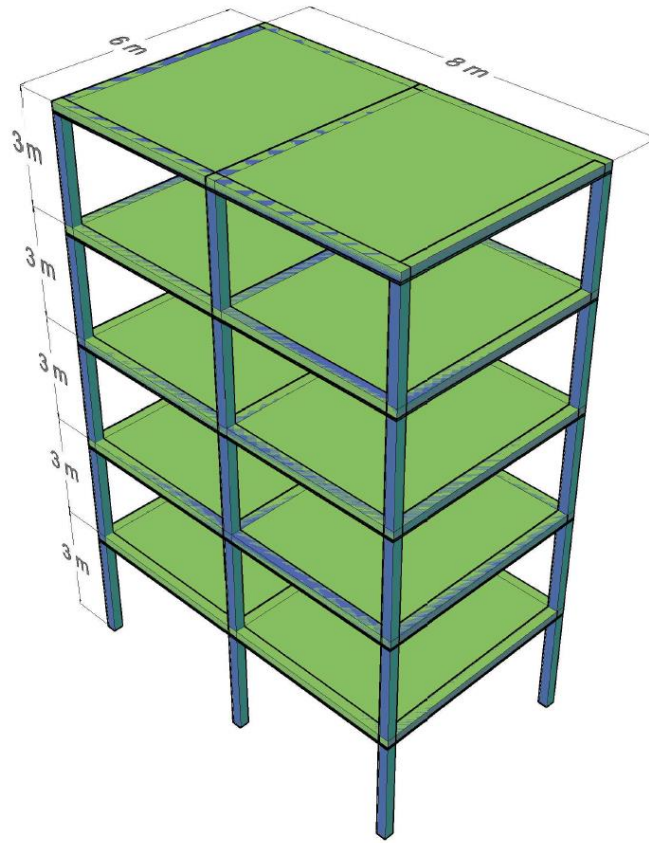


Figure 3-10 Schematic view of the case study in real scale

3.4.1 Scaling procedure

As the geometric scaling factor is set to $1/10^{\text{th}}$ the other parameters can be worked out accordingly. The analysis starts from scaling the mass of each floor. The approximate mass for each story of a real building in this size is 40 metric tonnes or 40,000 kg. As the scale factor for length is 0.1 and the scale factor for acceleration and mass density is considered as 1 (the same material) the dimensional analysis shall be as follow:

λ scale factor in length = $1/10$

L real length

l scaled length

M real mass

m scaled mass

A real acceleration

a scaled acceleration

D real density

d scaled density

T real time

t scaled time

$$l/L = \lambda = 1/10$$

$$d/D = 1 \text{ (same material)}$$

$$D \sim ML^{-3}$$

$$d/D = ml^{-3}/ML^{-3} = 1$$

$$m/M = L^{-3}/l^{-3} = (L/l)^{-3} = (1/\lambda)^{-3} = 10^{-3} = 1/1000$$

thus, mass scaling factor is λ^3 or $1/1000$.

Which determines 40kg of mass for each story.

The same procedure shall be followed in order to work out the scale factor for time and the period of the scaled structure.

$$A \sim LT^{-2}$$

Therefore,

$$a/A = lt^2/LT^2 = 1$$

$$t^2/T^2 = L/l = 1/\lambda = 10$$

$$(t/T)^2 = 10$$

$$t/T = 10^{-1/2} = 1/\sqrt{10} = 1/3.162 = 0.316$$

Same procedure shall be considered in order to work out other parameters scale factor as follow:

Table 3-1 Scaling relations in terms of geometric scaling factor

Parameter	Scaling relations	Factor for 1/10 th scale
Mass Density	1	1
Acceleration	1	1
Length	λ	1/10
Mass	λ^3	1/1000
Force	λ^3	1/1000
Time	$\lambda^{1/2}$	0.316
Frequency	$\lambda^{-1/2}$	3.162
Stress	λ	1/10
Stiffness	λ^2	1/100

3.5 Scaled model strucutre

Having found the scaled factors for required parameters, it is possible to design and build the scaled model. With respect to facilities available at the workshop the geometric scaling factor was chosen as 1/10th which has governed other scale factors. The scaled model built in the workshop is shown in Figure 3-11. The dimensions of the scaled model are shown in Figure 3-12. The structural system of the model is *moment frame* with rigid connections (structural members can take shear and axial forces as well as bending moments).



Figure 3-11 Scaled model structure built in the workshop

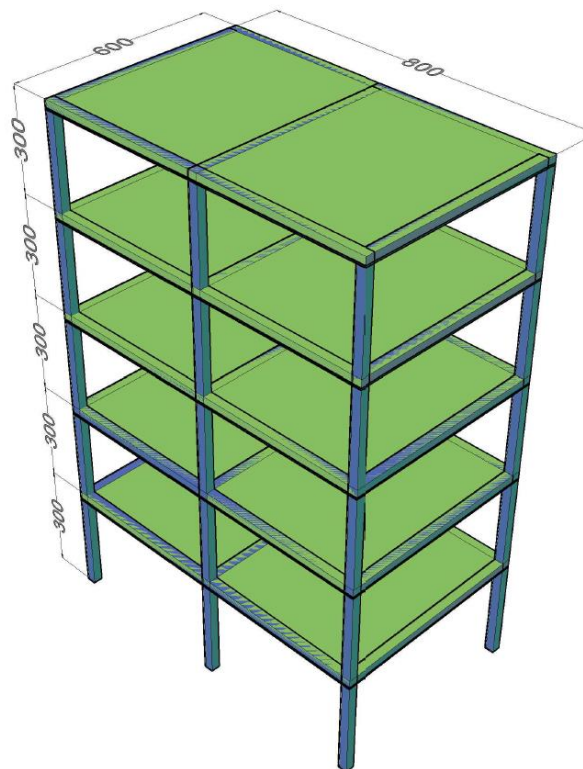


Figure 3-12 Scaled model dimensions (mm)

3.5.1 Mechanical characteristics of the scaled model

Mass: mass of the structure is the most important parameter after physical dimensions which has to be considered for scaling. As the typical mass of each story in real scale building is considered as 40,000 kg and the scale factor for mass is 1/1000 the mass of each story in scaled physical model is calculated as 40 kg. With respect to the materials used for building the structure the selection of materials and their weights are as follow:

5 kg steel works

10 kg wood works

25 kg concrete

Lateral stiffness: lateral stiffness of the structure is the next significant parameter in determining structure's dynamic characteristics. For a real scale structure of mentioned size (Figure 3-10) total lateral stiffness of each story is between 4600 and 4900 N/mm (Monfared, et al., 2013). According to the calculated scaling factor for stiffness (1/100), lateral stiffness of each story in scaled model is 460 to 490 N/mm. The lateral stiffness of stories has been examined through controlled tests in the workshop (Figure 3-13)

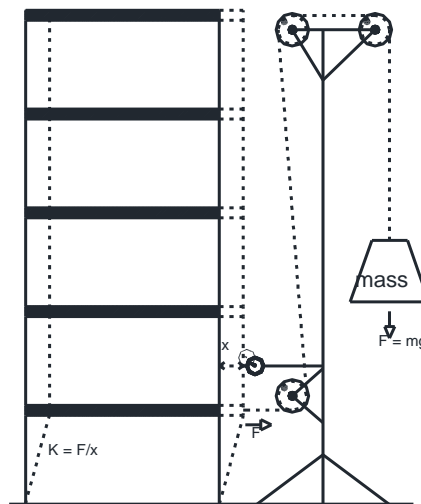


Figure 3-13 Lateral stiffness test diagram

Table 3-2 Results of lateral stiffness test

Force (N)	Measured Displacements (mm)	Mean Stiffness (N/mm)
10x9.81	0.22, 0.21, 0.19, 0.23	461.65
15x9.81	0.30, 0.31, 0.32, 0.30	474.68
20x9.81	0.40, 0.41, 0.42, 0.41	478.53
25x9.81	0.51, 0.54, 0.54, 0.53	462.74
Mean Lateral Stiffness Value (N/mm)		469.4

According to predicted values (460 to 490 N/mm) the mean stiffness value (469.4 N/mm) obtained from experiment is acceptable and used in analytical model.

Fundamental frequency and period: as it was discussed earlier in this chapter, the main purpose of seismic isolation is to shift the fundamental frequency of vibration to a smaller one. Therefore, fundamental frequency and corresponding period of vibration of the structure should be known. The fundamental frequency of vibration of the real building in this study is between 1.536 and 1.73 Hz and according to the scaling factor of $1/10^{0.5}$, the fundamental period of the scaled model is predicted between 4.857 and 5.47 Hz.

Prediction of mechanical characteristics of the scaled model is presented in Table 3-3.

Table 3-3 Prediction of scaled model mechanical characteristics based on scaling factors

Scaling	Real Building	1/10 Scaled model
Each Story Mass (kg)	40000	40
Lateral Stiffness (N/mm)	4600 to 4900	460 to 490
Natural Frequency (Hz)	1.536 to 1.73	4.857 to 5.47
Natural Period (s)	0.578 to 0.651	0.183 to 0.206

The dynamic characteristics of the scaled model based on laboratory tests are discussed in chapter 5.

3.5.2 Isolation system for scaled model

The isolation system for the scaled model is designed to resist the vertical loads and to isolate the structure from its base to a certain levels with capability of re-entering after shocks due to horizontal movements of base. Air-bearing solution is chosen for the purpose of isolation of the scaled model and it is used at two points underneath of the ground floor columns. In order to provide smallest level of contact between the structure and its base ball bearings are used underneath of other four columns (Figure 3-14) (Figure 3-15).

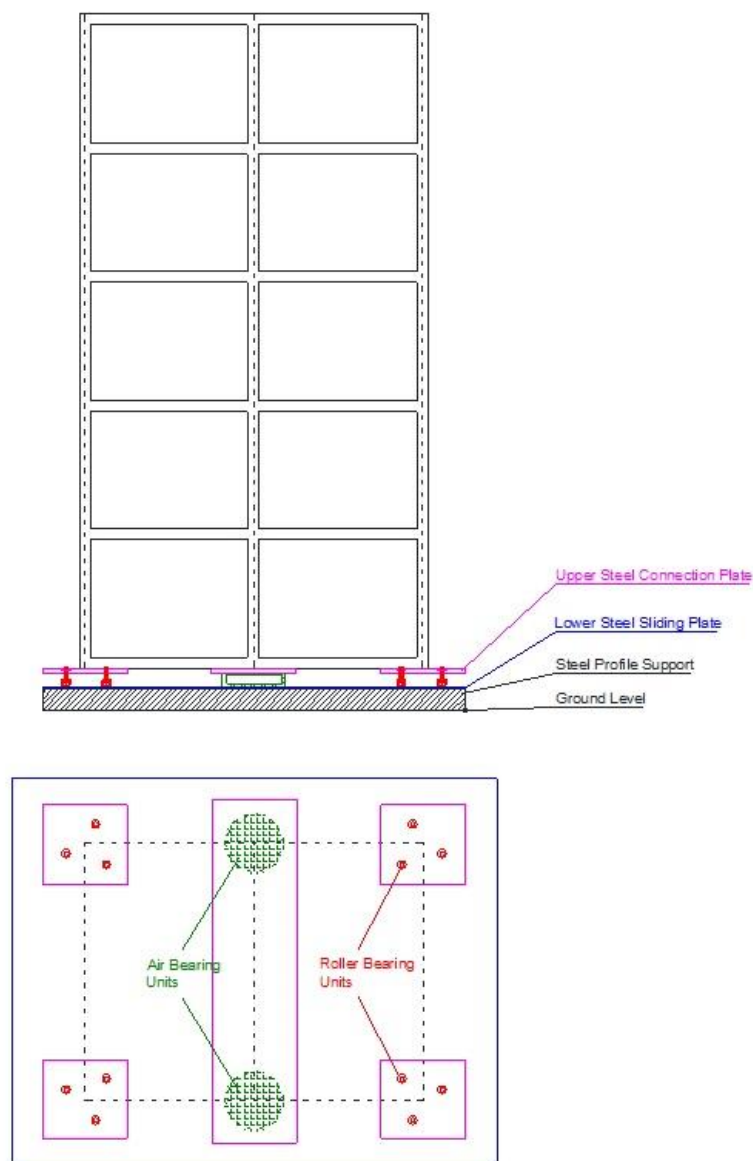


Figure 3-14 Isolation system for scaled model

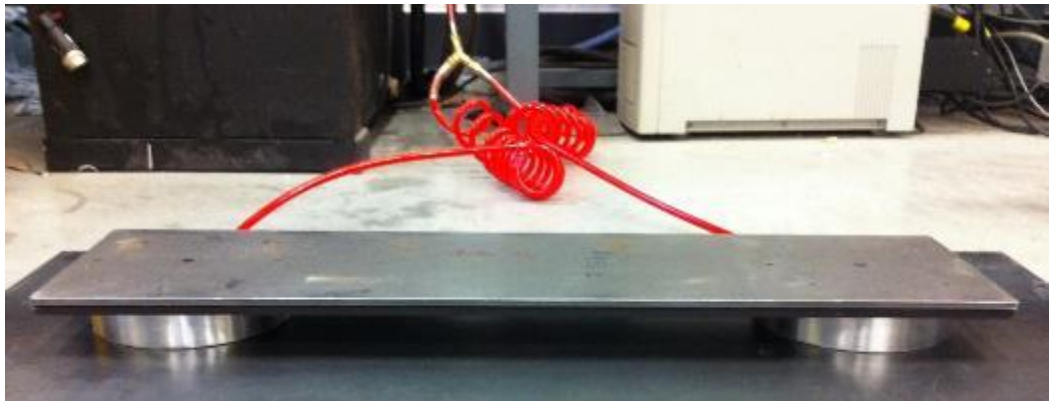


Figure 3-15 The air-bearing pallet to be installed underneath of the structure

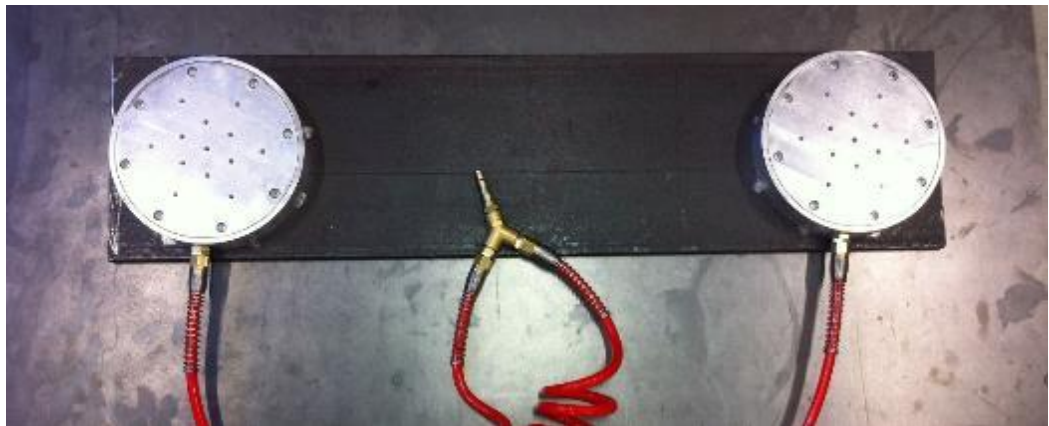


Figure 3-16 Beneath view of the air-bearing pallet



Figure 3-17 Beneath view of ball-bearing pallet

The steel sheet underneath of the isolation system is to provide minimum friction for ball bearings' movement as well as provide a smooth surface for air-bearings in operation (Figure 3-18). The air-bearing device design and specifications are fully discussed in chapter 4. The specifications of ball bearings used for the isolation system is given in appendix A.3 Roller bearing specifications.

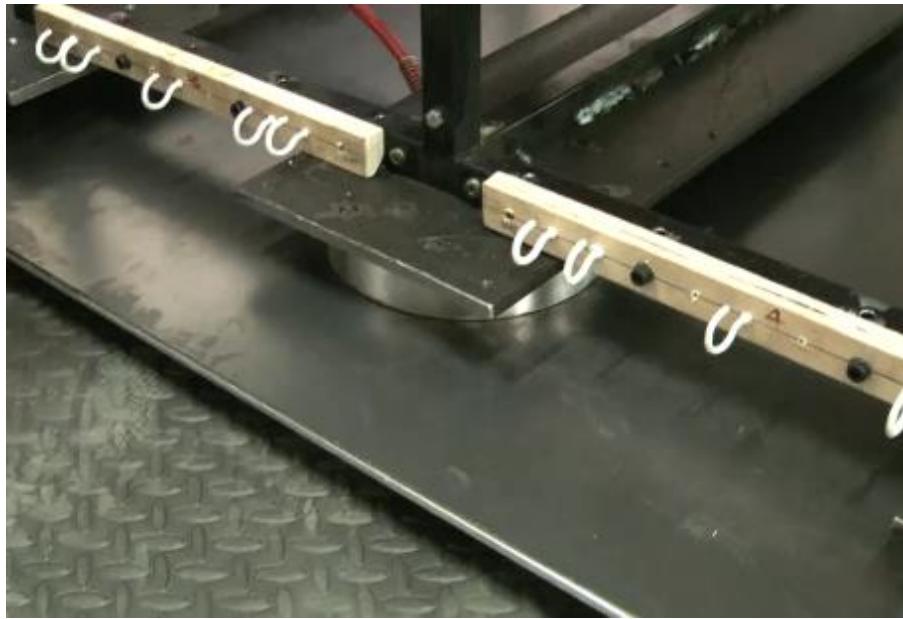


Figure 3-18 Air bearings installed underneath of the scaled model

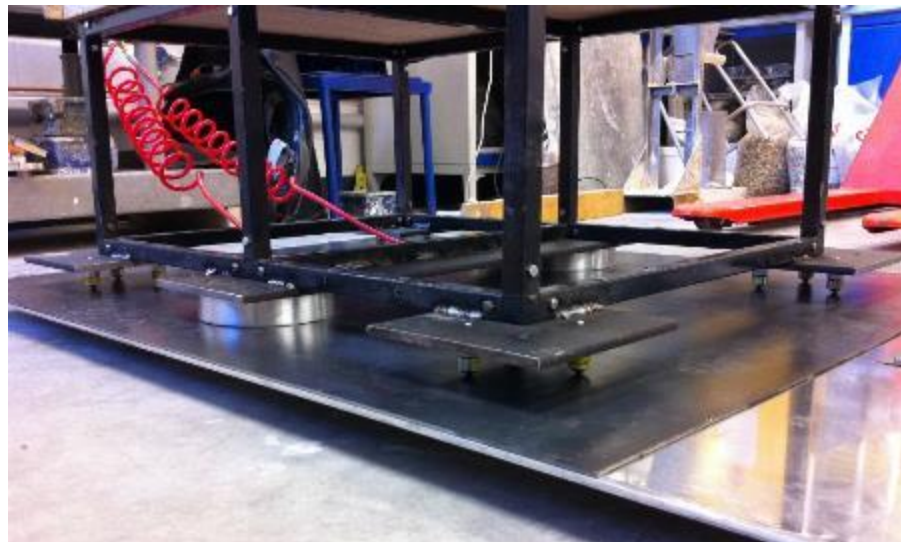


Figure 3-19 Air bearings and ball bearings installed underneath of the structure

In order to provide a suitable re-centring mechanism for proposed isolation system, bungee cords are selected, carefully measured for stiffness and used in the isolation

system for scaled model (Figure 3-20). As one of the advantages of the new system, with changing in the number of bungee cords, different stiffness values are obtained. Thus, it is possible to define different fundamental periods associated to the isolated structure.

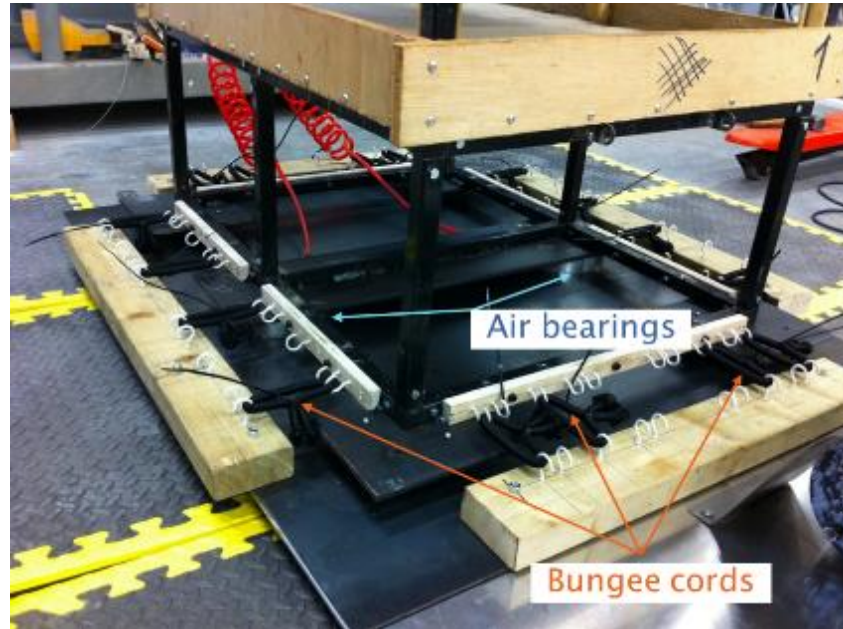


Figure 3-20 Isolation system for scaled model using bungee cords for re-centring

3.6 Analytical model of the scaled structure

An analytical model of the structure is comprised of a set of structural members includes structural floors (for mass definition), structural columns (for lateral stiffness definition) and structural foundation (fixed base or isolated). The analytical structural model of the scaled structure is shown in Figure 3-21. The analysis of structure is further simplified by assuming the structure as *shear building*.

The simplified model of the structure is obtained by assuming that all of the structural mass is lumped at the floor levels and the floor beams are rigid, whereas, the columns are axially rigid. These assumptions, along with assuming analysis just for one horizontal direction at a time, allow for the generation of a model of structure called shear-type building model. Therefore, displacements at each floor (or lumped mass)

level shall be described by one degree-of-freedom alone. Hence, only five degrees of freedom are needed to describe total displacements of the structure.

A structural system is supposed to have an infinite number of natural frequencies, however, if the lumped mass approach (shear-type building) is used, the number of natural frequencies reduced to a finite number corresponding to the number of lumped mass or degrees of freedom.

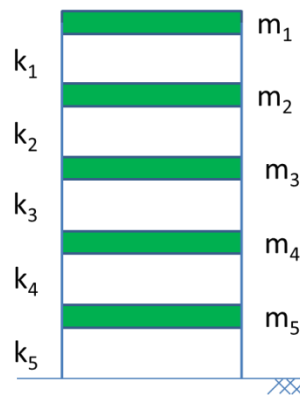


Figure 3-21 analytical model of the structure (fixed-base conditions)

3.6.1 Modal analysis

The analytical model is generated to find out the dynamic characteristics of the structure. Natural frequencies and periods of vibration are of interest in many engineering applications especially when seismic isolation is considered. *Modal Analysis* is widely accepted as a common type of dynamic analysis which is also referred to as an *eigenvalue analysis*.

Mode shapes of vibration which arise at the fundamental or natural frequencies are also discovered in addition to the frequencies. Mode shapes involve dimensionless representations of the shape that the structure experiences while vibrating at a particular frequency. This specific frequency is known as the *corresponding natural frequency* of the mode shape. These are known as the *undamped free vibration response* of the structure due to an initial disturbance (displacement or force) from the equilibrium position.

The solution derives from the general equation of motion (equation 3.3) by zeroing the damping and applied force terms as (Clough & Penzien, 2003)

$$M\ddot{U}(t) + KU(t) = \{0\} \quad (3.19)$$

In this equation M and K are mass and stiffness matrices respectively. $U(t)$ defines the displacement function.

Afterward, it is assumed that each node (lumped mass) is subjected to a sinusoidal functions of the peak amplitude for that node. If the displacement vector $U(t)$ has the following form:

$$U(t) = \emptyset \sin \omega t \quad (3.20)$$

which gives

$$\ddot{U}(t) = -\omega^2 \emptyset \sin \omega t \quad (3.21)$$

where \emptyset is the amplitude of displacement for each node and ω is the frequency of vibration, substituting equations 3.20 and 3.21 in equation 3.19 gives the eigenvalue equation as

$$K\emptyset - \omega^2 M\emptyset = \{0\} \quad (3.22)$$

Which has n solutions for n degrees of freedom corresponding to the structure. For a five-degree-of-freedom structure (the case study in this research) the total number of eigenvalues or natural frequencies is equal to five.

ω_i = natural frequencies ($i=1-5$)

$$\emptyset_i = \begin{pmatrix} \emptyset_{1,i} \\ \emptyset_{2,i} \\ \emptyset_{3,i} \\ \emptyset_{4,i} \\ \emptyset_{5,i} \end{pmatrix} = \text{natural mode shape of } i\text{th frequency}$$

Each eigenvalue or frequency has a corresponding eigenvector or mode shape. Since each of the eigenvectors cannot be null vectors, the eigenvalues are the roots of the following equation:

$$\det(K - \omega^2 M) = 0 \quad (3.23)$$

Having found the eigenvalues, the eigenvector corresponding to a specific mode shapes (and specific eigenvalue ω_i^2) is calculated as follow:

$$(-M^{-1}K)\phi_i - \omega_i^2 M\phi_i = 0 \quad (i = 1, 2, 3, \dots, n) \quad (3.24)$$

There will be a set of n equations and n unknowns - identical to ϕ_i elements - for an n degree-of-freedom system. Each eigenvector represents a mode shape which is unique in shape, but not in value (i.e. the mode shape vector for each mode does not have unique values). It may be scaled to any set of values, yet the relationship of one shape component to any other will be unique.

The *eigenvector matrix* ϕ is an $n \times n$ matrix where n is the number of degrees of freedom of the structure. The importance of eigenvector matrix is that it is utilized in computation of the *modal mass matrix* and subsequently *modal participation factor*. Modal participation factor is used to find the values of *effective masses* which expresses the importance of each mode in vibration (i.e. knowing which mode could be readily excited by base excitation).

For establishing modal participation factor it is necessary to define some other parameters as follow:

Generalized mass matrix: is an identity matrix defined as follow when the generalized-coordinate modal vectors are normalized (Clough & Penzien, 2003):

$$\hat{m} = \phi^T M \phi = I_n \quad (3.25)$$

Generalized mass matrix will not be an identity matrix, if the modal vector matrix is not normalized. However, non-diagonal elements have values very close to zero.

Influence vector: represents the displacements of the masses as a result of a unit displacement of ground. In case of a shear building this will be a unit vector:

$$\bar{r} = \begin{bmatrix} 1 \\ \vdots \\ 1 \end{bmatrix} \quad (3.26)$$

Coefficient vector: is a vector which defined as

$$\bar{L} = \Phi^T M \bar{r} \quad (3.27)$$

And subsequently, the modal participation factor Γ_i corresponding to i th mode is (Clough & Penzien, 2003)

$$\Gamma_i = \frac{\bar{L}_i}{\hat{m}_{ii}} \quad (3.28)$$

Then, the effective modal mass for mode i is

$$m_{eff,i} = \frac{\bar{L}_i^2}{\hat{m}_{ii}} \quad (3.29)$$

The effective modal mass is the part of the total mass responding to the ground motions in each mode (Clough & Penzien, 2003).

3.6.2 Modal analysis for scaled model

With respect to the mass and stiffness of stories in scaled model, modal analysis is carried out. Results of lateral stiffness tests presented in Table 3-2 are used with considering 40kg of mass for each story. The analysis are carried out with in Mathcad and for two conditions of basement; fixed base (FB) and base isolated (BI).

3.6.2.1 Fixed-base conditions

In the fixed base conditions, it is assumed that the structure is connected to the ground rigidly which resist any movement (horizontal and/or vertical) as well as rotations at the connection points. Recalling equation 3.22, and considering the model presented in Figure 2-1, the mass and stiffness matrices are defined as follow:

$$M = \begin{bmatrix} 40 & 0 & 0 & 0 & 0 \\ 0 & 40 & 0 & 0 & 0 \\ 0 & 0 & 40 & 0 & 0 \\ 0 & 0 & 0 & 40 & 0 \\ 0 & 0 & 0 & 0 & 40 \end{bmatrix} (kg)$$

$$K = \begin{bmatrix} 469400 & -469400 & 0 & 0 & 0 \\ -469400 & 938800 & -469400 & 0 & 0 \\ 0 & -469400 & 938800 & -469400 & 0 \\ 0 & 0 & -469400 & 938800 & -469400 \\ 0 & 0 & 0 & -469400 & 938800 \end{bmatrix} (N/m)$$

The procedure explained in section 3.6.1 shall then be followed to compute eigenvalues, eigenvectors, modal participation factors (MPFs) and finally effective modal mass.

Eigenvalues are computed as

$$\omega^2_i = \begin{bmatrix} 950.7 \\ 8100 \\ 20130 \\ 33220 \\ 43210 \end{bmatrix}$$

Therefore, natural frequencies and periods corresponding to each mode are:

$$\omega_i = \begin{bmatrix} 30.833 \\ 90.002 \\ 141.88 \\ 182.263 \\ 207.88 \end{bmatrix} (Rad/s) \quad f_i = \begin{bmatrix} 4.907 \\ 14.324 \\ 22.581 \\ 29.008 \\ 33.085 \end{bmatrix} (Hz) \quad T_i = \begin{bmatrix} 0.204 \\ 0.07 \\ 0.044 \\ 0.034 \\ 0.03 \end{bmatrix} (s)$$

The fundamental period of the structure is the first one which is the period of vibration of vibration of the first mode, 0.204 s. This is in good agreement with predictions which have been made earlier in this chapter (Table 3-3) recommending the natural period of the scaled model between 0.183 to 0.206 s.

Then eigenvectors corresponding to each mode are calculated as

$$\phi_1 = \begin{pmatrix} 0.597 \\ 0.549 \\ 0.456 \\ 0.326 \\ 0.17 \end{pmatrix}, \phi_2 = \begin{pmatrix} 0.549 \\ 0.17 \\ -0.326 \\ -0.597 \\ -0.456 \end{pmatrix}, \phi_3 = \begin{pmatrix} 0.456 \\ -0.326 \\ -0.549 \\ 0.17 \\ 0.597 \end{pmatrix}, \phi_4 = \begin{pmatrix} -0.326 \\ 0.597 \\ -0.17 \\ -0.456 \\ 0.549 \end{pmatrix}, \phi_5 = \begin{pmatrix} 0.17 \\ -0.456 \\ 0.597 \\ -0.549 \\ 0.326 \end{pmatrix}$$

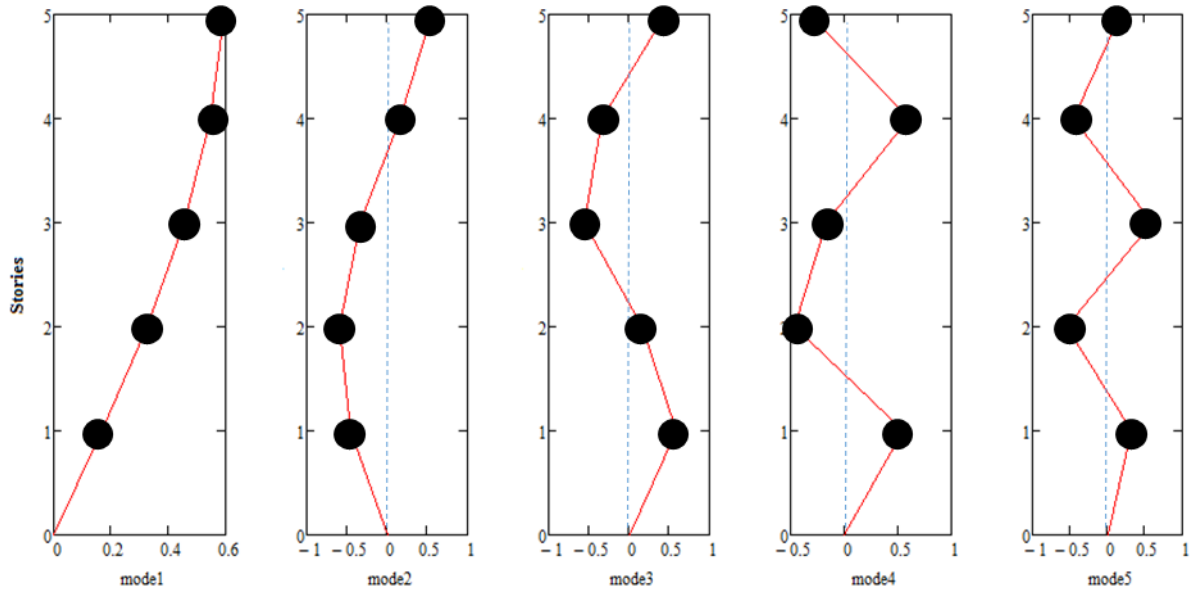


Figure 3-22 Mode shapes corresponding to the scaled structure

Having known the eigenvectors, mode shapes have been drawn (**Error! Reference source not found.**). Modal participation factors and effective modal masses are then computed as follow:

$$\Gamma_i = \begin{bmatrix} 2.097 \\ -0.66 \\ 0.348 \\ 0.194 \\ 0.089 \end{bmatrix} \quad m_{eff} = \begin{bmatrix} 175.906 \\ 17.435 \\ 4.843 \\ 1.502 \\ 0.314 \end{bmatrix}$$

It is understood from modal participation factors and effective mass matrix that the structure is highly likely subject to vibration at first mode at the time of excitation and mode number five is not likely to be excited. These values are often used in *modal superposition* method of dynamic analysis. It should be noted that the sum of the effective masses must be equal to the total mass of the structure (200 kg). Details of calculations for this section are given in appendix A.4 Modal analysis (fixed-base model).

3.6.2.2 *Isolated conditions*

Lateral stiffness of the isolation system will determine the fundamental frequencies and periods of the isolated structure. Therefore, seismic design codes provides engineers and designers with provisions which have to be considered in design of seismic isolation systems for buildings.

Desire period of the isolated structure shall be determined by defining the stiffness of the isolation system. The more stiff the isolation system, the smaller shift is observed in the effective isolated period. Therefore, Eurocode 8 recommended the following expression for identification of the effective isolated period (Eurocode8, 2011):

$$3T_f \leq T_{eff} \leq 3s \quad (3.30)$$

Where T_{eff} is the effective fundamental period of the isolated structure and T_f is the fundamental period of the superstructure assuming in fixed-base condition. The statement above is recommended for real building and for scaled model it is necessary to scale the time according to scaling relations in Table 3-1. Therefore, equation 3.30 changes to equation 3.31 for isolated condition as

$$3T_{fsc} \leq T_{effsc} \leq 3(0.316)s \quad (3.31)$$

Where, T_{fsc} and T_{effsc} represent period of the superstructure in fixed and isolated base conditions respectively.

The proposed isolation system is able to be set with different values in effective horizontal stiffness (with changing the number of bungee cords) and subsequently exhibits different effective periods. With respect to the fixed-base period of 0.204s (taken from the results of modal analysis in previous section) the limits for effective isolated period T_{effsc} are

$$0.612s \leq T_{effsc} \leq 0.948s \quad (3.32)$$

If the target period of the isolated structure is taken as four times of the fixed-base period for starting the calculations, T_{effsc} then is equal to $4(0.204) = 0.816s$, which is well lied in the range recommended by Eurocode 8:

$$0.612 < 0.816 < 0.948s.$$

A simple relation between effective period and effective stiffness shall determine the effective stiffness of isolation system for application in analytical model and further in experimental study.

$$T_{eff} = 2\pi \sqrt{\frac{M}{K_{eff}}} \quad (3.33)$$

In equation 3.33, M represents total mass of the structure and K_{eff} is the effective horizontal stiffness of the isolation system. It should be noted that the total mass of the structure in isolated conditions include additional mass base equals to the mass of each story (here 40kg). Mass base is the lowest level of superstructure to produce an ideal rigid slab immediately above the isolation system and act as a link between superstructure and isolation system. Therefore, the mass and stiffness matrices in isolated conditions have one more row and column to introduce characteristics of isolation system.

As discussed above the total mass of the structure is 240kg in isolated conditions and as explained earlier the target effective period is assumed as 0.816s, therefore, according to equation 3.33, the effective stiffness of the isolation system is calculated as 14229.5N/m. This value is applied in calculations as 14500N/m. Again the procedure explained in section 3.6.1 is followed for modal analysis of the isolated scaled structure.

$$M = \begin{bmatrix} 40 & 0 & 0 & 0 & 0 & 0 \\ 0 & 40 & 0 & 0 & 0 & 0 \\ 0 & 0 & 40 & 0 & 0 & 0 \\ 0 & 0 & 0 & 40 & 0 & 0 \\ 0 & 0 & 0 & 0 & 40 & 0 \\ 0 & 0 & 0 & 0 & 0 & 40 \end{bmatrix} (kg)$$

$$K = \begin{bmatrix} 469400 & -469400 & 0 & 0 & 0 & 0 \\ -469400 & 938800 & -469400 & 0 & 0 & 0 \\ 0 & -469400 & 938800 & -469400 & 0 & 0 \\ 0 & 0 & -469400 & 938800 & -469400 & 0 \\ 0 & 0 & 0 & -469400 & 938800 & -469400 \\ 0 & 0 & 0 & 0 & -469400 & 483900 \end{bmatrix} (N/m)$$

Where, M and K are mass and stiffness matrices of the scaled model in isolated conditions. As one additional level is now added to the structure, the number of degrees of freedom is 6; therefore, 6 number of natural frequencies, periods and mode shapes are expected.

Natural frequencies and periods corresponding to each mode are:

$$\omega_i = \begin{bmatrix} 7.593 \\ 57.075 \\ 108.75 \\ 153.399 \\ 187.712 \\ 209.294 \end{bmatrix} (Rad/s) \quad f_i = \begin{bmatrix} 1.208 \\ 9.084 \\ 17.308 \\ 24.414 \\ 29.875 \\ 33.31 \end{bmatrix} (Hz) \quad T_i = \begin{bmatrix} 0.827 \\ 0.11 \\ 0.058 \\ 0.041 \\ 0.033 \\ 0.03 \end{bmatrix} (s)$$

The fundamental period of the structure is now 0.827s which in good agreement with 0.816s of initial assumptions.

$$\phi_1 = \begin{pmatrix} -0.42 \\ -0.418 \\ -0.414 \\ -0.408 \\ -0.4 \\ -0.389 \end{pmatrix}, \phi_2 = \begin{pmatrix} -0.552 \\ -0.399 \\ -0.135 \\ 0.166 \\ 0.421 \\ 0.56 \end{pmatrix}, \phi_3 = \begin{pmatrix} -0.498 \\ 0.004 \\ 0.502 \\ 0.494 \\ -0.012 \\ -0.506 \end{pmatrix}, \phi_4 = \begin{pmatrix} -0.407 \\ 0.409 \\ 0.405 \\ -0.411 \\ -0.403 \\ 0.414 \end{pmatrix}, \phi_5 = \begin{pmatrix} 0.288 \\ -0.577 \\ 0.29 \\ 0.286 \\ -0.577 \\ 0.293 \end{pmatrix}, \phi_6 = \begin{pmatrix} -0.149 \\ 0.408 \\ -0.557 \\ 0.558 \\ -0.409 \\ 0.151 \end{pmatrix}$$

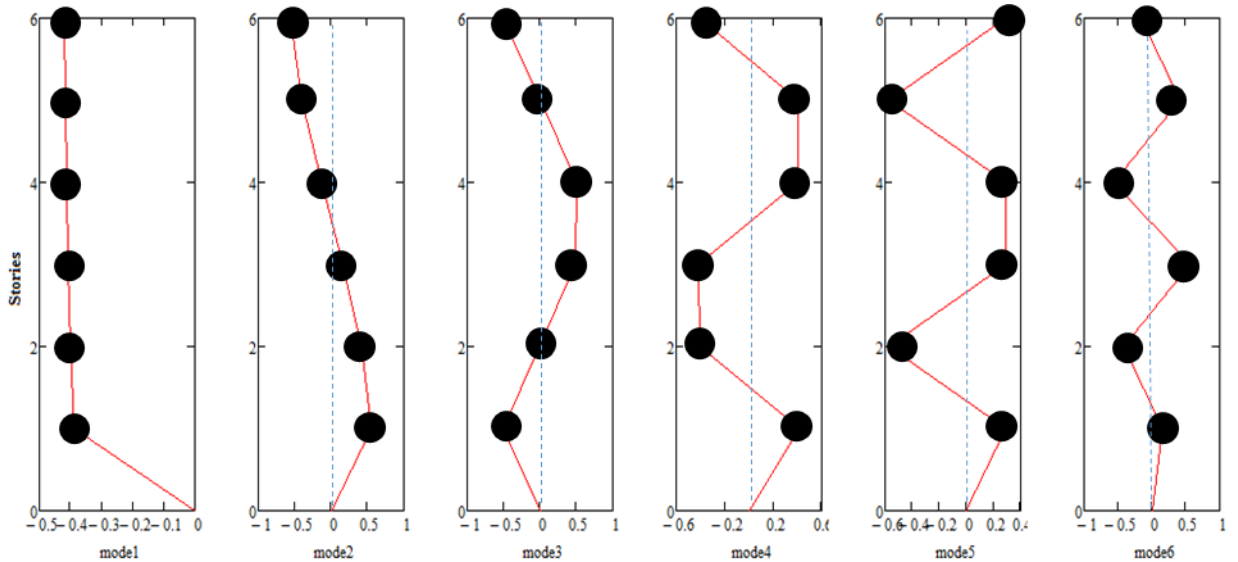


Figure 3-23 Mode shapes of isolated scaled structure

Mode shapes are shown in Figure 3-23. Modal participation factors and effective modal masses are then computed as follow:

$$\Gamma_i = \begin{bmatrix} -2.449 \\ 0.062 \\ -0.015 \\ 0.0064 \\ 0.003 \\ 0.0013 \end{bmatrix} \quad m_{eff} = \begin{bmatrix} 239.83 \\ 0.155 \\ 0.0096 \\ 0.0016 \\ 0.0003 \\ 0.0000 \end{bmatrix}$$

It is concluded from modal participation factors and effective mass matrix that the structure is highly likely excited at the first mode of vibration. Full computation details are presented in A.5 Modal analysis (base isolated).

3.6.2.3 Discussion

Comparing the results from modal analysis of the structure (scaled model) once again reveals the importance of period shifting in the response analysis of the structures. It is understood from modal participation factors in two conditions (fixed base and isolated) that the effect of second, third, fourth and fifth modes of vibration are negligible thanks to the isolation system. The most effective mode in isolated structure is the first mode which is shifted far beyond the likely period of devastating shocks.

In addition, comparison of the mode shapes of the structure in fixed-base and isolated conditions, illustrates how relative story drifts are reduced in isolated structure. According to the results from analysis of the scaled structure, the first mode of vibration is the most significant one (i.e. structural vibration in this mode is highly likely). There are great reductions in the values corresponding to story drifts in fixed base condition compared to isolated (Table 3-4).

Table 3-4 Story drifts

Stories	drifts (non-dimensional)	
	fixed base	isolated
5th - 4th	0.048	0.002
4th - 3rd	0.093	0.004
3rd - 2nd	0.13	0.006
2nd - 1st	0.156	0.008
1st - base	0.17	0.011
base - zero	-	0.389

The smaller the inter-story drifts, the less damage is expected in the structure after earthquake shocks.

3.7 Conclusion

In this chapter the philosophy of seismic base isolation was discussed and a case study was introduced along with the principals of scaling for a scaled structure. The analytical model of the case study was presented and the dynamic properties of the structure were investigated. It was shown how the appropriate base isolation system can reduce the effects of dynamic loads on the structure in theory, with shifting the period of the structure to a greater one and reducing story drifts as the cause of damage. The results will be further discussed and compared with experimental tests results in chapter five.

As the main element of the new isolation system is air bearings, chapter four presents the design and development of air-bearing devices through numerical simulations and laboratory tests.

4 **Air-bearing device design and development**

4.1 Introduction

The air-bearing units used for the purpose of this study are categorised as **flat air bearing** made of Aluminium materials. With respect to the size of the structure (5-story scaled building model), available materials in the market and capabilities of the CNC machine in the workshop, a 3D model for the device was generated in a CAD software and analysed through a numerical modelling then the results have been validated via laboratory tests and analytical study. The geometry and number of nozzles have been further optimized to achieve best performance for air bearing devices.

4.2 Air bearing design

The air bearing designed for this study is a flat air bearing in which the nozzle outlet blow a vertical jet of air directly to the surface underneath and unlike the cushion type bearings there is no rubber made cushion below the device to maintain the air volume. Flat bearings maintain a finite separation between mechanical components by means of the pressurized flow of air through the gap between two surfaces. A well-known example of this kind is an air hockey table, where a puck is floated above the table surface by an array of vertical jets of air (Hendriks, 2001). Using flat air bearings there is no contact between “moving parts” and thus no friction and no wear on surfaces.

The design of the bearing for this study consists of the design of the nozzle shape for flat type air bearing. The size of the chamber of the bearing is restricted by the maximum of 200mm and 50mm for exterior diameter and height respectively. These dimensions are all determined by the space restrictions at the base of the structure. According to these constraints and the capabilities of the CNC machine in the workshop, the geometry of the air-bearing device is determined as shown in Figure 4-1 and Figure 4-2.

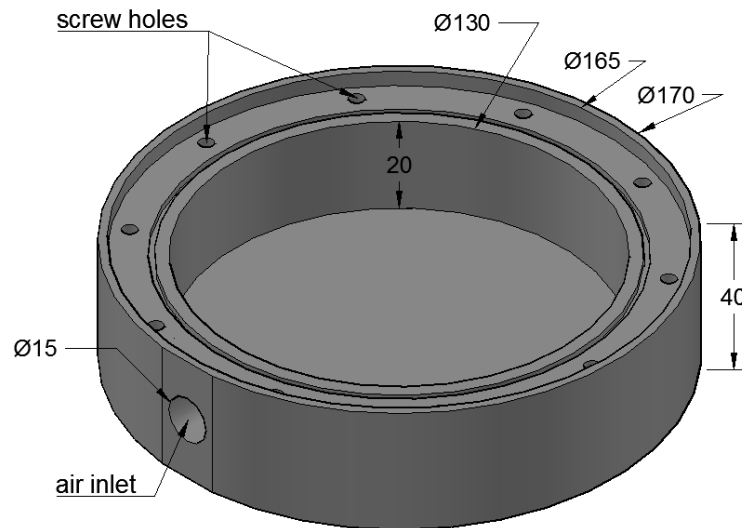


Figure 4-1 Air-bearing device chamber (dimensions in mm)

The seal of the bearing is attached to the chamber through the designated screw holes on the wall of the chamber.

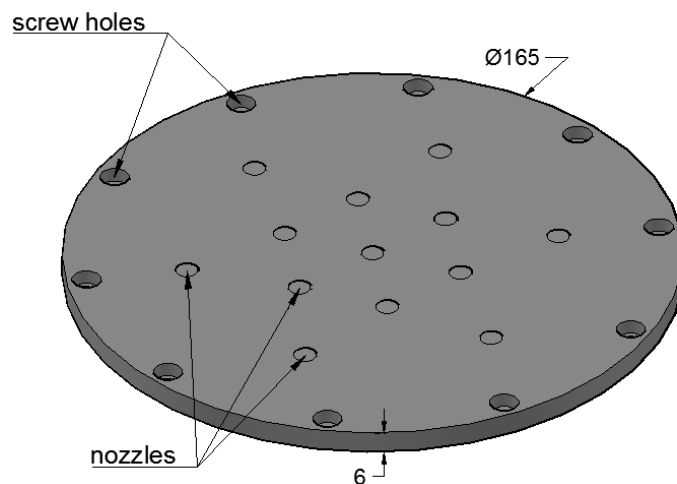


Figure 4-2 Air-bearing seal with nozzles (dimensions in mm)

The changeable seal gives the opportunity of testing different nozzle shapes and numbers. Having known the feasible size and geometry for the bearings, it is possible to model it in a CAD software and analyse the fluid flow with respect to the maximum pressure available at the workshop. Simulations are to determine the optimum geometry for nozzles and further optimisation of the number of nozzles. The primary shape of nozzle for this type of air bearing consists of an orifice with a cylindrical pocket. The shape considered for initial simulation is a conical shape shown in Figure 4-3.

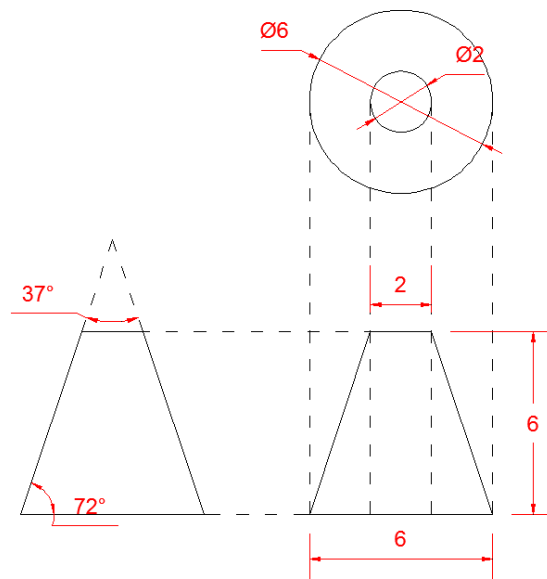


Figure 4-3 Nozzle geometry used in air-bearing design

The flow enters the nozzle from 2mm diameter side and exits from 6mm diameter. In fact, the inlet of the nozzle is designed to have the smaller diameter than its outlet. The flow that enters the nozzle reaches Mach velocity rapidly due to high pressure differences between inlet and outlet. As the flow becomes supersonic, the nozzle should have divergent shape to maintain the high velocity otherwise, the flow velocity will drop to subsonic area.

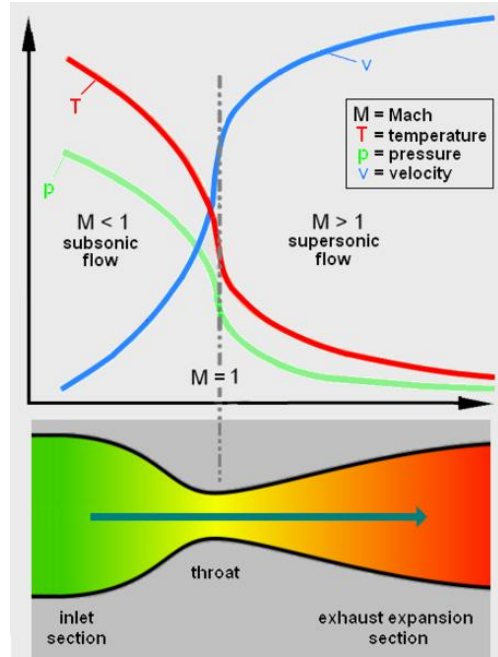


Figure 4-4 The effects of divergence in nozzle shape on flow parameters (Beychok, 2010)

The higher velocity is desire as it produces higher momentum.

In order to gain an insight into what happens to the flow inside the chamber and nozzle, it is necessary to create a computer simulation with respect to the geometry constraints and boundary conditions. The simulation also provides valuable information about the fluid characteristics such as pressure, velocity and consequently mass flow rate. Mass flow rate can be used to validate the total momentum force generated in nozzle. Next section will discuss the simulation method in light of the governing equations of fluid flow.

4.3 Simulation methods

4.3.1 Governing equations

The governing equations of the fluid flow could be described by the problems of continuum mechanics. In continuum motion the governing equation are as follow (Aris, 1989):

$$\frac{d}{dt} \int_{V_M(t)} \rho \phi(\mathbf{x}, t) dV = \frac{\partial}{\partial t} \int_{V_M(t)} \rho \phi dV + \oint_{\partial V_M(t)} d\mathbf{S} \cdot (\rho \phi \mathbf{U}), \quad (4.1)$$

In equation 4.1, \mathbf{U} is the velocity vector and $d\mathbf{S}$ is the outward pointing unit vector normal to $\partial V_M(t)$. The rate of change of ϕ in V_M can be written regarding its volume and surface sources:

$$\frac{\partial}{\partial t} \int_{V_M(t)} \rho \phi dV + \oint_{\partial V_M(t)} d\mathbf{S} \cdot (\rho \phi \mathbf{U}) = \int_{V_M(t)} Q_V(\phi) dV + \oint_{\partial V_M(t)} d\mathbf{S} \cdot \mathbf{Q}_S(\phi), \quad (4.2)$$

The differential form of the above is:

$$\frac{\partial \rho \phi}{\partial t} + \nabla \cdot (\rho \phi \mathbf{U}) = Q_V(\phi) + \nabla \cdot \mathbf{Q}_S(\phi). \quad (4.3)$$

Equation 4.3 is a governing equation for all continuum mechanics problems in general (Aris, 1989). The equation is transformed to different conservation equations by changing parameter ϕ .

The conservation laws valid for any continuum are as follow:

- Conservation of mass ($\phi = 1$)

$$\frac{\partial \rho}{\partial t} + \nabla \cdot (\rho \mathbf{U}) = 0 \quad (4.4)$$

- Conservation of linear momentum ($\phi = \mathbf{U}$)

$$\frac{\partial \rho \mathbf{U}}{\partial t} + \nabla \cdot (\rho \mathbf{U} \mathbf{U}) = \rho \mathbf{g} + \nabla \cdot \boldsymbol{\sigma} \quad (4.5)$$

- Conservation of energy ($\phi = e$)

$$\frac{\partial \rho e}{\partial t} + \nabla \cdot (\rho e \mathbf{U}) = \rho \mathbf{g} \cdot \mathbf{U} + \nabla \cdot (\boldsymbol{\sigma} \cdot \mathbf{U}) - \nabla \cdot \mathbf{q} + \rho Q. \quad (4.6)$$

Where

- ρ is the density,
- \mathbf{U} is the velocity vector,
- $\boldsymbol{\sigma}$ is the stress tensor,
- e is the total specific energy,
- Q is the volume energy source.

The system is still indeterminate as the number of unknown quantities is larger than the number of equations. There is a need to introduce additional conservative relations to increase the number of equations and close the system.

Considering the fluid as a Newtonian fluid, the following set of equations can be used (Jasak, 1996):

Defining the internal energy as a function of pressure P and temperature T :

$$u = u(P, T). \quad (4.6)$$

The total energy e can be defined as the sum of the kinetic energy e_k and internal energy:

$$e = e_k + u(P, T) = \frac{1}{2} \mathbf{U} \cdot \mathbf{U} + u(P, T) \quad (4.7)$$

The equation of state:

$$\rho = \rho(P, T), \quad (4.8)$$

The Fourier's law of heat conduction:

$$\mathbf{q} = -\lambda \nabla T, \quad (4.9)$$

Where

- \mathbf{q} is the heat flux,
- λ is the transport coefficient

Generalised form of the Newton's law of viscosity (Jasak, 1996):

$$\sigma = -\left(P + \frac{2}{3}\mu \nabla \cdot \mathbf{U}\right) \mathbf{I} + \mu[\nabla \mathbf{U} + (\nabla \mathbf{U})^T]. \quad (4.10)$$

Where

- μ is viscosity
- \mathbf{I} is the unit tensor

The constitutive relations above, together with the governing equations of continuum mechanics can create a close system of partial differential equations for a Newtonian fluid:

Continuity equation:

$$\frac{\partial \rho}{\partial t} + \nabla \cdot (\rho \mathbf{U}) = 0 \quad (4.11)$$

Navier-Stokes (momentum) equation (Jasak, 1996):

$$\frac{\partial \rho \mathbf{U}}{\partial t} + \nabla \cdot (\rho \mathbf{U} \mathbf{U}) = \rho \mathbf{g} + \nabla \cdot \left(P + \frac{2}{3} \mu \nabla \cdot \mathbf{U} \right) + \nabla \cdot [\mu (\nabla \mathbf{U} + (\nabla \mathbf{U})^T)], \quad (4.12)$$

Energy equation:

$$\begin{aligned} \frac{\partial \rho e}{\partial t} + \nabla \cdot (\rho e \mathbf{U}) &= \rho \mathbf{g} \cdot \mathbf{U} + \nabla \cdot (P \mathbf{U}) \\ &- \nabla \cdot \left(\frac{2}{3} \mu (\nabla \cdot \mathbf{U}) \mathbf{U} \right) + \nabla \cdot [\mu (\nabla \mathbf{U} + (\nabla \mathbf{U})^T) \cdot \mathbf{U}] \\ &+ \nabla \cdot (\lambda \nabla T) + \rho Q. \end{aligned} \quad (4.13)$$

As functions of thermodynamics state variables, the transport coefficients λ and μ are defined as follow:

$$\lambda = \lambda(P, T), \quad (4.14)$$

$$\mu = \mu(P, T). \quad (4.15)$$

4.3.2 Turbulence modelling

The state of continuous instability in a flow is called turbulence. Irregularity in the flow, increased diffusivity and energy dissipations are some characters of a turbulent flow (Jasak, 1996). Below the model used in this project to represent turbulence is described briefly.

Several deferent approaches can be conducted in order to model a turbulent flow. The Direct Numerical Simulation or DNS is a way in which the governing equations are

numerically integrated (Eswaran & Pope, 1988). The Large Eddy Simulation (LES) is another way in which a spatial filter is applied in order to separate different length scales which was first introduced by (Deardorff, 1970). Both two ways are among the pioneers in fluid turbulence numerical analysis yet demanding high computer specifications and rendering time.

An alternative approach is separation of the local value of the variable into the mean value and the fluctuation around the mean. In this case the characteristics of turbulent flow governs the selection of averaging method.

Reynolds averaging technique: One of the popular techniques is Reynolds averaging technique in which all flow parameters are presented as mean value plus a fluctuation value as follow:

$$\phi(\mathbf{x}, t) = \bar{\phi}(\mathbf{x}, t) + \phi'(\mathbf{x}, t), \quad (4.18)$$

where $\phi'(\mathbf{x}, t)$ is the fluctuation about the mean value and the mean value is defined as below:

$$\bar{\phi}(\mathbf{x}, t) = \lim_{N \rightarrow \infty} \frac{1}{N} \sum_{i=1}^N \phi_i(\mathbf{x}, t), \quad (4.19)$$

In this equation N is the number of identically performed experiments.

The following form of the averaged will be obtained if the above procedure is applied to the compressible¹ Navier-Stokes equation:

$$\frac{\partial}{\partial t}(\rho \bar{\mathbf{U}}) + \nabla \cdot (\rho \bar{\mathbf{U}} \bar{\mathbf{U}}) = \mathbf{g} - \nabla \bar{p} + \nabla \cdot (\nu \nabla \bar{\mathbf{U}}) + \overline{\mathbf{U}' \mathbf{U}'}. \quad (4.20)$$

The term $\overline{\mathbf{U}' \mathbf{U}'}$ is called the Reynolds stress tensor. The Reynolds stress represent effects of the turbulence and has to be modelled to close the system of equations (Ramezanpour, 2009).

¹ It should be noted that this analysis is based on compressible flow principals.

In order to express the Reynolds stress tensor in terms of the known quantities, Reynolds averaged turbulence modelling is necessary. One of the approaches is the Standard k - ω which is used for modelling in this study.

Standard k - ω model: ANSYS Fluent is employed for numerical modelling of air-bearing unit designed for this study. The standard k - ω model incorporated by ANSYS Fluent works based on Wilcox k - ω model (ANSYS, 2015). Wilcox k - ω model incorporates modifications for low-Reynolds number effect, compressibility and shear flow spreading (Wilcox, 2006). The standard k - ω model is based on model transport equations for the turbulence kinetic energy (k) and the specific dissipation rate (ω) and is an empirical model. The accuracy of the model for predicting free shear flows have been improved over the years by adding production terms to both k and ω equations.

Transport equations for the standard k - ω model: Following transport equations define k and ω :

$$\frac{\partial}{\partial t}(\rho k) + \frac{\partial}{\partial x_i}(\rho k u_i) = \frac{\partial}{\partial x_j} \left(\Gamma_k \frac{\partial k}{\partial x_j} \right) + G_k - Y_k + S_k, \quad (4.21)$$

$$\frac{\partial}{\partial t}(\rho \omega) + \frac{\partial}{\partial x_i}(\rho \omega u_i) = \frac{\partial}{\partial x_j} \left(\Gamma_\omega \frac{\partial \omega}{\partial x_j} \right) + G_\omega - Y_\omega + S_\omega. \quad (4.22)$$

Where

- Γ_k is the effective diffusivity of k
- Γ_ω is the effective diffusivity of ω
- G_k is the generation of turbulence kinetic energy due to mean velocity gradients
- G_ω is the generation of specific dissipation rate
- Y_k is the dissipation of k
- Y_ω is the dissipation of ω
- S_k and S_ω are user defined source terms

The effective diffusivities for the k - ω model are defined as follow:

$$\Gamma_k = \mu + \frac{\mu_t}{\sigma_k} \quad (4.23)$$

$$\Gamma_{\omega} = \mu + \frac{\mu_t}{\sigma_{\omega}} \quad (4.24)$$

In these equations:

- μ_t is the turbulent viscosity
- σ_k is the turbulent Prandtl number for k
- σ_{ω} is the turbulent Prandtl number for ω

The relation between k and ω is defined as follow:

$$\mu_t = \alpha^* \frac{\rho k}{\omega} \quad (4.25)$$

Note that in the high-Reynolds number form of the k- ω model, $\alpha^* = \alpha_{\infty}^* = 1$.

4.4 Numerical solutions

As there is no analytical solution for partial differential equations governing fluid flow problems and on the other hand, experimental study is costly and time taking for high number of design variables, the best option to analyse and finalise the air-bearing design is using numerical methods for the solution of mathematically defined fluid flow governing equations. CFD (Computational Fluid Dynamics) analysis is employed for solving the problem of fluid flows in this study in order to determine the optimised geometry of the nozzles.

4.4.1 Geometry

CFD analysis starts with generating the geometry of the model. It should be noted that, all geometry components are parametric in this model which enables the user to change them for desire dimensions. The general geometry of the air-bearing unit used in this study is shown in Figure 4-5.

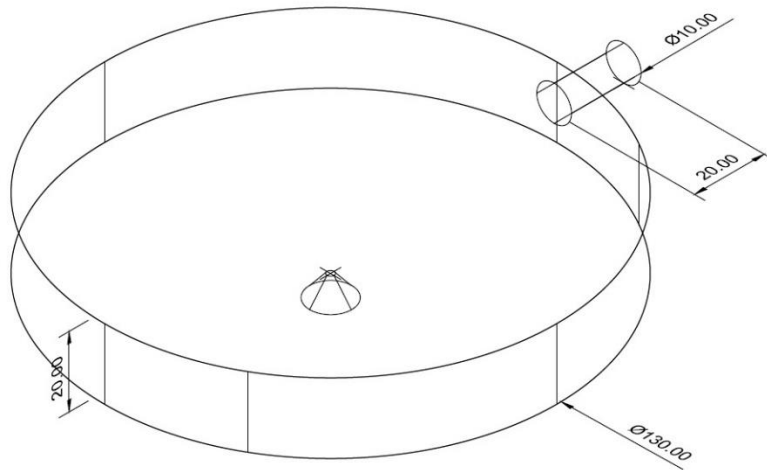


Figure 4-5 CFD model volume (dimensions in mm)

The geometry of CFD model is a cylinder shape volume with diameter of 130 mm and height of 20 mm. The inlet has the length of 20mm and diameter of 10 mm. The outlet is a nozzle to the centre of bottom plate Figure 4-6.

The thickness of bottom plate is 6mm and the material of the device is Aluminium. The air-bearing unit can lift up with producing a thin layer of air flow underneath of the bottom. The air pressure on the inlet of the unit is set to 5bars (gauge). The CFD model for this analysis is responsive when applying changes in inlet and outlet boundaries.

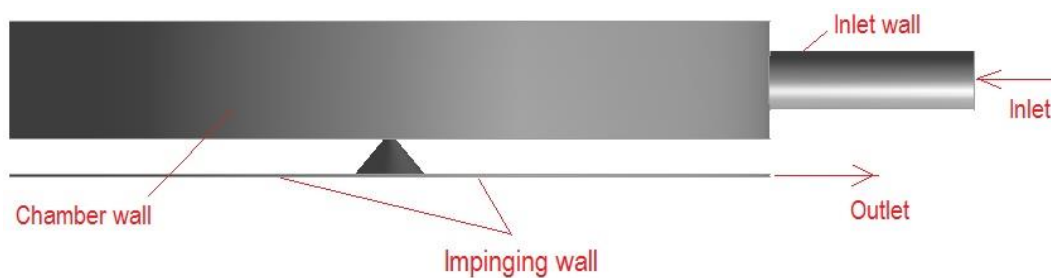


Figure 4-6 Geometry of flow domain

4.4.2 Discretisation

Discretisation is known as the process of transferring the continuous equations or function into separate complements. This is the primary step toward making the system of equations or model suitable for numerical analysis. Discretisation consists of three key steps:

Equations discretisation: The partial differential equations of governing equations are expressed in algebraic form, in terms of discrete quantities defined at each cell in the domain. Therefore, equation 4.3 becomes

$$a_p \phi_p^{t+\Delta t} = \sum_{f=1}^{nb} a_{nb} \phi_{nb}^{t+\Delta t} + S_K \quad (4.26)$$

Where a_p and a_{nb} represent the cell centre and neighbouring cell coefficient respectively. The cell centre coefficient is calculated as follow (Brennan, 2001):

$$a_p = \sum_{f=1}^{nb} a_{nb} - S_L \quad (4.27)$$

In equations 4.26 and 4.27, S_K and S_L are dimensionless source terms in integration.

Temporal discretisation: Time domain is divided into finite number of time intervals or steps in transient problems.

Domain discretisation: The problem space or the domain of the model is divided into finite number of volumes or regions, known as control volume or mesh.

The numerical solution in this study is based on finite volume method in which the integral form of the governing equations on each control volume or cell is considered. Therefore, the flow domain is subdivided into tetrahedral cells where governing equations are solved subsequently. Control volume or cells fill the whole domain volume and do not overlap. With respect to the geometry of the domain and the solution method, the discretisation can be carried out in two different methods:

Structured grid: The cells (meshes) have regular connectivity made it more effective for simple geometries. The suitable mesh choices are quadrilateral in two dimensional domains and hexahedra in three dimensional domains. As the neighbourhood relationships between cells are defined by storage arrangement, this model is highly space and time efficient with higher resolution than unstructured grid (Castillo, 1991).

Unstructured grid: The best option when irregular geometries for domain is governing the problem conditions. According to cells irregular connectivity, unstructured grids can

be arranged in any convenient manner which provides more freedom in refinement in specific regions. In comparison to structured meshes, this model can be highly space and time inefficient as it calls for explicit storage of neighbourhood relationships. These kind of grids normally hire triangle shapes in two dimensional and tetrahedral in three dimensional domains (Mavriplis, 1996).

4.4.3 Mesh generation

For this geometry, approximately, 3 million tetrahedral unstructured cells are generated with prism layer mesh at the boundaries to capture velocity gradients near the walls¹. There is higher mesh density inside the nozzle in order to capture shock waves and expansion fans (Figure 4-7).

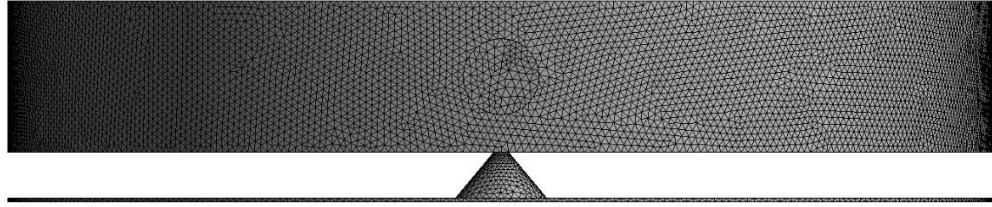


Figure 4-7 Mesh generation by ANSYS Mesh

4.4.4 Numerical setting

For this research, density base solver has been employed with implicit steady state condition for time frame. In order to reduce the errors, high order of discretisation schemes has been used. For momentum equations, third order MUSCL scheme has been adopted and for rest of the parameters second order upwind method has been implemented. To avoid instabilities in the solution domain, Courant number (CFL) was set to be below one. As the simulations are carried out for compressible flow, therefore, the air has been considered as ideal gas. As explained before $k - \omega$ turbulent model was selected to solve Reynolds stress model.

¹ This is due to capture boundary layer effect near the wall.

4.4.4.1 Boundary conditions

The partial differential equations governing the problem needs boundary conditions in order to close the system of equations. The solver used for this study is FLUENT commercial package. The set of boundary conditions implemented are as below:

The **inlet boundary condition** is defined as “pressure inlet” of 5bar gauge. The flow inside the chamber and inside the nozzle is solved for different pressure ratios. The inlet pressure to the chamber is known; on the other hand the velocity and mass flow rate are unknown. The relationship between variables in the case of compressible flow is as follow:

$$p_t = p_s \left(1 + \frac{\gamma - 1}{2} M^2 \right)^{\frac{\gamma}{\gamma - 1}} \quad (4.28)$$

Where,

p_t is total pressure,

p_s is the static pressure,

γ is the specific heat ratio and

M is Mach number defined as below:

$$M = \frac{u}{\sqrt{\gamma R T_s}} \quad (4.29)$$

In the above equation, u represents the velocity, T_s is the static temperature and R denotes the gas constant. The static temperature relationship with total temperature is described as

$$\frac{T_t}{T_s} = 1 + \frac{\gamma - 1}{2} M^2 \quad (4.30)$$

The **outlet boundary condition** is defined as “pressure outlet” which is atmospheric conditions pressure of 1.013bar (zero gauge).

The solid wall boundary condition is utilised for solid regions, with no slip conditions. In order to take into account the effect of viscosity of the flow on the solid walls, the wall boundary conditions are imposed the shear stress for laminar flows, which are calculated (based on the velocity gradient at the wall) as below:

$$\tau_w = \mu \frac{\partial u}{\partial n} \quad (4.31)$$

Where,

τ_w is shear stress at the wall and

μ is the coefficient of friction.

4.4.5 Numerical results

CFD model in this study is a parametric model with capability of applying changes in all geometry parameters.

The CFD was applied for three different nozzle geometries (Table 4-1) and a gap height of 1 mm between the bottom of the air-bearing device and the flat surface. In all three cases the inlet diameter was set to 2mm, however, the simulation was performed for three different outlet diameters.

Table 4-1 Simulation cases definition

Simulation case	Inlet diameter (mm)	Outlet diameter (mm)
2-3	2	3
2-6	2	6
2-12	2	12

4.4.5.1 Mach contours analysis

In order to determine the optimum slope for conical nozzle, the effect of velocity in nozzle should be considered. Figure 4-8, Figure 4-9 and Figure 4-10 show the contours of Mach number in the cross-sectional area of nozzle and gap for three different nozzles. Mach number is the ratio of actual velocity over the velocity of sound which is helpful

for investigating the velocity of compressible flow in a specific field and observation of shock waves.

In a flow field, **Stagnation point** is a point with zero local velocity (Clancy, 1975). According to Bernoulli equation, pressure and velocity have inverse relationship; the pressure is at its maximum level when the velocity is minimum. Therefore, in fluid flow where the velocity is zero or near zero (stagnation point), the static pressure is maximum. This pressure is called Stagnation pressure. With reference to Figure 4-8 to Figure 4-10, the largest area of stagnation pressure exists in the case of nozzle with 2 mm inlet and 6 mm outlet (Figure 4-9). The stagnation area creates a cushion of air that the air bearing stands on it. Therefore, it can produce more uplift pressure underneath of the bottom plate of air-bearing unit.

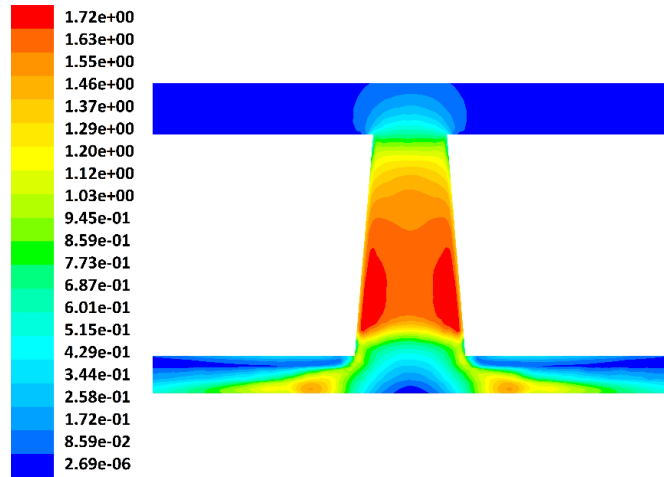


Figure 4-8 Output results for Mach number (nozzle 2-3 side view)

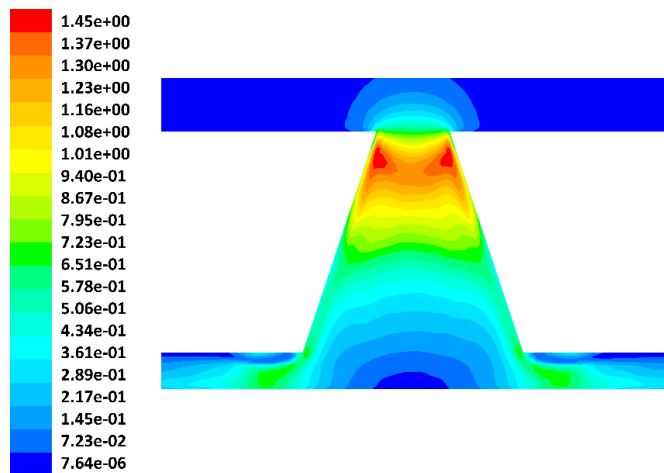


Figure 4-9 Output results for Mach number (nozzle 2-6 side view)

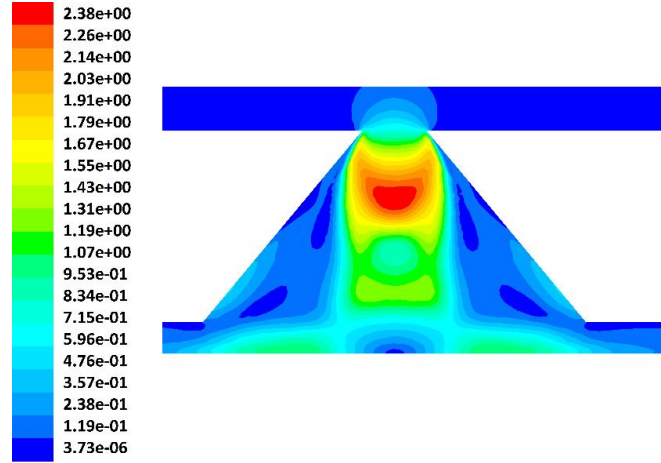


Figure 4-10 Output results for Mach number (nozzle 2-12 side view)

A comparison of Figure 4-9 and Figure 4-10, shows that in the nozzle with 12mm outlet diameter, there is a large separation zone on the nozzle wall. This is due to high adverse pressure gradient that separates the flow. The circulation zone, as a result of pressure gradient, is a non-desirable phenomenon as it blocks the air flow. Although, the maximum velocity is not happening in the nozzle 2-6, due to larger stagnation area and less separation zone, the optimum shape for the nozzle will be 2mm inlet diameter and 6mm outlet diameter (a conical shape).

4.4.5.2 Mass-flow rate analysis

One of the fundamental concepts of physics is the conservation of mass which implies that the amount of mass remains constant in a problem domain; mass is neither created nor destroyed. The mass of an object is the volume that the object occupies times the density of the object. For a fluid the density, volume, and shape of the object can all change within the domain with time.

The conservation of mass (continuity) determines that the mass flow rate \dot{m} through a nozzle is constant and equal to the product of the density ρ , velocity u , and flow area A :

$$\dot{m} = \rho \cdot u \cdot A \quad (4.32)$$

It is understood from the above equation that any increase in velocity for a constant density and given area, will increase the mass flow rate. However, as a result of compressibility effects in real fluid the density does not remain constant. Therefore, it

is essential to take into account the effect of change in density in higher velocities. Recalling equation 4.29 and substitute for velocity in equation 4.32, the compressible form of the mass flow rate equation is derived as

$$\dot{m} = \rho \cdot A \cdot M \sqrt{\gamma R T} \quad (4.33)$$

Equation of state determines density as follow:

$$\rho = \frac{p}{RT} \quad (4.34)$$

As the flow is assumed to maintain the constant value of entropy, **isentropic**¹ flow governing equations are applied:

$$p = p_t \left(\frac{T}{T_t} \right)^{\frac{\gamma}{\gamma-1}} \quad (4.35)$$

$$T = \frac{T_t}{1 + \frac{1}{2}(\gamma - 1)M^2} \quad (4.36)$$

Where, p_t and T_t are total pressure and total temperature respectively.

By collecting terms and substituting 4.34, 4.35 and 4.36 into 4.33 the equation for mass flow rate is derived as

$$\dot{m} = \frac{A \cdot p_t}{\sqrt{T_t}} \cdot \sqrt{\frac{\gamma}{R}} \cdot M \left(1 + \frac{\gamma - 1}{2} \cdot M^2 \right)^{-\frac{\gamma+1}{2(\gamma-1)}} \quad (4.37)$$

The maximum flow rate occurs when the Mach number is equal to one (Bailey, 1961). This phenomenon is known as **choking** of the flow (Bernstein, et al., 1967). If $M = 1$ is replaced in equation 4.37, the value of the choked mass flow rate is determined as

$$\dot{m} = \frac{A \cdot p_t}{\sqrt{T_t}} \cdot \sqrt{\frac{\gamma}{R}} \cdot \left(\frac{\gamma + 1}{2} \right)^{-\frac{\gamma+1}{2(\gamma-1)}} \quad (4.38)$$

¹ Isentropic flow occurs, if the changes in flow variables are small and gradual, e.g. the ideal gas flow through a nozzle.

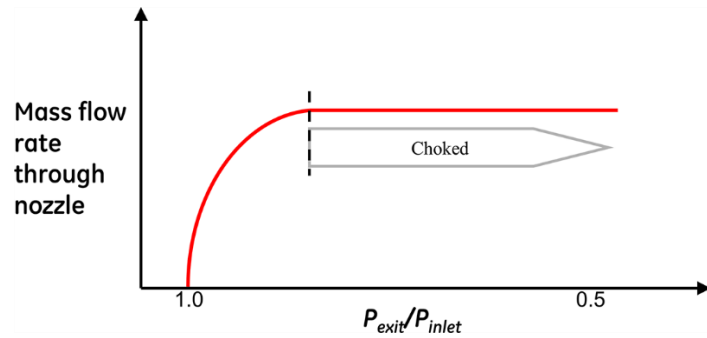


Figure 4-11 Mass flow rate through a nozzle at different pressure ratios (Tiwari, et al., 2013)

The mass flow rates are calculated at cross section area where $M = 1$ using equation 4.38 for three case studies. The results are presented in Table 4-2.

Table 4-2 Mass flow rate calculated for three different cases

Nozzle inlet diameter (mm)	Nozzle outlet diameter (mm)	Outlet/Inlet	flow rate (kg/s)
2	3	1.5	0.0313
2	6	3	0.0388
2	12	6	0.0327

The higher mass flow rates provides more momentum force. It is understood from table above, that nozzle 2-6 demonstrates the highest mass flow rate through the nozzle. These values will be used further on for validation of the numerical modelling.

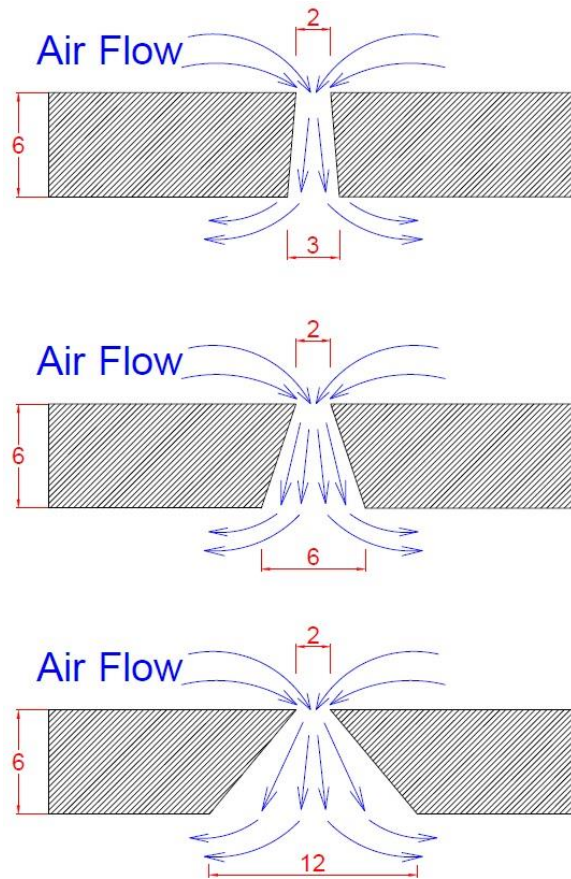
4.5 Experimental study

Laboratory tests were conducted to validate the results from numerical study on air-bearing unit in terms of choosing the optimum option for nozzle shape (Figure 4-12). Three different types of nozzle (investigated in numerical study) were tested and the optimum option was chosen for producing highest vertical force.

Two sets of test were carried out. The first set of tests were performed to determine the best nozzle type in terms of conical shape to verify numerical modelling. And the second set of tests were performed to determine the optimum number of nozzles for the air bearing device to take desirable loads at the same inlet pressure.

4.5.1 Air-bearing device

The air-bearing devices used for laboratory tests were made up of aluminium in the Mechanical workshop at Anglia Ruskin University (Figure 4-13 and Figure 4-14). Three types of bottom plate were made with three different types of nozzles as described in Figure 4-12.



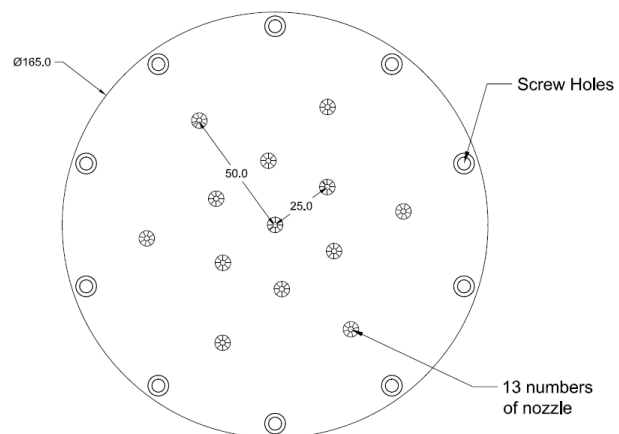
**Figure 4-12 Three different types of nozzle used in numerical study and laboratory tests
(dimensions in mm)**



Figure 4-13 The bottom plate of air bearing device made in workshop



Figure 4-14 Air-bearing device componenets



**Figure 4-15 The air-bearing device bottom plate dimensions and position of nozzles
(dimensions in mm)**

4.5.2 Tests

Tests on the air-bearing units were designed to examine the ability of each type of air-bearings in lifting designated loads. Therefore, a high precision gauge was employed to measure lift gaps at different loads and different number of nozzles.

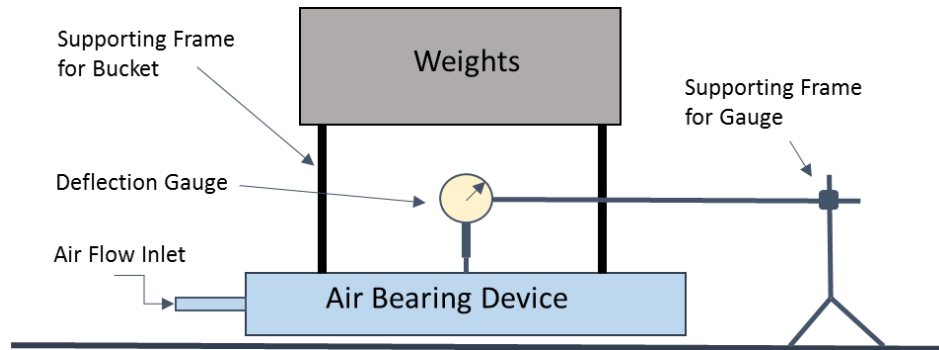


Figure 4-16 Air-bearing tests diagram

Based on the capacity of air compressor in the workshop, two different pressures are examined (5 bar and 7 bar). Inlet pressure to the chamber of air-bearing device is adjustable with an air regulator valve (Figure 4-17).



Figure 4-17 Air valve to adjust the pressure

4.5.3 Experimental results

Nozzle type: In order to validate the results from numerical study, which shows the best performance of 2-6mm diameter nozzle, three different nozzle types (Figure 4-12) were tested in the workshop with different loading on top of the air-bearing device and recording the vertical lift read by the gauge. Table 4-3 shows the performance of air-bearing device for three different types of nozzle with different loadings on 5 bar pressure.

Table 4-3 Lifting capacity of each nozzle type investigated by experiments

	Nozzle type ($D_{in} - D_{out}$)		
	2 – 3	2 – 6	2 – 12
Weight (kg)	Lift (mm)		
1.6 ¹	0.7	0.95	0.52
2.0	0.45	0.68	0.39
2.2	0.41	0.55	0.37
2.4	0.38	0.48	0.35
22.6	0.26	0.28	0.26

It is understood that the best performance belongs to the nozzle 2-6 as it provides the highest lift among others in the same pressure inlet.

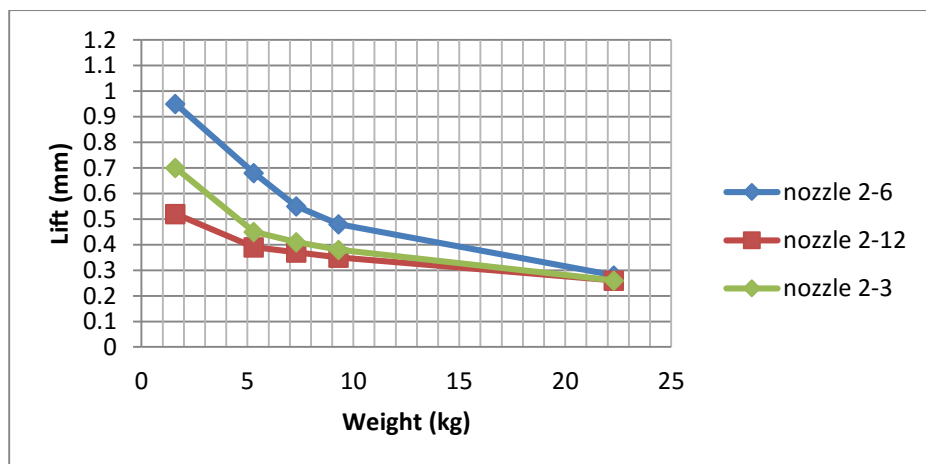


Figure 4-18 Lift against Weight diagram and trend lines for three different nozzles

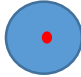
¹ 1.6 kg is the self-weight of the device

Number of nozzles: In order to determine the optimum number of nozzles, the same procedure for loading and measuring lifts are conducted. As the nozzle 2-6 showed the best performance, this time tests are conducted just on the 2-6 type nozzle and for different numbers of nozzle to the bottom plate of air-bearing device to optimise the number of nozzles.

Three sets of test for this part includes:


- Just one nozzle to the centre of bottom plate is open
- One nozzle to the centre and 6 far around
- One nozzle to the centre and 12 nozzles around (Figure 4-15)

Table 4-4 Lifts corresponding to different loadings for air bearing with one nozzle at the centre




one nozzle at the centre				
@ 7 bar			@ 5 bar	
Weight (kg)	Lift (mm)	vertical stiffness (N/m)	Lift (mm)	vertical stiffness (N/m)
1.6	0.72	21800	0.52	30184.62
3.6	0.66	53509.09	0.44	80263.64
5.6	0.61	90059.02	0.41	133990.2

Table 4-5 Lifts corresponding to different loadings for air bearing with one nozzle at the centre and six nozzles far around



one nozzle at the centre + 6 far around				
@ 7 bar			@ 5 bar	
Weight (kg)	Lift (mm)	vertical stiffness (N/m)	Lift (mm)	vertical stiffness (N/m)
1.6	1.09	14400	0.63	24914.29
3.6	0.63	56057.14	0.43	82130.23
5.6	0.55	99883.64	0.34	161576.5

Table 4-6 Lifts corresponding to different loadings for air bearing with one nozzle at the centre and 12 nozzles around



one nozzle at the centre + 12 around				
@ 7 bar			@ 5 bar	
Weight (kg)	Lift (mm)	vertical stiffness (N/m)	Lift (mm)	vertical stiffness (N/m)
1.6	1.82	8624.176	0.95	16522.11
3.6	0.99	35672.73	0.76	46468.42
5.6	0.73	75254.79	0.68	80788.24

Results from these tests show the best performance in terms of lifting capacity when all nozzles are open.

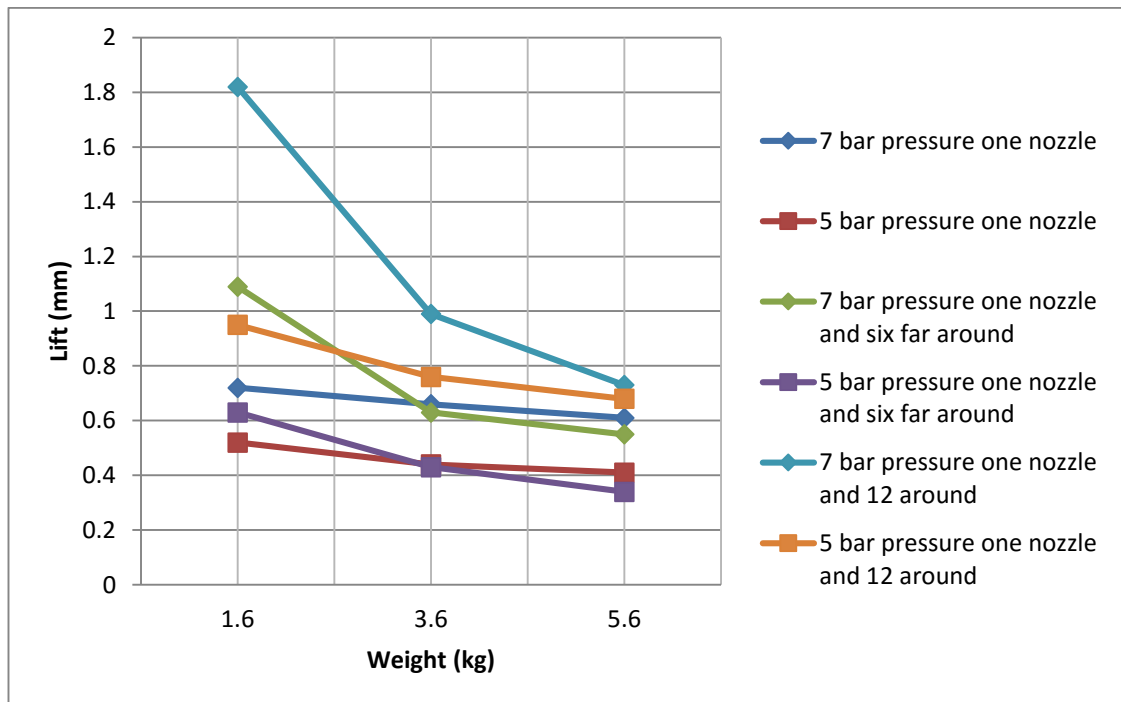


Figure 4-19 Lifts against weights for three different distribution of nozzles to the bottom plate

Figure 4-19 shows how the changes in the number of nozzles for air bearing affect the total gap lifts. With reference to the results from this set of tests, it is understood that the

device with 13 number of nozzles has the best performance in terms of lifting the weights. However, the increase in number of nozzles can not necessarily benefit the level of performance for this particular air bearing as the air bearing with one nozzle to the centre and six nozzles far around produces less lifting than the air bearing with just one nozzle to the centre does, in small loading conditions. This is because - in small loadings - the gap between cylinder and the ground is high and it forces the air to escape from six outer nozzles easier and hence, less effectiveness on producing lift. In such circumstances one single nozzle in centre produces better lift.

The other purpose of this test has been the investigation of the effects of pressure on the performance of air bearing. Therefore, two different pressure (5 and 7 bar) have been examined on the options for the third nozzle arrangement (one at the centre and 12 around). Figure 4-20 shows the trends how the lifting capacity of a specific air bearing can be different based on changes in pressure. The trends in this figure give an insight into choosing a desire pressure when lifting larger loads. It is understood that 5 bar pressure produces better consistency when larger loads are considered. This could be due to lower gap height and negative influence of shock waves in 7 bar pressure compared to the 5 bar pressure. Therefore, and based on these findings, 5 bar pressure is chosen for dynamic tests on the structure.

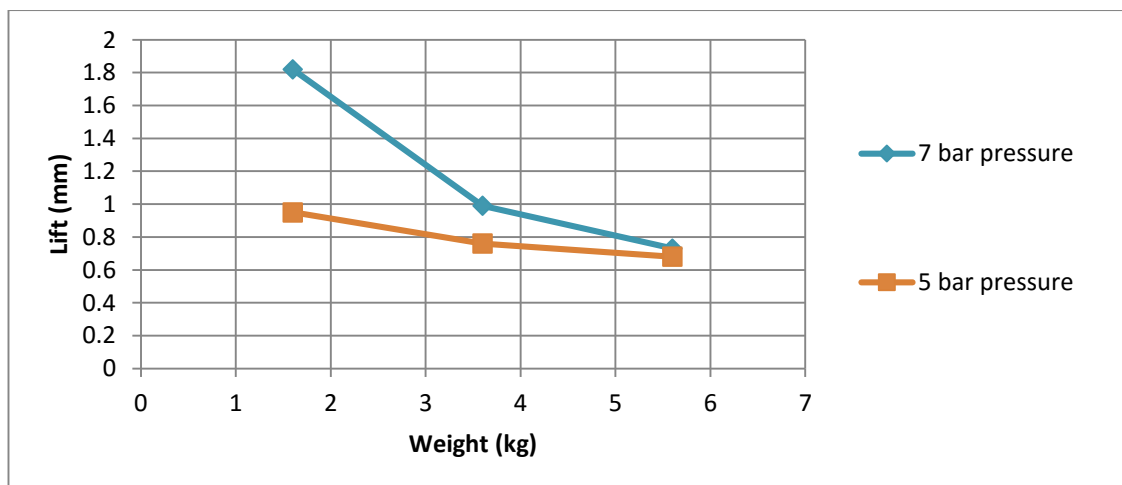


Figure 4-20 Different pressures on air bearing with one nozzle at the centre and 12 around

4.6 Validation

Validation of the results from numerical study with respect to the results from experimental observations is presented here.

4.6.1 Numerical study and experiments

The parameter which can be investigated in this part is Mass-flow rate. The defined mass flow rate of the compressor, used for producing pressurised air, can be obtained from its data sheets (appendix A.6 Air pump specifications). The actual mass flow rate of the compressor is calculated with respect to the volume rate of flow given by its manual as 1665 Litre per second at 5bar pressure. Since the mass density of air is known (1.225 kg/m^3), the actual mass flow rate of the flow is simply calculated as 0.034 kg/sec. Comparing the numerical derived mass flow rates to the actual mass flow rate of compressor, shows reasonable agreement and accuracy for numerical simulations.

Table 4-7 Comparison of mass flow rates (kg/s)

Nozzle type	Numerical	Actual	Difference
2-3	0.0313	0.034	7.99%
2-6	0.0388	0.034	14.11%
2-12	0.0327	0.034	3.7%

Table above shows that there is less than 15% errors in all cases. Although, the compressor data sheet does not provide mass flow rates for different pressure ratios corresponding to different nozzle geometries, it is anticipated that there will be less error in mass flow rate calculations if the data for different pressure ratio is available.

4.6.2 Numerical validations

To validate the numerical study, following tests were conducted.

4.6.2.1 Grid dependency

One of the most important parameters that affects accuracy of the CFD solutions is the quality of numerical grid. Grid dependency tests has been conducted on all cases where

extra numbers of mesh did not provide any change to the solutions. It is important for the refinement to be substantial and systematic. Systematic refinement means that the grid is refined in all direction with the same ratio. The number of cells that are used for these simulations were two, three and four million that the three-million cell showed the best and robust results.

4.6.2.2 *Y-plus distribution*

The Boundary layer is almost laminar in viscous sub-layer and fully turbulent in log-law region. As mentioned before turbulence models are valid for fully turbulent flows, therefore semi empirical formulas “wall functions”, are used to model flow properties between the wall and log-law region. In log-law region the profile is

$$u^+ = \frac{1}{\kappa} \ln y^+ + B = \frac{\bar{u}}{u_\tau} \quad (4.39)$$

where κ is von Karman constant ($\kappa = 0.41$), u_τ is the shear velocity given by $u_\tau = \sqrt{|\tau_w|/\rho}$ and τ_w is the shear stress at the wall, \bar{u} is the mean velocity parallel to the wall, B is an empirical constant related to the thickness of viscous sublayer and y^+ is dimensionless parameter which shows distance from the wall and is defined as

$$y^+ = \frac{\rho u_\tau y}{\mu} \quad (4.40)$$

In viscous sublayer $u^+ = y^+$ but in buffer layer where $5 < y^+ < 30$, neither law holds. In buffer layer the effect of viscosity and turbulent are equally important.

For turbulence modelling spatial considerations are required for grid resolution near the wall. y^+ values need to be in log-law region; therefore, it was important to keep the y^+ values around thirty. This has been achieved with especial consideration for near wall meshes.

4.7 Conclusion

In this chapter design and development of the air-bearing device needed for experimental study for the research were discussed. It was explained that how the

numerical modelling can help in saving time and costs for designing a device which works with the principles of fluid's flow.

According to the results obtained from controlled laboratory tests compared to those obtained from numerical modelling, it was concluded that the best option for nozzle conical shape is 2 mm diameter inlet and 6 mm diameter outlet. This conclusion stands for the purpose of handling heavier load at the same pressure on the proposed geometry for air-bearing device.

Although the numerical model has its own limitations such as lack of dynamic mesh generator, it has been a useful tool for a comparative study which played a valuable role to determine the size and shape of nozzles.

Findings from laboratory tests were considered as validations for numerical modelling. The results from laboratory tests were further used for determination of the number of nozzles being implemented on the air-bearing device. The optimum number and position for nozzles were then chosen as 13 nozzles.

It was also concluded that the best pressure is 5 bar in comparison to 7 bar pressure (two available stable levels of pressure can be provided in the lab) for taking larger loads.

5 Experimental study on the model structure

5.1 Introduction

An original investigation has been undertaken in order to gain an insight into the dynamic behaviour of the scaled model in practice. In this chapter, specifications of the model and measurement devices, tests' method, tests' results and analysis of results are presented. The empirical results from laboratory tests are used for validation of findings from analytical analyses and further comparisons with numerical simulations.

5.1.1 Experimental study (general argument)

An experimental study is an investigation procedure performed to verify, disprove, or establish the validity of a hypothesis. The experimental study is usually conducted to test a particular conjecture which is defined as an expectation or assumption about how a particular phenomenon or process works. However, in some cases, an experiment may also be carried out without a specific prediction or expectation about what the experiment is supposed to reveal. Experiments can also provide insight into reasons and effects of a phenomenon by explaining what outcome occurs when a particular factor is changed. The results of an experiment - if it is carefully conducted – can support or disprove the hypothesis (Popper, 2002).

In the scientific methods of experimental studies, an experiment is an empirical procedure that adjudicates between contending models or hypotheses (Cooperstock,

2009) (Griffith, 2001). Researchers also conduct experimental study to test existing theories or new suppositions to support or disprove them (Wilczek & Devine, 2006).

The primary component of a scientific method in physical sciences and in engineering is experimental study. Experiments are used to test how hypothesis and theories about a physical process work under particular conditions. Experimental works in engineering usually replicate identical procedures in hopes of producing identical results.

5.1.1.1 General principles of an experimental study

There are different ways of outlining the components of an experimental study with respect to scientific methods in engineering sciences. The following classification of components are generally agreed by scientific community and philosophers of science (Jevons, 1958) (Godfrey-Smith, 2003) (Ørsted, 1998):

Characterizations: definitions, observation, and measurements of the problem or subject of inquiry.

Hypotheses: hypothetical or theoretical explanations of observations and measurements of the problem or the subject of inquiry.

Predictions: including deductive reasoning from the theory or hypothesis.

Experiments: tests of the subject of inquiry with respect to above mentioned statements.

The methodological elements and organization of procedures mentioned above tend to be more applicable to natural sciences than social sciences.

It is difficult to formulate the statement of method, however, it is often presented as a sequence of steps as follow:

- Making hypotheses or conjectures
- Deriving predictions from hypotheses as logical consequences
- Performing experiments based on predictions

5.1.2 Experimental study for this research

The purpose of this research is defined as introduction of an innovative system for seismic base isolation. The new system which was introduced in chapter 3 is based on the advantages of air bearing for isolation. This is supported by the theory of producing a thin layer of air underneath of a structure and above its base to decouple the structure from horizontal movements. In order to predict the behaviour of the structure in isolated conditions, the analytical model was introduced and explained in chapter 3. For supporting the hypothesis experimental study has been conducted and will be explained in details in this chapter.

The method for the experimental study in this research is in accordance with the general principles mentioned in the previous section as follow:

5.1.2.1 Formulating the question

The question can be very specific in scientific methods of experimental study. In this research the key question arose from the gap of the knowledge with respect to the dynamic behaviour of structures under earthquake loadings. That is finding a better way of seismic isolation which overcome the drawbacks of current system along with keeping the advantages known for those systems. The new system then was defined with respect to the principles of seismic isolations (i.e. lengthening the fundamental period and imposing some levels of damping) and state of the art technology (i.e. air bearing and early warning system).

5.1.2.2 Hypothesis

A hypothesis is defined based on the knowledge obtained through formulating the question. The hypothesis might be very specific, or be the desired outcome.

“A scientific hypothesis must be falsifiable, meaning that one can identify a possible outcome of an experiment that conflicts with predictions deduced from the hypothesis; otherwise, it cannot be meaningfully tested” (Popper, 2002).

Hypothesis in this study explain the dynamic behaviour of the scaled model structure in which it is assume that the response of the structure to dynamic loads are reduced and

damages are alleviated. The hypothesis is defined based on established theories of structural analysis.

5.1.2.3 Prediction

Determining the logical consequences of the hypothesis is involved in this step. It is typical to select one or more predictions and conduct further testing. In this research, the fundamental frequencies and periods of a structure and structural response (displacement and acceleration) were predicted through an analytical model analysis, and damping was to be measured as unpredicted value.

5.1.2.4 Testing

Experimental test involves investigation of whether the real world behaves as predicted by the hypothesis. The purpose is to determine whether observations of the real world are in agreement or disagreement with the predictions derived from a hypothesis. In this research the relevant dynamic tests were conducted to determine the fundamental frequencies of the structure in isolated and unisolated modes and to perform a comparative study on the response of the structure in two different conditions of base (fixed and isolated) with applying three different loadings.

5.1.2.5 Analysis

Analysis determines what the results of conducted tests show and what they mean to the researcher. The analysis of results decide if the evidence has falsified the hypothesis or they support the hypothesis. In this research, the analyses were performed on the results obtained from tests and consequently, the final conclusion on whether the evidences are strong enough, to support the robustness of the new proposed isolation system, was drawn.

5.2 Test rig

The test rig configuration comprises of the scaled structure and proposed isolation system. The proposed test rig satisfies the following criteria:

- Tests are suitable for the scaled model.
- Tests replicate the same vibration observed in the real conditions.
- The structure does not experience unrealistically high loading that might change the failure mechanism.
- The test specification is suitable for laboratory based testing and appropriate for analytical and numerical modelling evaluations.

In this research free vibration tests on the scaled structure are considered in order to observe the dynamic behaviour of the scaled structure to compare with analytical and numerical simulations.

5.3 Dynamic test

Dynamic tests involve measuring the dynamic response of a structure to excitation. This includes free vibration tests and force vibration tests.

There are different methods of generating excitation for free vibration test. The simplest way is employing ambient excitation, produced from earthquake, wind or traffic. The main drawback in this approach is the lack of control over amplitude, direction and duration of applied loading. Another approach is the snap-back test in which a structure is suddenly released from an imposed initial loading or displacement and the ensuing free vibration recorded in terms of acceleration or displacement (Butterworth, et al., 2004).

The most well-known force vibration test is shaking table test, in which a mechanical exciter applies a varying force of known frequency and amplitude to a designated basement on which the structure is mounted. Shake tables for dynamic test purposes are also able to produce simulated ground motions, including reproduction of previous earthquake records.

With respect to the aims and objectives of this research, the scope of experimental study was defined to

- verify the fundamental frequency of the structure,
- perform a comparative study on the maximum acceleration and story drifts exerted in the structure due to similar loading conditions and different base configuration (isolated and unisolated), and
- extracting damping properties of the structure.

In order to accomplish these pre-defined goals, the method of snap-back test is chosen for dynamic tests (Figure 5-1). As it is shown in figure below, an initial displacement (due to the hanged mass) is applied on top of the structure. As a result of a sudden release of the mass (cutting the rope) the structure vibrates on its natural frequency (free vibration).

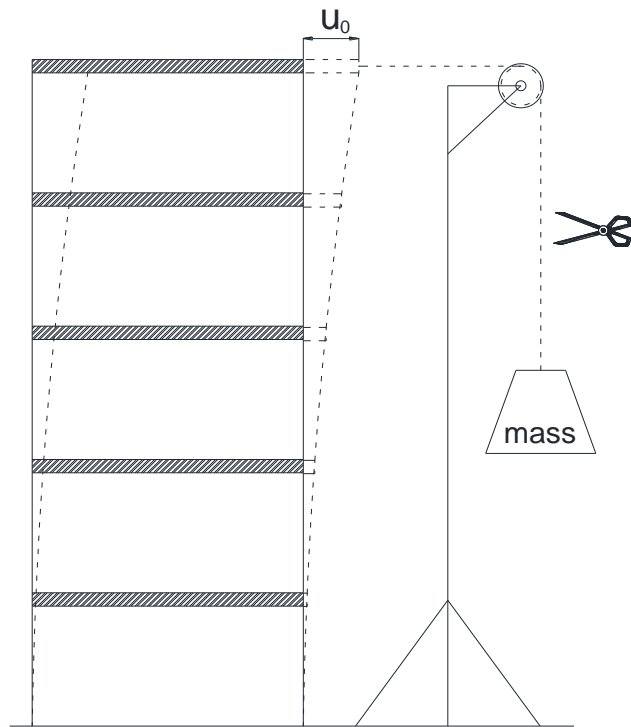


Figure 5-1 Schematic view of the snap-back test

In order to observe the performance of the proposed isolation system designed for the scaled structure, it is necessary to investigate the dynamic behaviour of the structure. To

gain an insight into dynamic behaviour of the structure, experimental tests in two different sets with two different base configurations were performed on the structure.

Tests were conducted with three different loading 5kgf, 10kgf and 15kgf. The input level of the force was adjusted to make certain that the natural frequency of the structure is triggered and for comparative study. The adjustment allowed to achieve near maximum accelerations and also to maintain the response of the structure within a range predetermined for linear behaviour.

5.4 Tests' procedure

The experimental testing was completed in six sessions, three sessions for each base condition (isolated and unisolated); each session corresponds to different loading (5kgf, 10kgf and 15kgf).

The procedure was designed to test the structure with fixed-base configuration first (Figure 5-2). Upon completion of testing fixed-base structure, the structural base configuration was changed to isolated condition with installing the isolation devices to the designated points as shown in Figure 5-3.



Figure 5-2 Fixed-base configuration

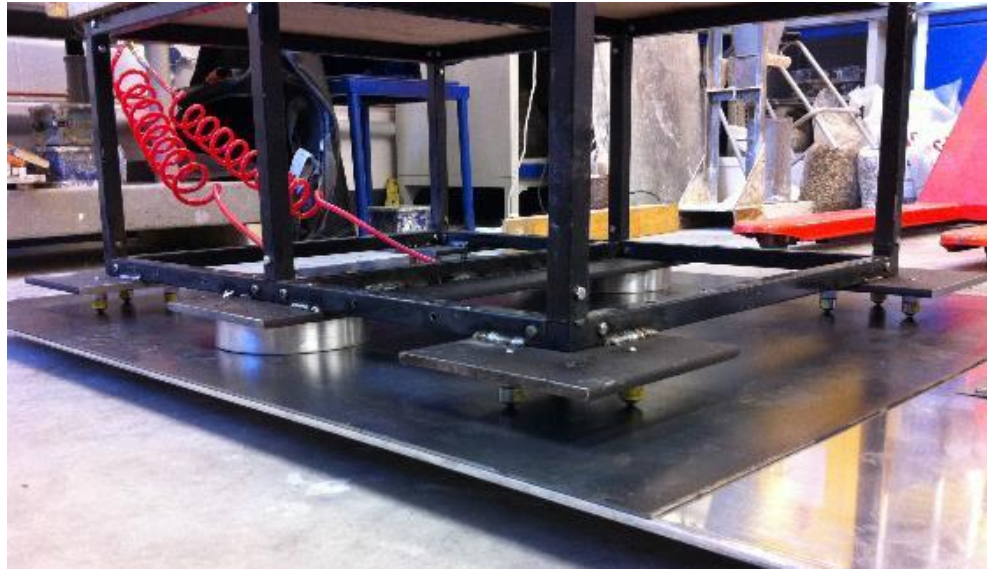


Figure 5-3 Base-isolated configuration

5.4.1 Fixed base

The first set corresponds to the structure with Fixed-base configurations, meaning that the structure is fixed to the grounds underneath through thick steel base plates and strong screw bolts at the bottom of each column as shown in Figure 5-32.

This is identical to the conditions of ordinary foundations in which the columns at base are fixed to their foundation with translational and rotational constraints.

5.4.2 Base isolated

The second set of tests corresponds to the structure with Base-isolated configurations, meaning that the columns at base are connected to the isolation system through the thick base plates as shown in Figure 5-3. The isolation system then decouples the super-structure from the ground underneath.

5.5 Measurement devices

The measurement devices were provided by a Swiss company namely GeoSIG, specialist in dynamic measuring and structural monitoring solutions. The measurement devices' are listed below with details of their functionality.

5.5.1 Data acquisition

GMSplus as the latest generation of GeoSIG measurement systems is used for acquiring data from accelerometers. The main advantages can be summarised as high performance, flexibility in operation and enhanced connectivity. The instrument is equipped with software which processes data in real time. As a self-contained instrument GMSplus is supplied with an uninterruptible power-supply (A 12 VDC, 7.0 Ah battery), which can provide more than 24 hours autonomy. The external power supply cable (100-240 VAC) will be used to connect the instrument to the main. The instrument is capable of being connected to a desktop or laptop through its ports and relevant cable. It includes an ethernet cable and connector to ensure fast and reliable data transfer (GeoSIG, 2015). Full specifications and certificate of calibration are given in appendix A.7 GMSplus specifications and calibration.

5.5.2 Sensors

Accelerometers have been chosen as the sensor of measurements, as acceleration recorded data are easily convertible to other parameters such as velocity and displacement. AC-43 accelerometer types are used for acceleration measurements with full scale range of $\pm 2g$ and up to 100Hz bandwidth. The accelerometer type is MEMS Force Balance Accelerometer with dynamic range of 95dB. The AC-43 accelerometer works based on the modern MEMS (Micro Electro-Mechanical Systems) technology, in which sensing cells are assembled in a way that optimizes their performances. MEMS cells include linear accelerometer sensing elements which measure the capacitance variation in response to any movement or inclination and a factory trimmed interface chip that converts the capacitance variations into analogue or digital signal proportional to the motion (GeoSIG, 2013). Sensors should be tested and calibrated prior to start the tests to ensure reliable data records. Hence, accelerometers verification tests and

calibrations have been carried out by GeoSIG. Full specifications and calibration certificates are given in appendix A.8 Accelerometer specifications and calibration.

5.5.3 Data communication software

The software used for data communication is GeoDAS, the product of GeoSIG. The software enables users to obtain recorded data and view the diagrams and perform some analyses. The program is basically used for acquisition of data provided by any standard GeoSIG instrument and also for instrument configuration. An RS-232 cable with USB converter is provided along with the software for communication between data acquisition system and computer.

5.6 Data analysis and results

By analysing signals from measurement devices, one can learn more about the nature of the vibration of the structure. Data analysis in this case is basically divided into two parts; *Time domain* and *frequency domain* analysis; each of which provides a different view or insight into the mechanism of the vibration of the structure.

Time domain analysis is the study of signals (accelerations or displacement records) as a function of time. The plot of vibration parameters (acceleration, velocity or displacement) versus time provides information needed for characterization of the dynamic behaviour of a structure in terms of detecting the peaks levels or identifying the periods and furthermore, estimating the decay rate. These are known as the typical results of time domain analysis.

Frequency domain analysis refers to the study of signals as function of frequency which provides the plot of vibration parameters (or square root of them or other common types of representation) versus frequency. It is possible to transform any time history signal into the frequency domain. The most well-known mathematical transformation technique of time signals is Fourier Transformation after the French mathematician Jean-Baptiste Joseph Fourier (Sterken, 2003). Fourier Transform is based on the assumption that any periodic signal can be represented in the form of a series of sine

waves; each of which has its own frequency and peaks. In vibration analysis of a structure, these peaks and their frequencies are important and meaningful.

The next sections discuss the vibration data obtained from the experimental tests on the scaled structure. The data are represented in the form of acceleration and displacement signals in time domain and analysed data in frequency domain.

5.6.1 Absolute acceleration on top of the structure

In this section, the experimental results are presented in the form of a comparison of the absolute acceleration on top of the structure due to specific loading in both fixed base and isolated conditions. As mentioned before three snap-back test runs were performed for each base condition which included a specific load in magnitude (5kgf, 10kgf and 15kgf) applied to the structure in order to ensure that the first two fundamental frequencies of vibration are triggered; and to check the effects of increase in applied load on natural frequencies for further validations.

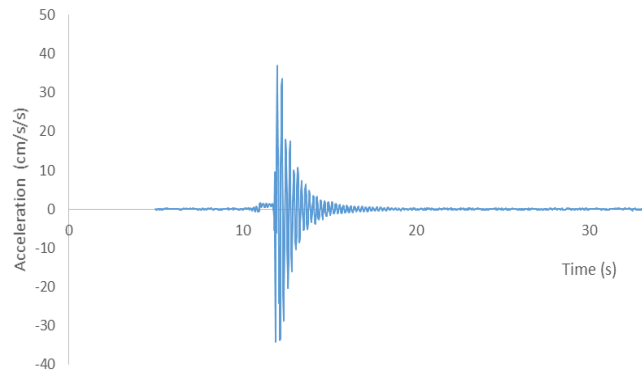


Figure 5-4 Acceleration on top of the structure in horizontal direction due to 5kgf snap-back test (Fixed-base); maximum absolute value = 36.96 cm/s²

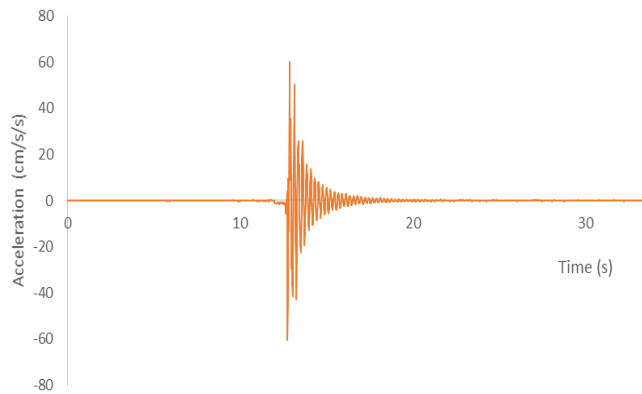


Figure 5-5 Acceleration on top of the structure in horizontal direction due to 10kgf snap-back test (Fixed-base); maximum absolute value = 60.65 cm/s²

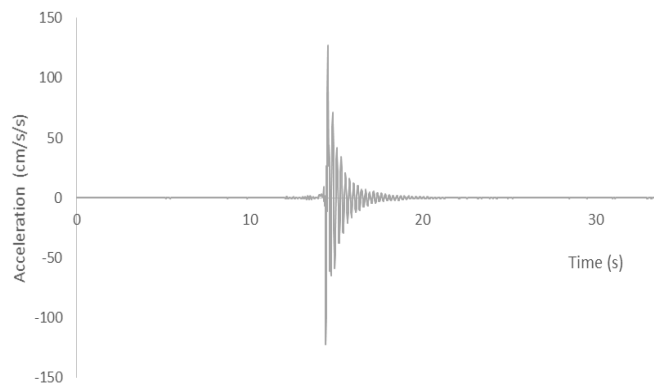


Figure 5-6 Acceleration on top of the structure in horizontal direction due to 15kgf snap-back test (Fixed-base); maximum absolute value = 126.82 cm/s²

Figure 5-4 to Figure 5-6 show the magnitude of accelerations on top of the structure (5th story) due to application of 5kgf, 10kgf and 15kgf respectively in horizontal direction in snap-back tests. Figure 5-7 illustrated how the maximum acceleration experienced on

top of the structure can be affected by magnitude of applied load. As it was expected, the greater the applied load in snap-back test, the greater magnitude of acceleration is exerted to the structure. This further confirms the consistency of the structural system of the scaled model.

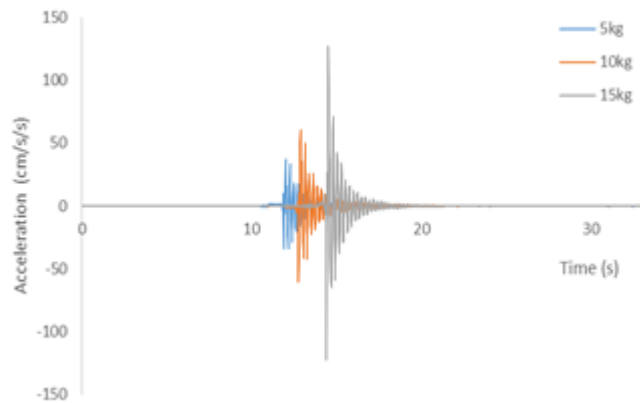
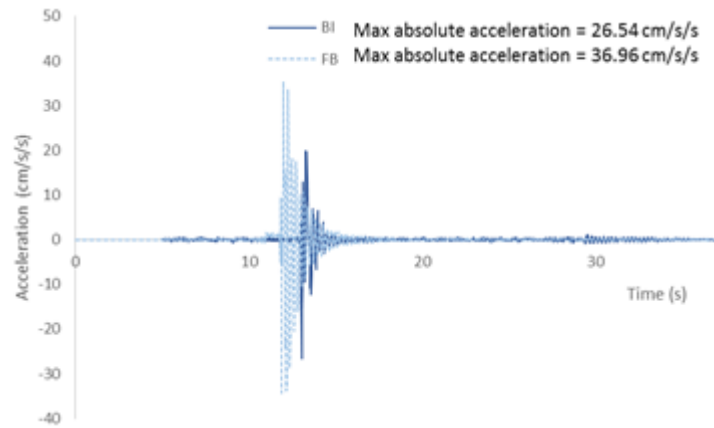


Figure 5-7 The effects of applied load magnitudes in accelerations experienced on top of the structure (Fixed-base conditions)

It is understood that the maximum absolute acceleration is increased by 77% when the applied load is increased by 100% from 5kgf to 10kgf; likewise the increase in acceleration is 270% when the applied load is increased by 300% from 5kgf to 15 kgf.

By changing the conditions of base from fixed to isolated, it is expected that the maximum absolute acceleration exhibits some levels of reduction. Figure 5-8 to Figure 5-10 show how the acceleration experienced on top of the structure is reduced thanks to the new base isolation system. Reduction in levels of acceleration on the structure is a must for any seismic isolated system and as it was discussed earlier, base isolation solution is the best known way of practice in this area. It was observed that the present isolation system exhibits a great performance in reduction of absolute acceleration and therefore, is able to reduce the potential structural damage.



**Figure 5-8 Acceleration on top of the structure due to 5kgf in snap-back test;
Fixed base (FB) and Base isolated (BI) conditions**

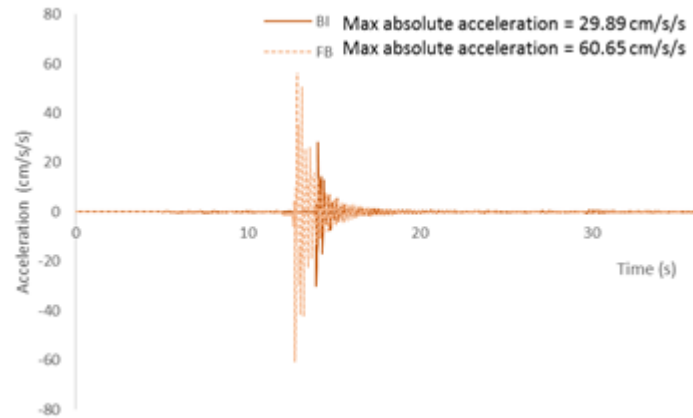


**Figure 5-9 Acceleration on top of the structure due to 10kgf in snap-back test;
Fixed base (FB) and Base isolated (BI) conditions**

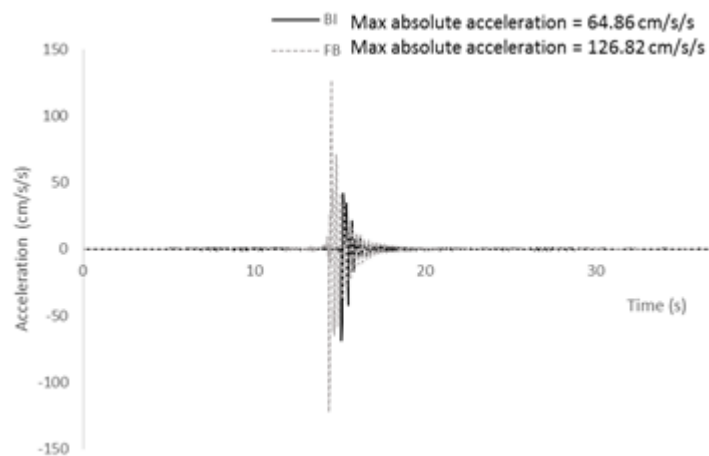


**Figure 5-10 Acceleration on top of the structure due to 15kgf in snap-back test;
Fixed base (FB) and Base isolated (BI) conditions**

Results of acceleration response confirms the reduction of 28%, 51% and 49% in absolute acceleration in snap-back test for 5kgf, 10kf and 15kgf respectively. Therefore, the present isolation system demonstrates adequate level of isolation and exhibit a great performance against horizontal input. The performance of the structure against different types of earthquake is investigated through numerical simulation and results are given and discussd in the next chapter.

5.6.2 Natural frequencies and periods

The natural frequencies of a structure demonstrate the sensitivity of the structure to different loading frequencies. If the loading frequencies coincide with the natural frequencies of a structure, its vibration increases dramatically which increase the acceleratin in the structure (resonance). In order to reduce the resonance effect, one way is to shift the fundamendl fresquency of the structure to a smaller one. Base-isolation systems - if applied appropriately – can shorten the natural frequency of vibration of the structure to smaller one (far from the devastating frequency of earthquake shocks) by providing a layer of low horizontal stiffness to the base of the structure. This is investigated in this chapter by anlysis of the data obtained from experimental laboratory tests on the scaled structure in the workshop.

Data analysed in the last section were in time domain; if data in time domain are transferred to frequency domain with using Fast Furier Transformation, it is possible to analyse data in frequency domain and the analysis is called Frequency Response Analysis. The peaks in frequency response diagrams then reperesent the natural frequency of vibration of the structure (Avitabile, 2001).

5.6.2.1 Fast Fourier Transformation (FFT)

FFT is refered to as the discrete Fourier Transform (DFT) of a collected block of time signal which represents the frequency spectrum of the time signal. It computes the DFT of a sequence rapidly by factorizing the DFT matrix into a product of mostly zero factors (Ramirez, 1975). In order to transform real data readings from time domain to frequency domain it is necessary to know the number of points, intervals and sampling rates (Harris, 1978). The time-frequency relationship is as follow:

- if data is sampled at N equi-spaced points in time domain, where $n = 0, 1, \dots, N-1$, then the time signal consists of N real numbers; therefore, if the time interval between samples is known as dt , the total length of the sample record is T and $T = N.dt$.
- if the sampling rate (the number of readings per time unit) is equal to f_s , there will be $f_s/2$ number of data at positive frequencies and $f_s/2$ number of data at negative frequencies where, $f_s = N/T$.
- if the frequency resolution (frequency separation of the data points) is considered as df , the bandwidth (the maximum frequency of the display) is equal to F_{max} and $F_{max} = f_s/2 = (N/2).df$.

therefore, the time and frequency domain relationship is defined as

$$dt = \frac{1}{2F_{max}} \text{ (secs)} \quad (5.1)$$

$$df = \frac{1}{T} \text{ (Hz)} \quad (5.2)$$

In the laboratory tests conducted for this study, accelerometers with sampling rate of 50 per seconds are used which determines the time increments of 0.02s and the bandwidth of 25Hz. The algorithm of FFT and MATLAB implementation code for frequency response analysis of this part is given in appendix A9.

The results from FFT analysis of acquired data from snap-back tests on the scaled structure are presented here with relevant discussion. The most important understanding from frequency response analysis is perhaps, detection of fundamental frequency of vibration. This is the position of the peaks (regardless of its unit) on the frequency axis and is obtainable by analysing the recorded displacement values on top of the structure (5th story). Figure 5-11 demonstrates the fundamental frequencies of the structure in fixed-base (FB) and base-isolated (BI) conditions.

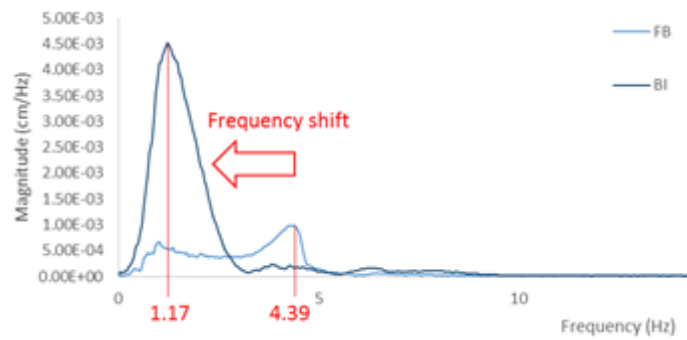


Figure 5-11 The effect of isolation system in shifting the fundamental frequency of the structure to a lower one

It is understood from Figure 5-11 that the isolation system shifts the fundamental frequency of the structure to a smaller one. It means that the isolation system shifts the fundamental period of vibration of the structure to a longer one from 0.228s to 0.855s. Therefore, the adequate isolation performance of the system is confirmed.

The results are also in accordance with what were expected from analytical model of the structure presented in chapter 3 of this dissertation. It was predicted that the fundamental periods of the structure in fixed-base and base-isolated conditions should be around 0.204s and 0.827s respectively (section 3.6.2). It is now confirmed that the fundamental periods of the vibration of the structure are 0.228s and 0.855s for fixed-base and base-isolated respectively. The results of experimental study therefore show the difference of 10% for fixed-base and 3.3% for base-isolated conditions in the value of fundamental periods in comparison to the analytical model of the structure.

It is understood from the diagram of frequency response in Figure 5-11 that the maximum displacement on top of the structure is increased in isolated structure. This increase in displacement was predictable as adding a layer of low stiffness to the base of the structure, simply means that the maximum absolute displacement on each story tends to increase with respect to the fact that the isolation stiffness is considerably lower than the stiffness of each story. Therefore, it is expected that the structure moves more like a rigid body when isolated. This can be observed when considering the displacement response of the top three stories at their peaks.

5.6.3 Story drifts

Inter – story drifts is defined as the relative displacement between two adjacent stories at a certain time and is known as one of the important causes of structural damage (Wu & Samali, 2002). In order to gain an insight into the performance of the structure when subject to a certain loading condition in fixed-base and base-isolated settings, the relative displacements are investigated and compared. By double integration of acceleration values obtained from accelerometer readings, the displacement values are calculated.

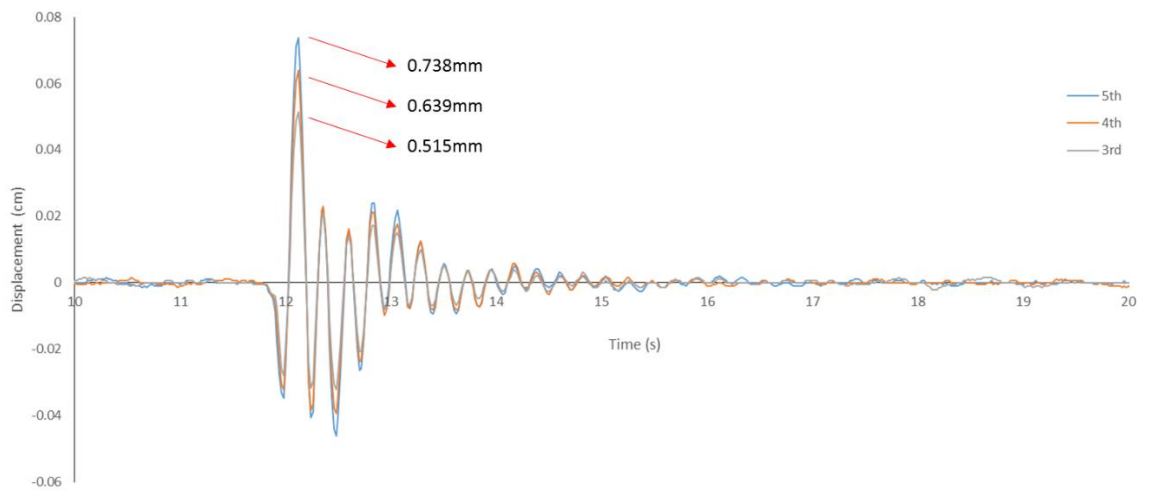


Figure 5-12 Displacement values on top three levels of the structure in snap-back test (5kgf), in Fixed-base condition

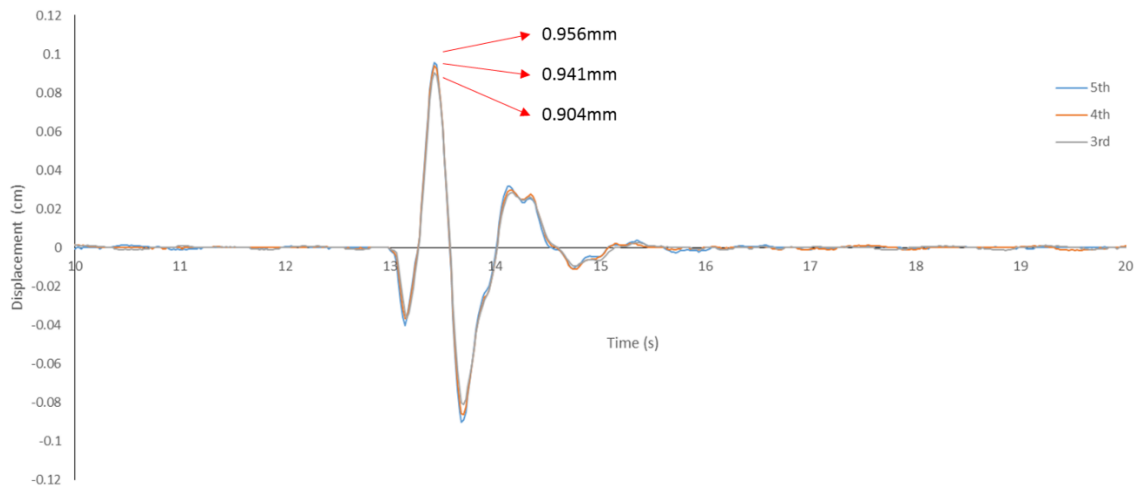


Figure 5-13 Displacement values on top three levels of the structure in snap-back test (5kgf), in Base-isolated conditions

Table 5-1 Story drifts on top of the structure in Fixed-base (FB) and Base-isolated (BI) conditions in snap-back test with 5kgf

FB	Displacement (mm)	Drifts (mm)	BI	Displacement (mm)	Drifts (mm)
Story			Story		
5 th	0.738	0.099	5 th	0.956	0.015
4 th	0.639	0.124	4 th	0.941	0.037
3 rd	0.515	-	3 rd	0.904	-

Figure 5-12 and Figure 5-13 are depicting the graph of displacement values in time domain when the structure is subject to the same loading conditions and different base configurations. Table 5-1 shows the values of absolute displacements on top three levels of the structure and calculated story drifts.

It can be seen that the base-isolated model demonstrates a dramatic reduction in the story drifts. These are 85% reduction for fifth story and 70% for the fourth story. This reduction implies that there would be a much lower level of structural damage in isolated structure compare to unisolated structure when the structure is subject to a horizontal load as a result of the reduction in horizontal relative displacement exerted in the structure.

Figure 5-14 and Figure 5-15 show the displacement time-history response of the structure on top three stories and Table 5-2 compares the results. Great reductions in story drifts are again observed; the story drift corresponds to the 5th story demonstrates 43% reduction in isolated conditions compare to unisolated conditions. Likewise the drift corresponds to 4th story is reduced by 41%.

In order to gain an insight into the sensitivity of structure to greater loading in snap-back test, the tests have been run for 15kgf and the results are shown in Figure 5-16 and Figure 5-17; the comparison of results are given in Table 5-3.

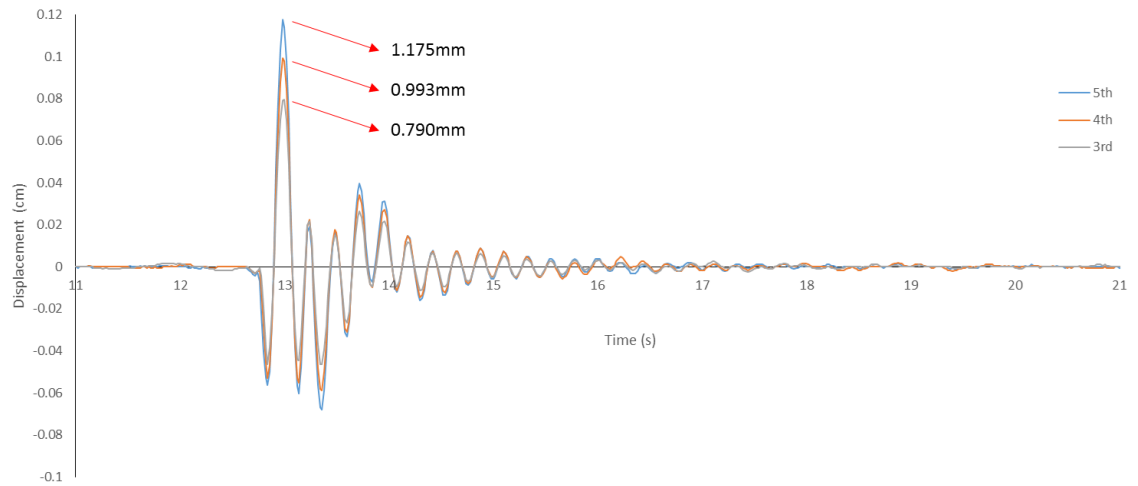


Figure 5-14 Displacement values on top three levels of the structure in snap-back test (10kgf), in Fixed-base condition

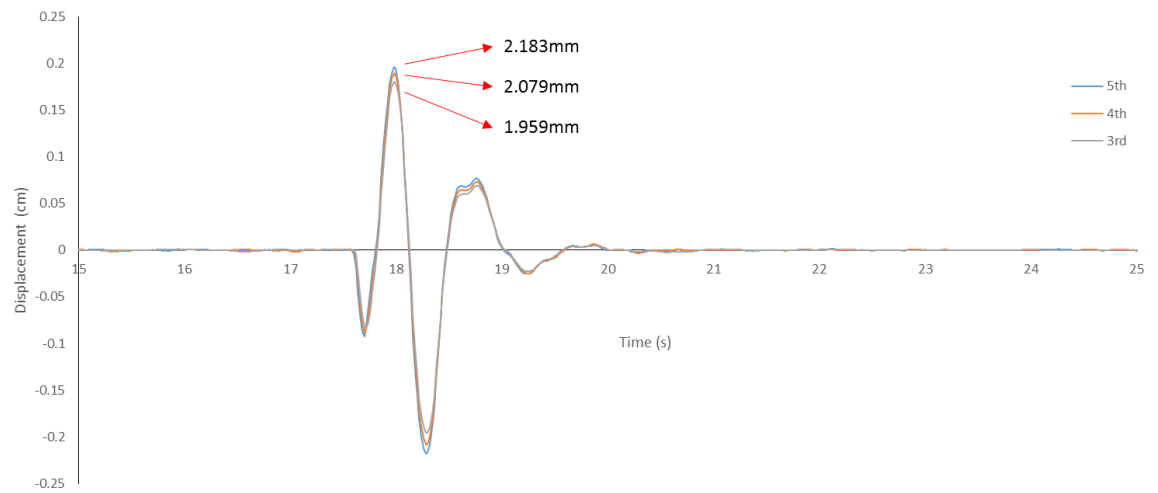


Figure 5-15 Displacement values on top three levels of the structure in snap-back test (10kgf), in Base-isolated conditions

Table 5-2 Story drifts on top of the structure in Fixed-base (FB) and Base-isolated (BI) conditions in snap-back test with 10kgf

FB	Displacement (mm)	Drifts (mm)	BI	Displacement (mm)	Drifts (mm)
Story			Story		
5 th	1.175	0.182	5 th	2.183	0.104
4 th	0.993	0.203	4 th	2.079	0.120
3 rd	0.790	-	3 rd	1.959	-

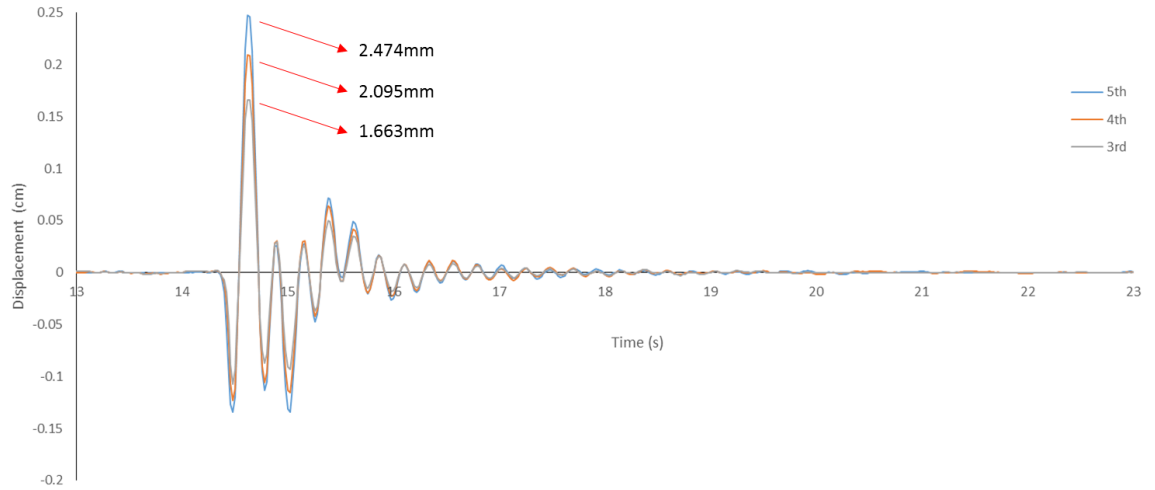


Figure 5-16 Displacement values on top three levels of the structure in snap-back test (15kgf), in Fixed-base condition

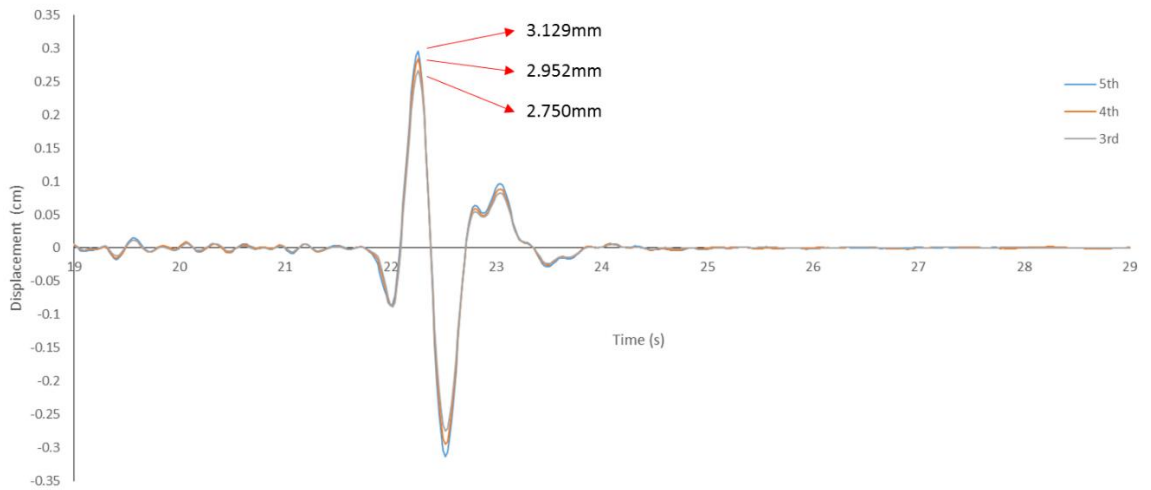


Figure 5-17 Displacement values on top three levels of the structure in snap-back test (15kgf), in Base-isolated conditions

Table 5-3 Story drifts on top of the structure in Fixed-base (FB) and Base-isolated (BI) conditions in snap-back test with 15kgf

FB	Displacement (mm)	Drifts (mm)	BI	Displacement (mm)	Drifts (mm)
Story			Story		
5 th	2.474	0.379	5 th	3.129	0.177
4 th	2.095	0.432	4 th	2.952	0.202
3 rd	1.663	-	3 rd	2.750	-

It is once again confirmed that the story drifts are reduced significantly (by 53% in both 5th and 4th level) in isolated structure. This implies that reduction in story drifts is an indisputable advantage of the proposed isolated system.

A comparison between the values of story drifts of structure subject to different amount of loadings suggests that the structure is more sensitive to the increase in loading when it is isolated. This will be investigated in the next chapter based on the results of numerical simulation of the structure subject to different earthquakes.

5.6.4 Damping

Damping values are empirical values that must be obtained by measurements. Damping is recognised as playing a major role in reduction of response and alleviation of the level of damage in a given structure. Even though, damping has been remained the most difficult dynamic property of the structure to predict when designing the structure. Unlike mass and stiffness, damping cannot be deducted from the physical property of the structure (Butterworth, et al., 2004). Accordingly, the assessment of damping relies mostly on measured data from experimental observations on the given structure or similar structures.

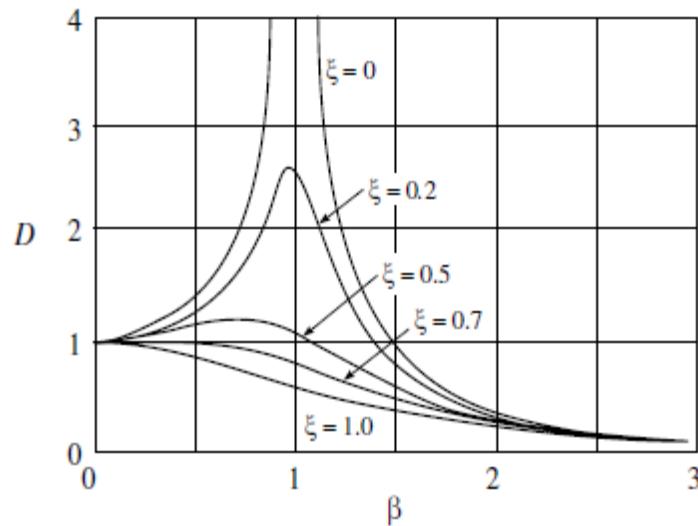


Figure 5-18 Effects of damping in response of the structures, where D denotes the response of the structure and β is the ratio of applied loading frequency to the natural free-vibration frequency (Clough & Penzien, 2003)

A structure with relatively low damping and with a natural frequency close to the natural frequency of the applied dynamic load could produce high level of damage under resonance conditions.

5.6.4.1 Definition

Damping in dynamic systems is defined as the phenomenon by which mechanical energy is dissipated (De Silva, 2007). The dissipated energy is usually converted into internal thermal energy. It is very important to gain a knowledge about the level of damping in a given structure. Damping properties will be used in structural analysis and further in structural tests and utilisations. Therefore, in order to develop a realistic dynamic model of a structure, the nature and level of damping should be known. It is also essential to have a good knowledge of system's damping when imposing dynamic environmental limitations is considered. The dynamic limitations involve maximum dynamic excitation the system can withstand under service conditions (De Silva, 2007). Moreover, knowledge of a system's damping is useful in making design modifications in systems with failure in acceptance tests.

In general, damping occurs through the dissipation of mechanical energy in vibrating system. Types of damping includes:

- Structural damping
- Material internal damping (viscoelastic and hysteretic)
- Viscous damping
- Interface damping
- Fluid damping
- Coulomb friction
- Stribeck damping

It is customary to represent various types of damping using equivalent viscous damping.

5.6.4.2 Measurement of damping

Two different approaches are known for measurement of damping in structures when time-history response of the structure is available; *time domain method* and *frequency domain method*.

In time domain methods the response of a structure which could be acceleration, velocity, or displacement is considered over a certain period of time. The damping ratio is then obtainable by employing relevant theories in vibration and appropriate calculations. There are three accepted methods for extracting damping from time history response of a structure (De Silva, 2007):

- Logarithmic decrement method
- Step-Response method
- Hysteresis loop method

In frequency domain methods the response of a structure versus different frequencies is considered as the source of calculations. Widely accepted methods of this approach are listed below (De Silva, 2007):

- Magnification factor method
- Bandwidth method

For structural analysis purposes when data of time-history response is available the most convenient way of estimating damping is *Logarithmic decrement method*. This method is used to measure the overall damping of a structure in this research.

5.6.4.3 Logarithmic decrement method

The method is perhaps the most popular one when using experimental data for measurement of damping. This method is basically used for single-degree-of-freedom (SDOF) systems but it can be also used for multiple-degree-of-freedom (MDOF) system when lower modes are targeted (Butterworth, et al., 2004).

When a system is excited by an impulse input which can be an initial condition (displacement or force), the system response takes the form of a time decay as

$$y(t) = y_0 \exp(-\zeta \omega_n t) \sin \omega_d t \quad (5.3)$$

Where,

$y(t)$ is the displacement response,

y_0 is the initial displacement,

ζ denotes damping ratio, and

ω_d represents the damped natural frequency and is given by

$$\omega_d = \sqrt{1 - \zeta^2} \omega_n \quad (5.4)$$

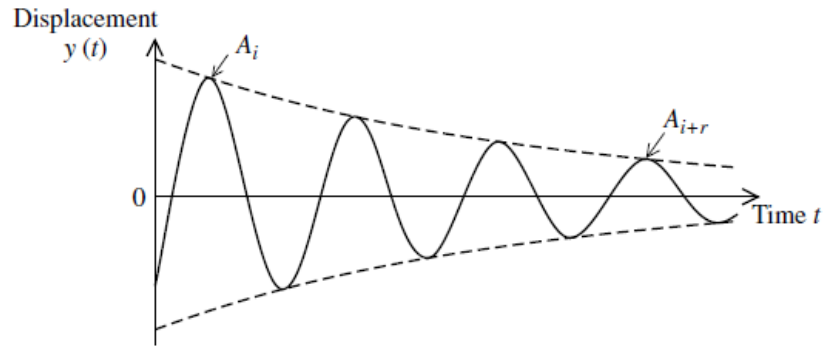


Figure 5-19 Impulse response of an oscillatory system (De Silva, 2007)

The response at $t = t_i$ can be denoted by y_i , and at $t = t_i + 2\pi r / \omega_d$ by y_{i+r} , thus, equation 5.3 can become

$$\frac{y_{i+r}}{y_i} = \exp\left(-\zeta \frac{\omega_n}{\omega_d} 2\pi r\right), \quad i = 1, 2, \dots, n \quad (5.5)$$

If A_i and A_{i+r} corresponds to the peak points in time decay function which are r cycles apart in time history (Figure 5-19), then,

$$\frac{A_{i+r}}{A_i} = \exp\left(-\zeta \frac{\omega_n}{\omega_d} 2\pi r\right) \quad (5.6)$$

Substitution of equation 5.4 in 5.6 gives

$$\frac{A_{i+r}}{A_i} = \exp\left(-\frac{\zeta}{\sqrt{1 - \zeta^2}} 2\pi r\right) \quad (5.7)$$

Then, the logarithmic decrement δ is given by

$$\delta = \frac{1}{r} \ln \left(\frac{A_i}{A_{i+r}} \right) = \frac{2\pi\zeta}{\sqrt{1 - \zeta^2}} \quad (5.8)$$

And damping ratio may be expressed as

$$\zeta = \frac{1}{\sqrt{1 + (2\pi/\delta)^2}} \quad (5.8)$$

For low damping ratios (typically under 10%), when $\omega_d \cong \omega_n$ the above equation becomes (De Silva, 2007)

$$\zeta = \frac{\delta}{2\pi} \quad (5.9)$$

Alternatively, when n cycles of damped vibration are needed for the amplitude to decay by a factor of k_d , in low damping ($\zeta < 0.1$)

$$\zeta = \frac{1}{2\pi n} \ln(k_d) \quad (5.10)$$

5.6.4.4 Results

The method of logarithmic increment is employed to measure overall damping of the structure for two different base configurations and three different impulse loadings. Figure 5-12 to Figure 5-17 are considered to determine the level of damping in each test. Results are presented in Table 5-4.

Table 5-4 Damping ratios extracting from displacement response of the structure

Base condition	Snap-back test loading (kgf)	Damping ratio (ζ) (% of critical)
Fix	5	5.9
	10	5.8
	15	6.5
Isolated	5	12.3
	10	12.4
	15	13.5

The above table reveals how the isolation system benefits the dynamic behaviour of the structure by damping the free vibrations (induced by an impulse force) and alleviation of shocks. The damping ratio is increased drastically for isolated structure, which is the direct result of isolation system. The unisolated structure exhibits around 6% damping ratio which is a reasonable level for a structure of this kind and the isolated structure shows 12% damping as a result of employing isolation system. The overall damping in the isolated structure is, indeed, the result of combination of *structural* damping and *isolation system* damping, yet it should not be confused with the sum of the two damping ratio. This means that the difference in the level of overall damping in the isolated structure compare to the unisolated structure (around 6%) does not necessarily denote the damping of isolation system (De Silva, 2007).

The table shows that there has been a slight increase in the level of damping when the applied force is increased. This is, in fact, due to the greater movement exerted in the structure due to greater loads and therefore, greater internal friction which produces more damping. This is in a good agreement with the work of Butterworth, et al. in 2004 (Butterworth, et al., 2004).

As it was discussed before, damping is beneficial for isolation systems. Any isolation system should demonstrate an increase in the level of overall damping in the given structure in practice. In this section it was shown - by the results obtained from practical tests – that the proposed isolation system provides the structure with a reasonable level of damping in vibrations. The empirical values of damping obtained from experimental tests will be further used in numerical simulation of the structure.

5.7 Conclusion

This chapter described and discussed the experimental study - the major part of this research - on a case study which is a scaled model of a five-story building. It was explained that how a hypothesis can be conducted in a scientific method through an experimental investigation.

The methods of experimental tests explained in this chapter can be used for further study as the followed approach (snap-back test) is categorised as a low-cost yet powerful procedures for extracting the dynamic parameters of a given structure.

The results from experimental study validated the findings from analytical model of the structure explained earlier in chapter 3. It was shown that the proposed isolation system is able to lengthen the fundamental period of a structure to a greater one which results in diminution in the level of peak acceleration exerted to the structure. It was also discussed that, however, the *maximum displacement* on top of the structure is increased by using the isolation system, *story drifts* are reduced by more than 40% in all cases (given loading conditions). Damping as an empirical parameter was measured with respect to the time-history response of the structure and employing *Logarithmic decrement* method. It was conclude that the proposed isolation system is able to increase the overall damping ratio from around 6% to 12%. The measured values for damping are further employed in numerical simulation.

In the chapter that follows, the numerical model of the building is described and the performance of the proposed isolation system under different earthquakes is investigated accordingly.

6 Computer simulation of the structure

6.1 Introduction

The numerical method enables researchers and engineers to solve complicated sets of equations and variables with numbers of constraints which all together define a problem. The time-history model of a structure is a mathematical model that uses numerical time-stepping procedure to obtain the structural behaviour over time. This will be a numerical simulation of sets of governing differential equations, obtained from physical parameters of the structure that cannot be solved analytically.

In investigation of the dynamic behaviour of a structure, it is common to generate a numerical simulation for a given building with respect to the development of computer technology these days. When study of the dynamic behaviour of a structure subjected to an earthquake or wind loads is considered, the best method is to examine a scaled real model of the given structure under scaled given loading. This approach which is possible through the use of shaking table in special fitted laboratories enable researchers to obtain the exact results. The drawback is that such facilities are not available everywhere and for everyone. In addition it is not possible and it is not rational to build a physical model for every given building. Therefore, the mathematical model of a structure is generated with respect to established physics laws. The physical model of the structures then can be represented with a mathematical model.

The mathematical model of a structure should be accurate and should simplify the problem with respect to the importance of parameters. Then the given problem is represented by sets of equations, variables and unknowns. The mathematical models of structures in dynamic analysis are not always simple to analyse as in majority of cases there are numbers of simultaneous differential equations to be solved. The analytical approach for solving the system of equations in these cases is almost impossible. Therefore, numerical methods are employed to solve the sets of equations and unknowns for a given problem.

The researcher or engineer who is looking at a problem in structural analysis can generate their own approach for a numerical solution of the given problem. However, there are programs and software available to be employed. One of the most powerful tools is SAP2000 which enables the user to perform dynamic analysis on a structure with respect to variety of parameters. One of the features this program provides is the use of previous earthquake records. The user can examine the target structure's dynamic behaviour under different past earthquake records. It is also possible to define an arbitrary dynamic loading in terms of force, acceleration or displacement to the program. Hence, the performance of a given structure can be investigated under the other earthquake records which are not available in the program predefined records.

In this research the numerical modelling of the structure is generated to gain an insight into its dynamic behaviour with and without proposed isolation system under different earthquakes. For this purpose, SAP2000 is chosen as the numerical simulator and analyser tool with respect to its ability in dynamic analysis.

The earthquake records are scaled by factor of 0.316 in time axis (according to scaling analysis, Table 3-1) to maintain the dynamic resemblance between the scaled model and real scale structure. The earthquake records are chosen from the records of past earthquakes with respect to their magnitude and duration.

6.2 Physical model

The physical model is what was explained in chapter 3, a scaled structure comprises of five story, in which the stories are linked through the columns.

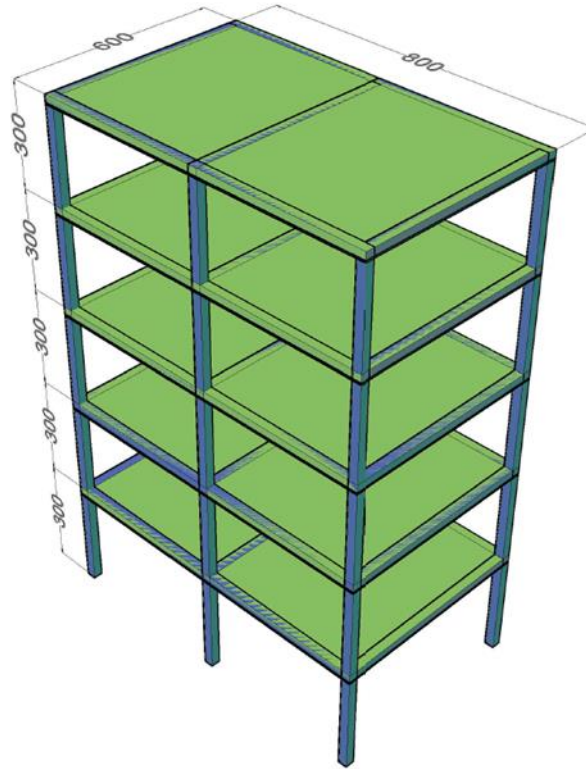


Figure 6-1 Physical model of the structure (dimensions in mm)

For simplification of the model in analysis, the structure is simulated as a *shear building* explained in section 3.6. (Figure 6-2).

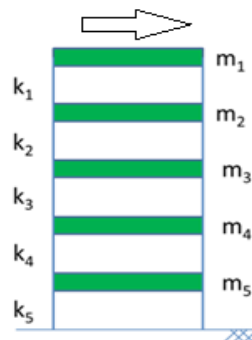


Figure 6-2 shear building model of the structure for dynamic analysis (direction of movement is shown)

Therefore, the model of the structure for analysis is comprises of masses which are connected through springs with relevant stiffness values.

6.3 Mathematical model

For the mass-spring model of the given structure the governing equations are defined by recalling equation 3.3 as

$$M\ddot{u} + c\dot{u} + Ku = -M\ddot{u}_g \quad (6.1)$$

Where, M , and K represent mass and stiffness matrix respectively as

$$M = \begin{bmatrix} 40 & 0 & 0 & 0 & 0 \\ 0 & 40 & 0 & 0 & 0 \\ 0 & 0 & 40 & 0 & 0 \\ 0 & 0 & 0 & 40 & 0 \\ 0 & 0 & 0 & 0 & 40 \end{bmatrix} (kg)$$

and

$$K = \begin{bmatrix} 469400 & -469400 & 0 & 0 & 0 \\ -469400 & 938800 & -469400 & 0 & 0 \\ 0 & -469400 & 938800 & -469400 & 0 \\ 0 & 0 & -469400 & 938800 & -469400 \\ 0 & 0 & 0 & -469400 & 938800 \end{bmatrix} (N/m)$$

for fixed-base structure and

$$M = \begin{bmatrix} 40 & 0 & 0 & 0 & 0 & 0 \\ 0 & 40 & 0 & 0 & 0 & 0 \\ 0 & 0 & 40 & 0 & 0 & 0 \\ 0 & 0 & 0 & 40 & 0 & 0 \\ 0 & 0 & 0 & 0 & 40 & 0 \\ 0 & 0 & 0 & 0 & 0 & 40 \end{bmatrix} (kg)$$

and

$$K = \begin{bmatrix} 469400 & -469400 & 0 & 0 & 0 & 0 \\ -469400 & 938800 & -469400 & 0 & 0 & 0 \\ 0 & -469400 & 938800 & -469400 & 0 & 0 \\ 0 & 0 & -469400 & 938800 & -469400 & 0 \\ 0 & 0 & 0 & -469400 & 938800 & -469400 \\ 0 & 0 & 0 & 0 & -469400 & 483900 \end{bmatrix} (N/m)$$

for base-isolated structure.

In equation 6.1, c denotes damping for which the values obtained from experiments are used (0.06 and 0.12 for fixed base and base isolated respectively). In the governing equation of motion (equation 6.1), \ddot{u}_g specifies the time-history acceleration of ground motion. These time-history records correspond to the past earthquakes acceleration values over time which are recorded by seismographs around the world.

Equation 6.1 provides n number of simultaneous equations with n unknowns corresponds to the degrees of freedom of the model. The unknown values in each run will be time-history of acceleration, velocity and displacement correspond to each degree of freedom.

6.4 Simulation

In order to numerically simulate the seismic responses of the structure, the basic equation of motion 6.1 is considered by the program in which \ddot{u}_g is the time history of a particular earthquake records acceleration. The seismic response is simulated only in one direction, this, on the other word, means just one degree of freedom is defined at each node. The mass and stiffness matrices together with scaled earthquakes are used to simulate the dynamic behaviour of the structure. Scaling of the earthquakes are necessary to maintain the dynamic similitude between the scaled model and real scale building. The scale is 0.316 on time axis of the real record.

6.4.1 Earthquakes

The first earthquake simulated is El-Centro 1940 (California) ground motion as a moderate earthquake with PGA (Peak Ground Acceleration) of 0.3188g. It is very important for engineers to gain insight about the performance of the target structure under a moderate ground motion as majority of earthquakes around the world are categorised in this range; therefore, it is common to use El-Centro earthquake data for structural dynamic analysis world-widely. In order to observe the performance of the isolated system, proposed in this study, subject to stronger earthquakes, Kobe 1995 (Japan) recorded data is used as a near field strong ground motion. Kobe peak ground

acceleration was recorded as 0.8209g, by seismometer, which categorised this earthquake as one of the greatest one recorded since the technology of seismometers came into practice. Another earthquake simulated in this study is Manjil 1990 (Iran) as a middle field record and long duration motion with PGA of 0.5146g.

Table 6-1 Earthquakes used for simulation

Earthquake	El-Centro (1940)	Kobe (1995)	Manjil (1990)
PGA (g)	0.3188	0.8209	0.5146
Magnitude (Richter)	6.9	6.9	7.4
Fault depth (km)	8.8	17.9	19
Station	Imperial valley	JMA ¹	Abbar station
Station distance (km)	12.2	1	12.6
Duration of records (sec)	31.2	48	53.52
Time step (sec)	0.02	0.02	0.02
Number of data points	1560	2400	2676
Earthquake specifications	Moderate ground motion with short duration	Near field strong ground motion	Middle range strong ground motion with long duration

The earthquake records are obtained from the database of USGS (available at <http://www.strongmotioncenter.org/>). The time axis for these earthquakes were scaled to 0.316 of the original ones for dynamic similarity and in order to keep the fundamental frequency of the structure consistent with dominant frequency of the earthquake records.

¹ Japan Metrological Agency

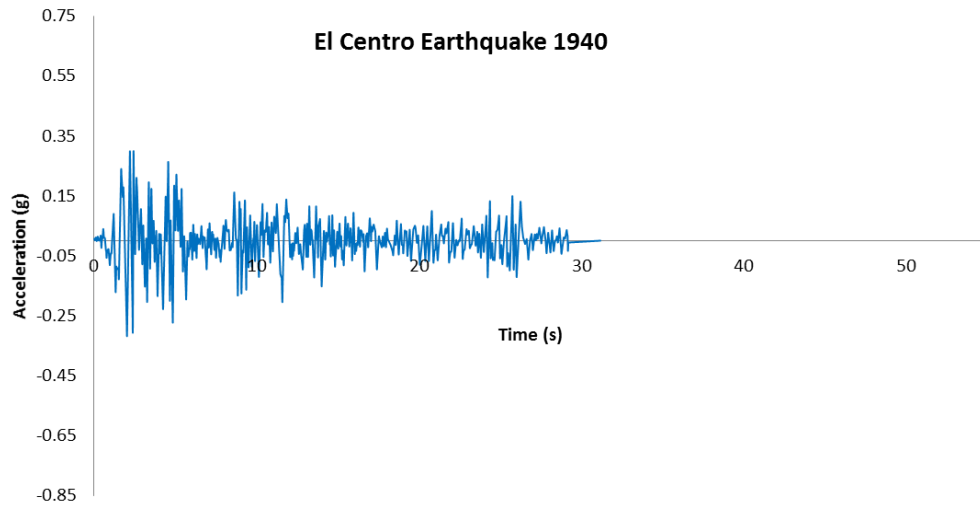


Figure 6-3 El-Centro earthquake acceleration data

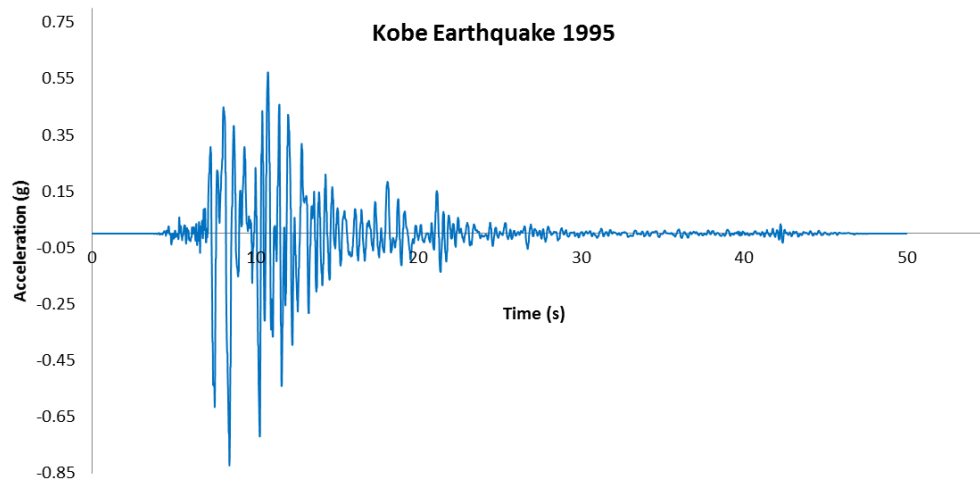


Figure 6-4 Kobe earthquake acceleration data

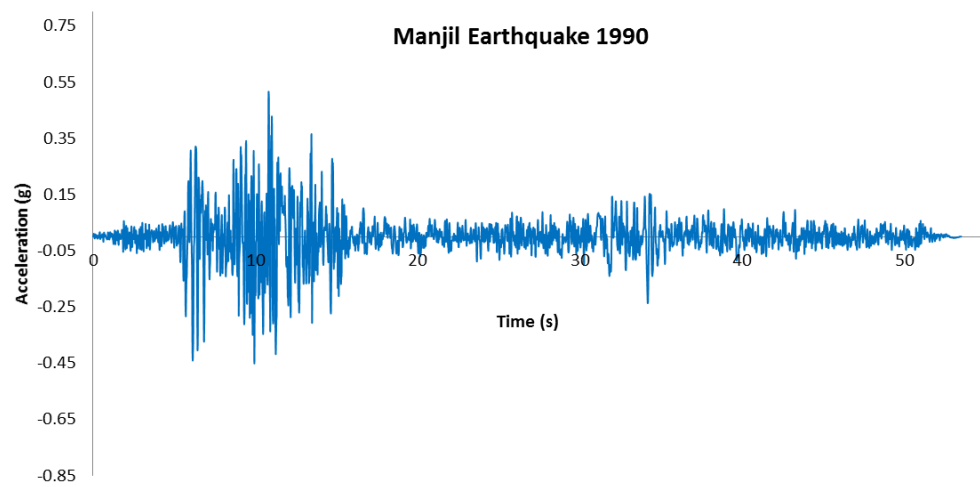


Figure 6-5 Manjil earthquake acceleration data

Time histories of the response quantities were then computed under the given earthquakes for isolated and unisolated structure.

6.5 Program settings

As a model of mass-spring is considered for simulation, it is necessary to define correct mass at each node, correct stiffness at each link and correct function for time history.

6.5.1 Mass

SAP2000 enables the user to define masses at desire nodes by using Assign menu and define a mass to the joint in the desire direction (here local axis 1).

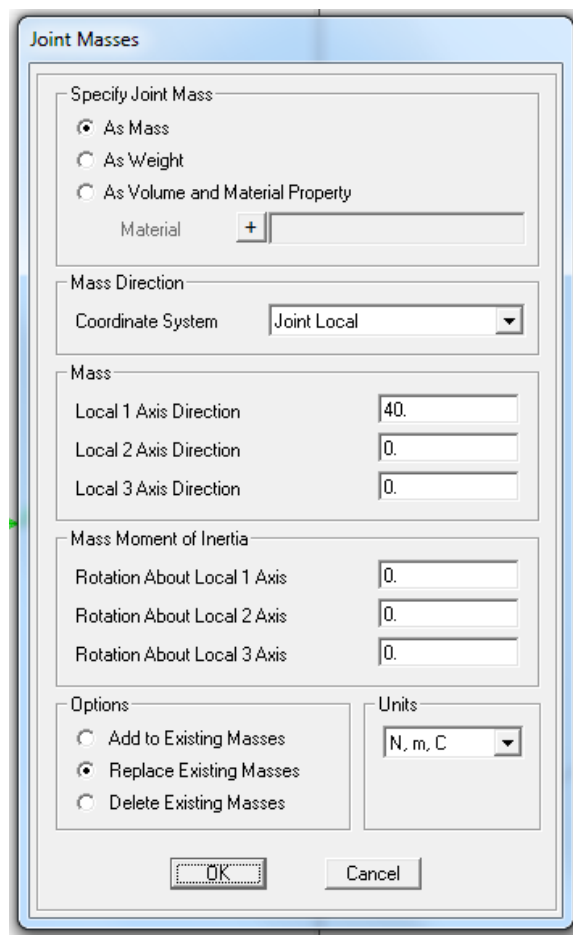


Figure 6-6 Assigning mass to the model in SAP2000

In the local axis 1, the defined mass in 40 corresponds to 40kg mass of each story.

6.5.2 Stiffness

In order to define the accurate stiffness to the model, it is necessary to draw the links between each nodes. This is possible using Define menu where the option for defining Links are available.

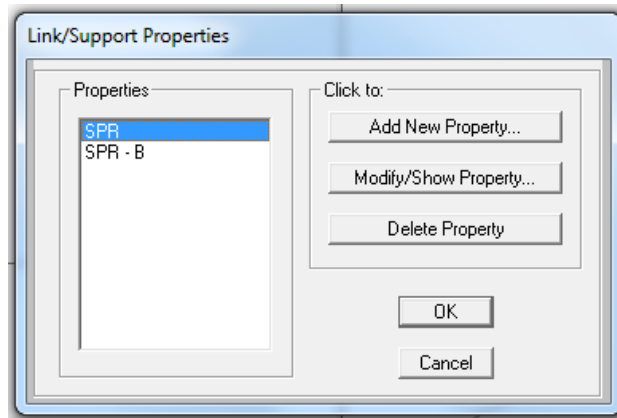


Figure 6-7 Defining lateral stiffness as Link in SAP2000

In the Link definition menu, SPR corresponds to lateral stiffness of each story and SPR-B represents the lateral stiffness of the isolation system.

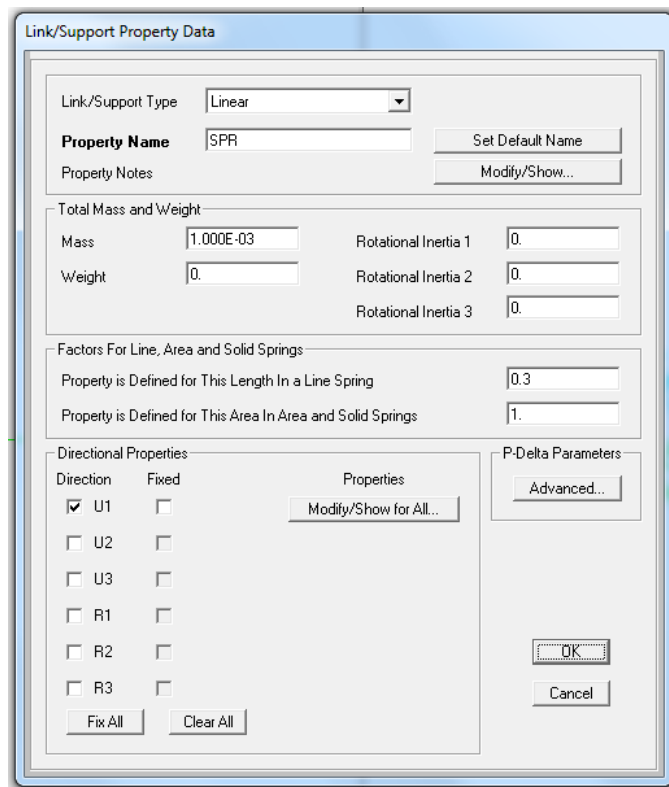


Figure 6-8 Definition of stiffness as Spring type Link in SAP2000

The mechanical properties of each Link can be defined by a Spring element as shown in Figure 6-8. The value and direction of stiffness, then, is defined in the properties menu as shown in Figure 6-9.

The screenshot shows the 'Linear Link/Support Directional Properties' dialog box. The 'Link/Support Name' field is set to 'SPR'. In the 'Directional Control' section, the 'U1' checkbox under the 'Direction' column is checked. The 'Stiffness Values' section has 'Stiffness Is Uncoupled' selected, and the 'U1' input field contains the value '469400'. The 'Damping Values' section has 'Damping Is Uncoupled' selected, and the 'U1' input field contains the value '0'. The 'Units' dropdown is set to 'N, m, C'. The 'OK' and 'Cancel' buttons are at the bottom.

Figure 6-9 Definition of properties for spring links in SAP2000

The value of 469400 N/m corresponds to the lateral stiffness of each story is entered for SPR element. Please note that, since the values for overall damping will be defined in analysis settings the value for damping is considered as zero for this element here.

6.5.3 Time history input

For time-history inputs the user needs to first define the function of a quantity (acceleration, displacement or force) over time. This is possible through Define menu and sub-menu namely Function; where the user is able to introduce a time-history records to the program. Time history records are text (*.txt) files format which in this study are obtained from past earthquake records from USGS (United States Geological Survey).

KOBE - KJM1km - PGA082 r01.txt - Notepad

PEER STRONG MOTIO	N DATABASE REC	ORD. PROCESSING BY PACIFIC ENG	INEERING.
KOBE 01/16/95 204	"6, KJM, 000"		
ACCELERATION TIME	HISTORY IN UN	ITS OF G. FILTER	POINTS: HP=0. 05
"NPTS= 2400, DT="	.02000 SEC		
1.58E-05	1.56E-05	1.55E-05	1.53E-05
1.50E-05	1.49E-05	1.48E-05	1.47E-05
1.44E-05	1.42E-05	1.41E-05	1.39E-05
1.36E-05	1.35E-05	1.34E-05	1.32E-05
1.30E-05	1.31E-05	1.30E-05	1.28E-05
1.29E-05	1.29E-05	1.23E-05	1.23E-05
1.15E-05	1.14E-05	1.07E-05	1.05E-05
1.02E-05	1.08E-05	1.06E-05	1.13E-05
1.11E-05	1.10E-05	1.19E-05	1.08E-05
1.06E-05	9.36E-06	9.20E-06	9.09E-06
8.84E-06	8.70E-06	8.61E-06	9.98E-06
9.80E-06	9.72E-06	9.60E-06	9.53E-06
9.35E-06	9.24E-06	9.18E-06	6.95E-06
6.71E-06	6.63E-06	6.49E-06	6.38E-06
6.17E-06	8.73E-06	8.62E-06	8.53E-06
8.35E-06	8.27E-06	8.17E-06	8.09E-06
4.67E-06	4.52E-06	4.45E-06	4.31E-06
4.12E-06	4.06E-06	7.87E-06	7.82E-06
7.64E-06	7.53E-06	7.45E-06	2.87E-06
7.24E-06	2.45E-06	2.35E-06	2.29E-06
2.10E-06	2.01E-06	7.24E-06	7.12E-06
6.95E-06	6.88E-06	6.80E-06	6.71E-06
5.65E-07	4.82E-07	4.27E-07	3.28E-07
			2.88E-07

Figure 6-10 A sample of *.txt file corresponds to the earthquake recorded data

Time History Function Definition

Function Name: KOBE

Function File:

File Name: Browse...
 \\anglia.local\fs\studentshome\mh749\my documents\my desktop\thesis writing\prototype

Header Lines to Skip: 4

Prefix Characters per Line to Skip: 0

Number of Points per Line: 5

Convert to User Defined View File

Values are:

☐ Time and Function Values

☒ Values at Equal Intervals of 6.320E-03

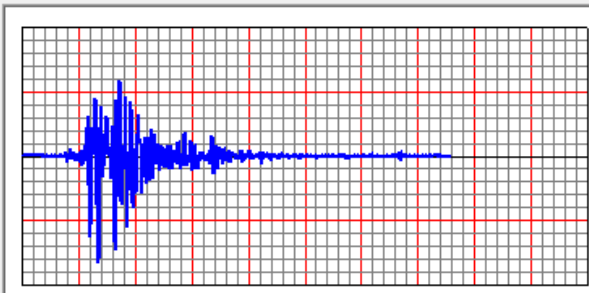
Format Type:

☒ Free Format

☐ Fixed Format

Characters per Item

Function Graph



Display Graph

OK Cancel

Figure 6-11 Definition of Kobe earthquake acceleration records as a function of time in SAP2000

Having known the sampling time for original record (which in this case is 0.02s) the user is able to scale the time axis to the predefined target scale. The target scale for this analysis was set to 0.316 for time, therefore, 0.00632 is entered as the intervals to the program (Figure 6-11).

Upon defining the function of time history, it is necessary to assign it to a Load Case for analysis by program. This is possible through Load Case Data setting from Define menu.

Load Case Data - Linear Modal History

Load Case Name: Notes:

Load Case Type:

Initial Conditions:
☒ Zero Initial Conditions - Start from Unstressed State
☐ Continue from State at End of Modal History
 Important Note: Loads from this previous case are included in the current case

Analysis Type:
☒ Linear ☐ Nonlinear
 Time History Type:
☒ Modal ☐ Direct Integration

Time History Motion Type:
☒ Transient ☐ Periodic

Modal Load Case:
 Use Modes from Case:

Loads Applied

Load Type	Load Name	Function	Scale Factor
Accel	U1	KOBE	9.81
Accel	U1	KOBE	9.81

☐ Show Advanced Load Parameters

Time Step Data:
 Number of Output Time Steps:
 Output Time Step Size:

Other Parameters:
 Modal Damping:

Figure 6-12 Load case data assignment to a time history function in SAP2000

As it is shown in Figure 6-12, the function is defined as acceleration with the scale factor of 9.81 which denotes the gravity acceleration. Please note that, the recorded data used for this analysis were acceleration readings by seismographs in unit of g. It should be noted that the damping ratio is defined to the program at this step. The damping values obtained from experiments are assigned to all modes of vibration here as 0.06 for fixed-

base and 0.12 for isolated structure. Considering the same damping ratio for all modes is a conservative assumption as the higher modes involves higher damping (Butterworth, et al., 2004).

6.6 Results

6.6.1 Frequencies and periods

In this section the results from computer simulation are presented and discussed. The first and most important item to look at is the fundamental frequency and period of the structure computed by the program. This will give an insight about the accuracy of simulation.

Table 6-2 Comparison of fundamental frequencies and periods

Measured by:	Fixed Base (FB)		Base Isolated (BI)	
	Frequency (Hz)	Period (sec)	Frequency (Hz)	Period (sec)
Computer simulation	4.91	0.204	1.21	0.828
Experiments	4.39	0.227	1.17	0.855
Analytical model	4.907	0.204	1.208	0.827

Results from computer simulation are in a closed correlation with the results obtained from experiments and are in accordance with the analytical model which confirms the accuracy of the computer simulation. Therefore, the performance of the present isolation system in lengthening the fundamental period of vibration of the structure is confirmed.

6.6.2 Accelerations

The performance of a structure in attenuation of acceleration, due to input dynamic loads, is also very important. In addition to structural damage caused by high acceleration due to an earthquake, the convenience of the occupiers and non-structural elements are affected significantly by a high level of acceleration. Following figures show the performance of the structure with respect to absolute acceleration exerted on top of the structure in the same loading and different base configurations.

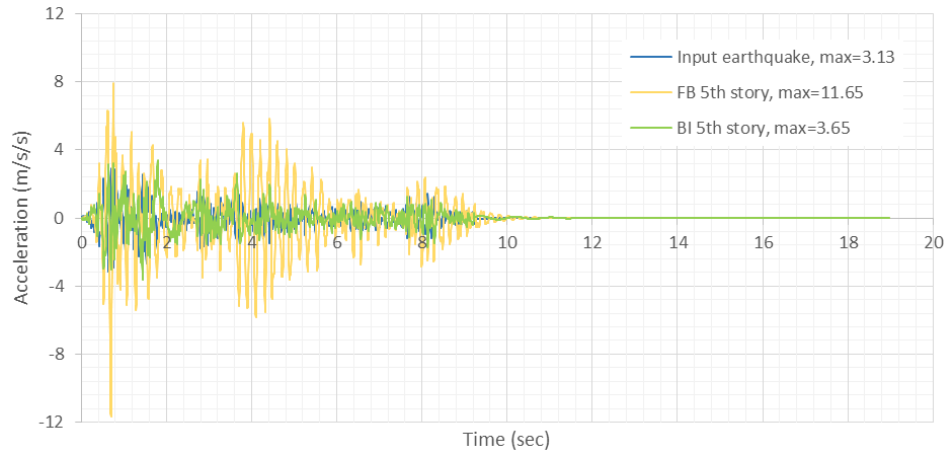


Figure 6-13 Acceleration response on top of the structure due to El-Centro earthquake (FB: Fixed base and BI: Base isolated)

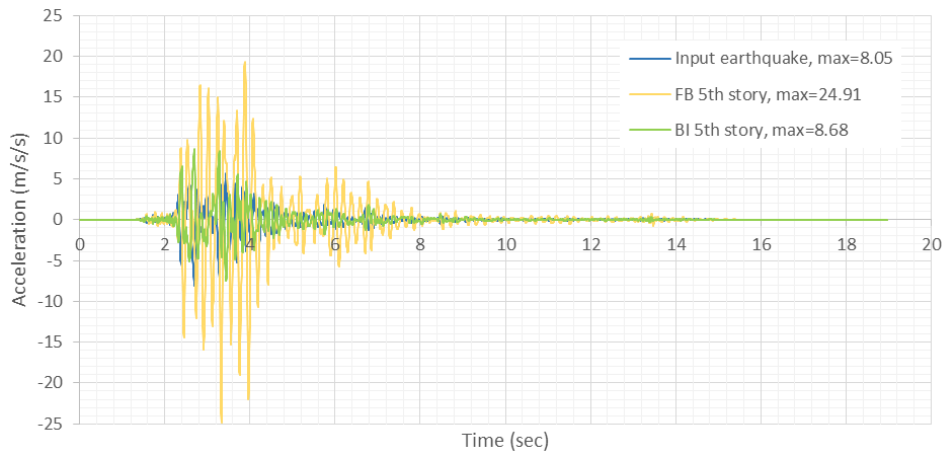


Figure 6-14 Acceleration response on top of the structure due to Kobe earthquake (FB: Fixed base and BI: Base isolated)

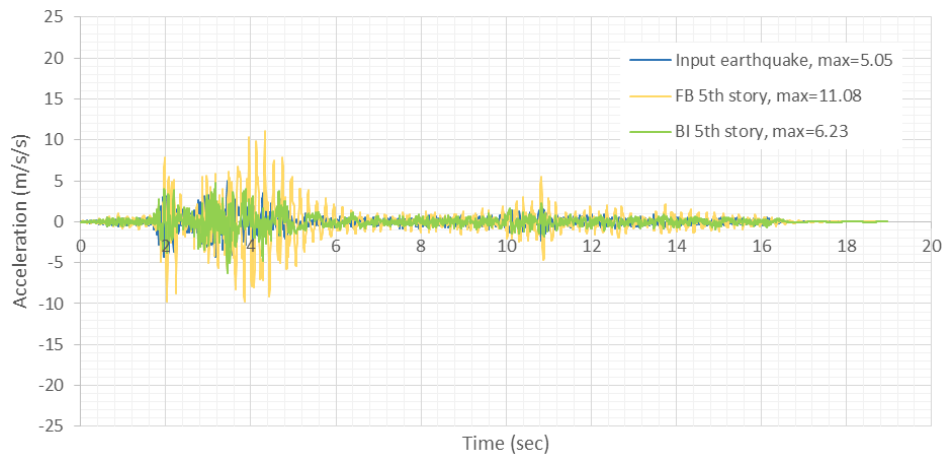


Figure 6-15 Acceleration response on top of the structure due to Manjil earthquake (FB: Fixed base and BI: Base isolated)

Table 6-3 Peak acceleration at each level of the structure due to input ground motion (m/s²)

		MASSB	1st	2nd	3rd	4th	5th
ELCE	FB	-	3.55466	6.04734	8.10146	10.20851	11.64578
	BI	3.41102	3.50343	3.57001	3.60977	3.63773	3.6542
	Reduction (%)		1.44	40.97	55.44	64.37	68.62
KOBE	FB	-	6.47916	12.85764	17.44105	22.07453	24.91162
	BI	8.08672	8.29152	8.44672	8.55902	8.63732	8.6815
	Reduction (%)		-27.97	34.31	50.93	60.87	65.15
MANJ	FB	-	6.78363	9.98996	10.18468	8.59338	11.0826
	BI	6.07364	6.1694	6.18779	6.19746	6.21461	6.23455
	Reduction (%)		9.05	38.06	39.15	27.68	43.74

The response of the structure is drastically reduced when the present isolation system is used. It is again confirmed that the present isolation system is able to reduce the level of acceleration in the structure to a much lower level; more than 50% reduction is observed on upper levels. It is observed that in a strong motion of Kobe, the acceleration on first level is not reduced due to the use of isolation system. This, however, does not have large effects as the value of peak acceleration at this level is low. It can be also concluded that an acceptable level of performance for the isolation system corresponds to all three cases of ground motion is observed. However, for Manjil ground motion which involves a longer time oscillation, the ratio of attenuation is lower than shorter oscillations such as El-Centro and Kobe.

6.6.3 Displacements

The other parameter which should be investigated is displacement in different levels of the structure. Following figures correspond to the displacement response of the structure with different base configurations and subject to three mentioned earthquakes.

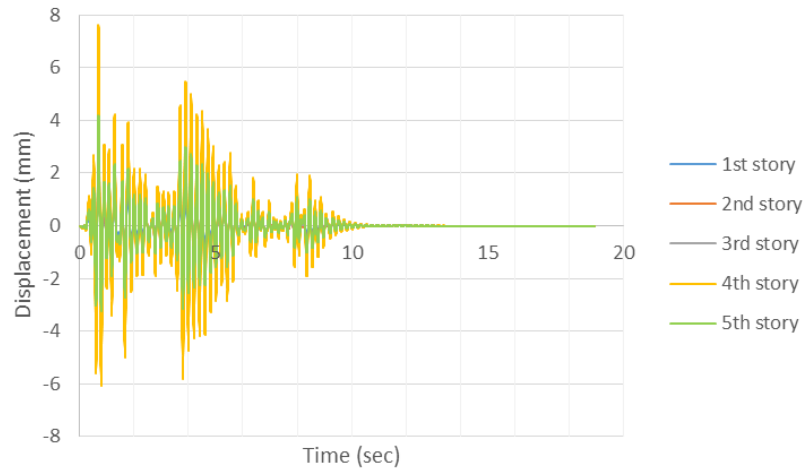


Figure 6-16 Displacement response of the fixed-base structure due to El-Centro earthquake

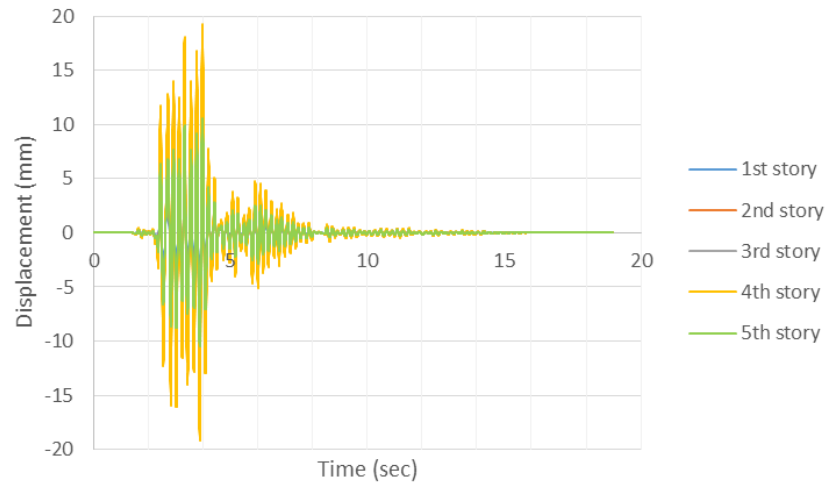


Figure 6-17 Displacement response of the fixed-base structure due to Kobe earthquake

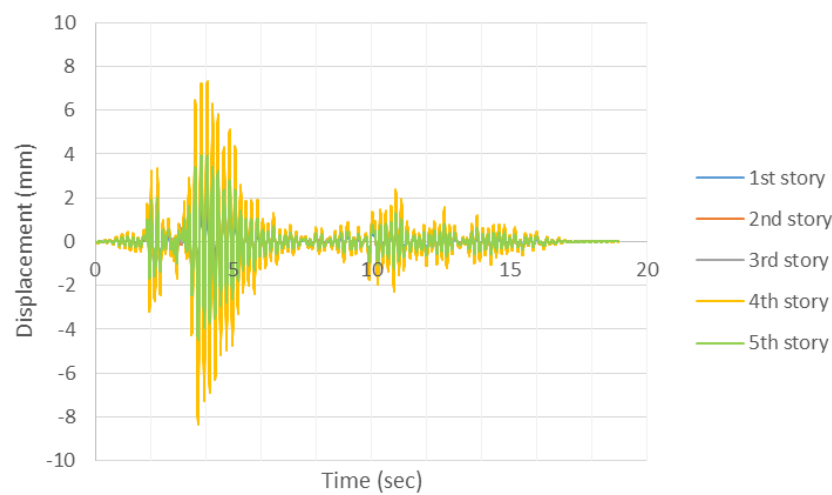


Figure 6-18 Displacement response of the fixed-base structure due to Manjil earthquake

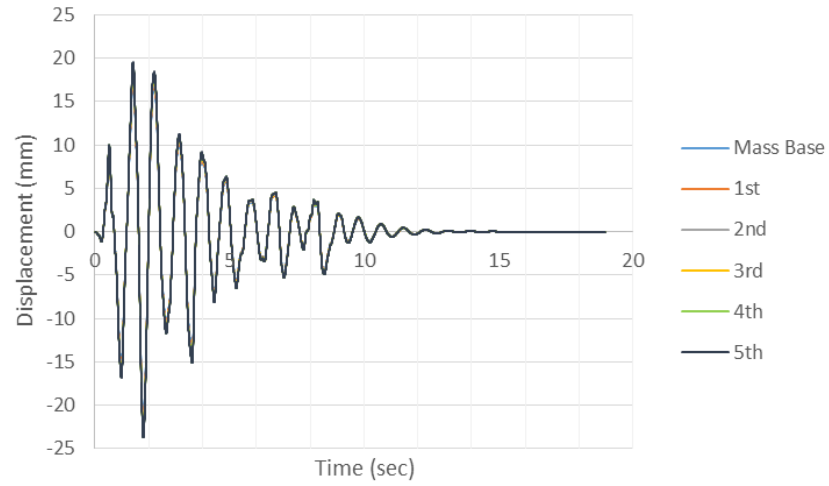


Figure 6-19 Displacement response of the base-isolated structure due to El-Centro earthquake

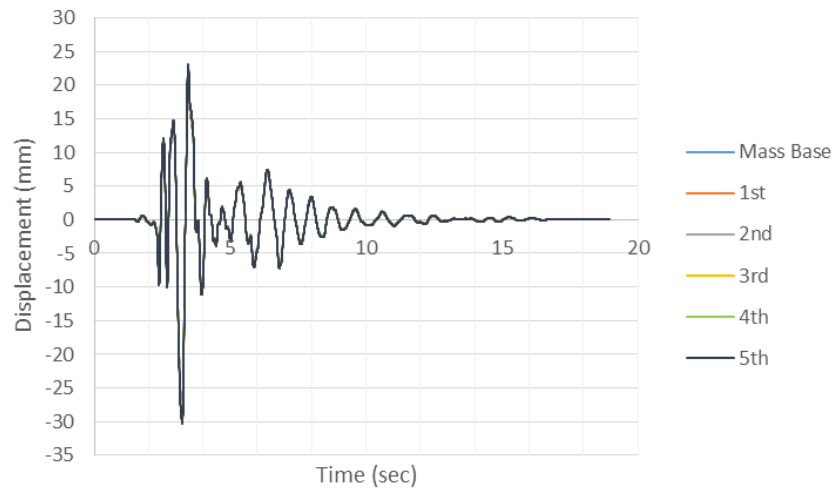


Figure 6-20 Displacement response of the base-isolated structure due to Kobe earthquake

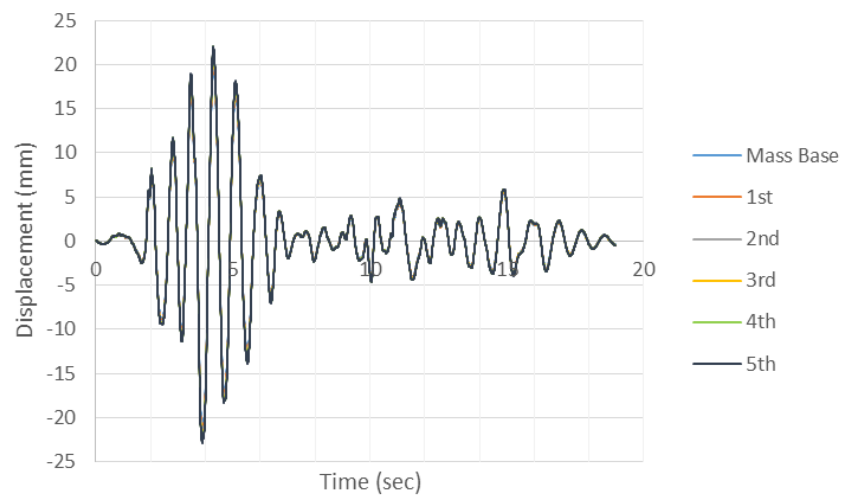


Figure 6-21 Displacement response of the base-isolated structure due to Manjil earthquake

Table 6-4 Displacements and story drifts due to El-Centro earthquake (mm)

		MASSB	1st	2nd	3rd	4th	5th
Fixed-Base	Displacement	-	2.174	4.307	6.191	7.626	4.204
	Story drift	-	-	2.133	1.884	1.435	3.422
Base-Isolated	Displacement	21.958	22.536	23.007	23.364	23.604	23.724
	Story drift	-	0.578	0.471	0.357	0.240	0.120

Table 6-5 Displacements and story drifts due to Kobe earthquake (mm)

		MASSB	1st	2nd	3rd	4th	5th
Fixed-Base	Displacement	-	5.921	11.354	15.909	19.252	10.552
	Story drift	-	-	5.433	4.554	3.344	8.700
Base-Isolated	Displacement	28.110	28.829	29.397	29.815	30.090	30.226
	Story drift	-	0.719	0.568	0.418	0.275	0.136

Table 6-6 Displacements and story drifts due to Manjil earthquake (mm)

		MASSB	1st	2nd	3rd	4th	5th
Fixed-Base	Displacement	-	2.881	5.340	7.176	8.357	4.459
	Story drift	-	-	2.459	1.836	1.181	3.898
Base-Isolated	Displacement	21.255	21.800	22.229	22.549	22.762	22.869
	Story drift	-	0.544	0.430	0.319	0.213	0.107

The isolated structure accommodates a large amount of displacement during the earthquakes but the story drifts are reduced significantly in comparison to the unisolated structure. The story drift known as one of the major causes of damage in structures during earthquakes. Again, the appropriate performances of the present isolation system under moderate and strong earthquakes are confirmed based on the displacement response of the structure.

6.6.4 Base-shear

One of other important measures in earthquake engineering is the base-shear in a structure due to an earthquake. The base-shear maximum values for fixed-base and base-isolated structure subject to three mentioned earthquakes are presented in the following table.

Table 6-7 Maximum base-shear force (N)

	El-Centro	Kobe	Manjil
Fixed base	1020	2779	1352
Base isolated	318	407	308

Base-shear force is a horizontal load exerted to the structure basement at the time of earthquake. A great reduction in base-shear is observed in the isolated structure.

6.6.5 Earthquake input energy

The performance of the present isolation system can be investigated with evaluating the input energy to the structure due to the earthquakes (Figure 6-22 to Figure 6-27).

Table 6-8 Maximum input energy by different earthquakes (N-m)

	El-Centro	Kobe	Manjil
Fixed base	15.40	97.45	20.80
Base isolated	11.07	29.38	13.77

A significant reduction in maximum input energy to the structure is observed when a strong ground motion – Kobe – is considered. It can be concluded that the performance of the isolation system in terms of reduction in the input energy is better when considering strong earthquakes in comparison to moderate earthquakes.

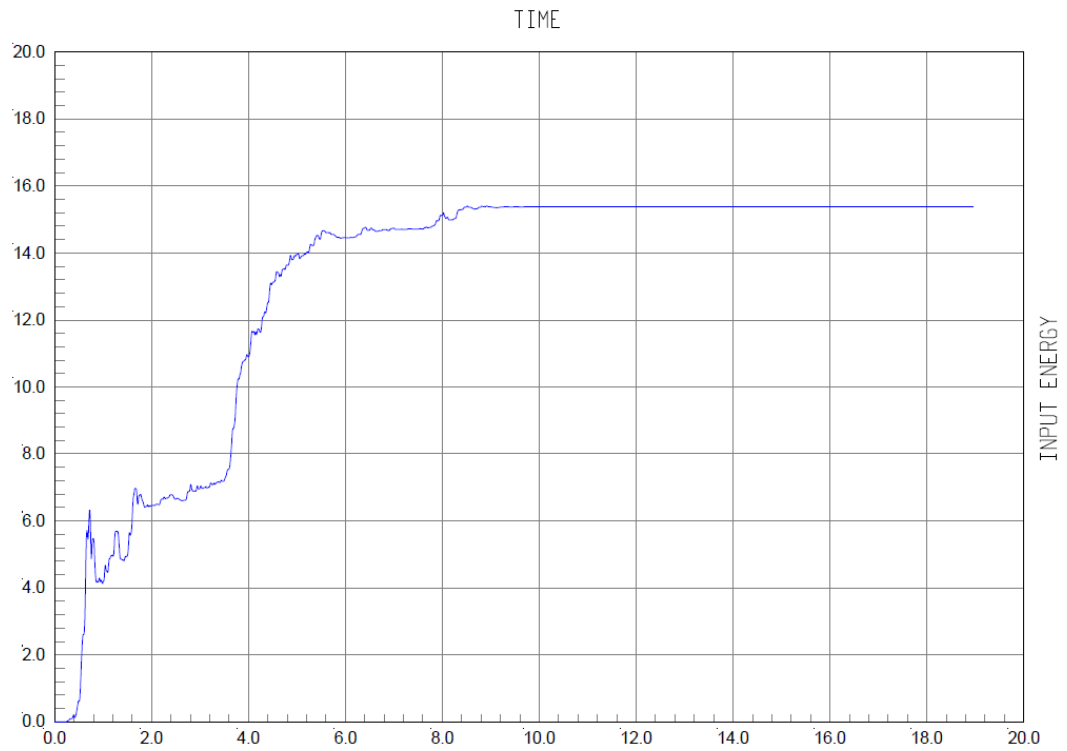


Figure 6-22 Input energy trend over time due to El-Centro earthquake on fixed-base structure (N-m)

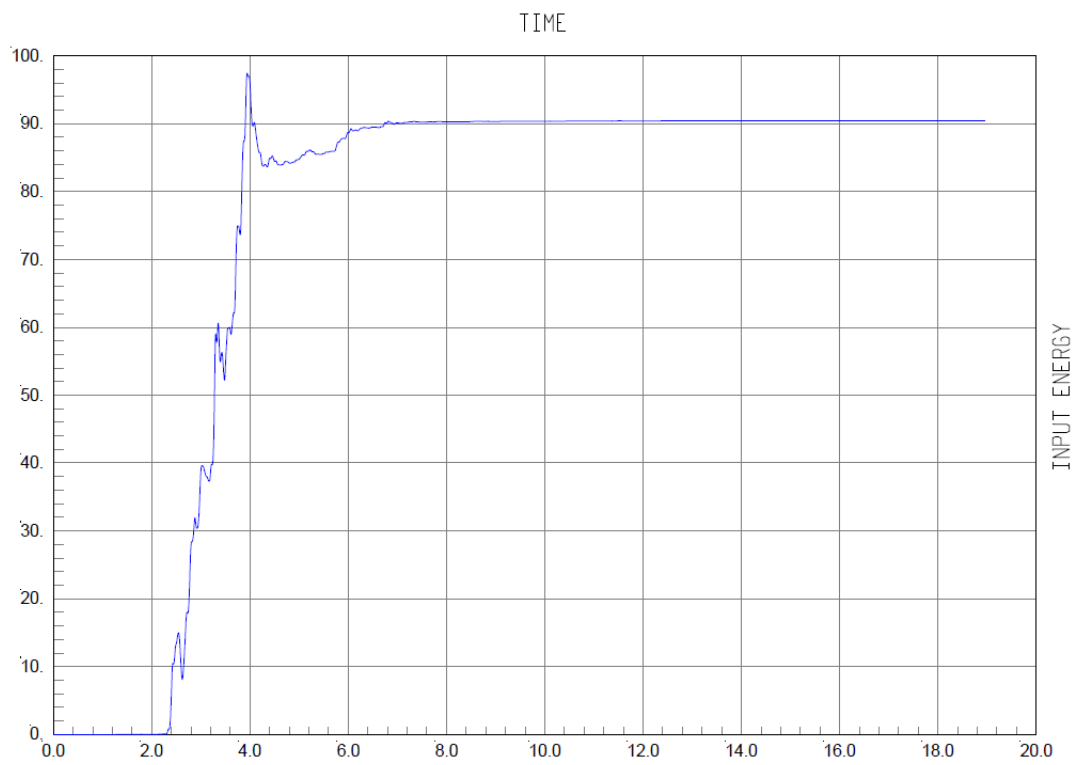


Figure 6-23 Input energy trend over time due to Kobe earthquake on fixed-base structure (N-m)

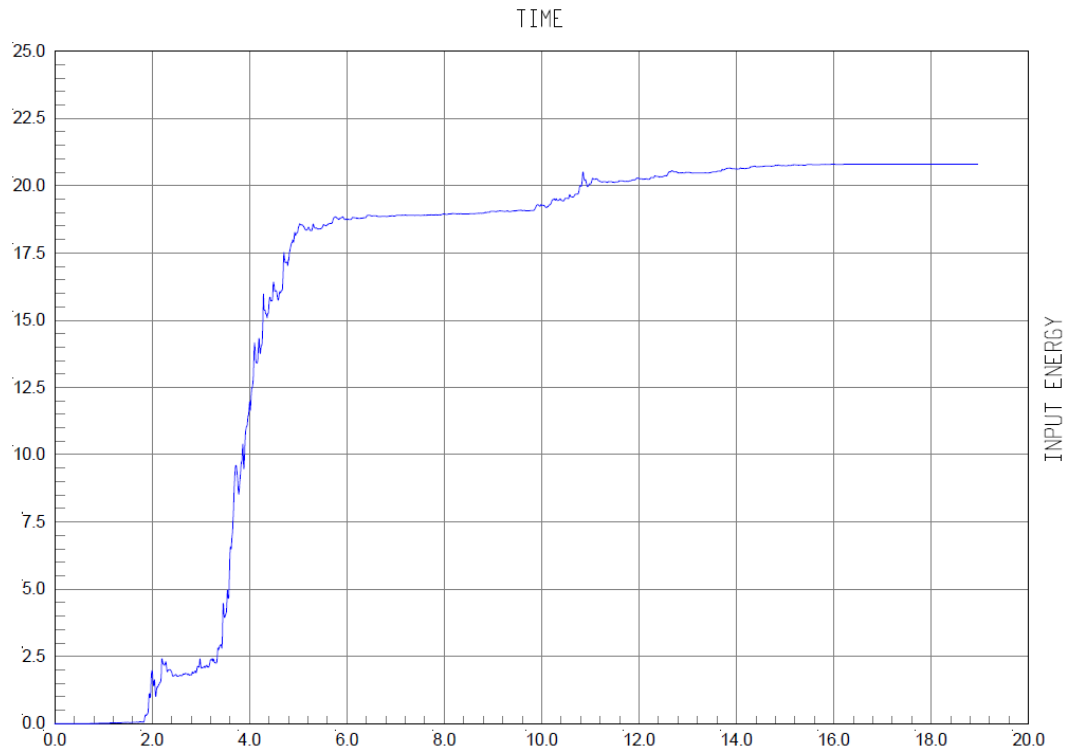


Figure 6-24 Input energy trend over time due to Manjil earthquake on fixed-base structure (N-m)



Figure 6-25 Input energy trend over time due to El-Centro earthquake on base-isolated structure (N-m)

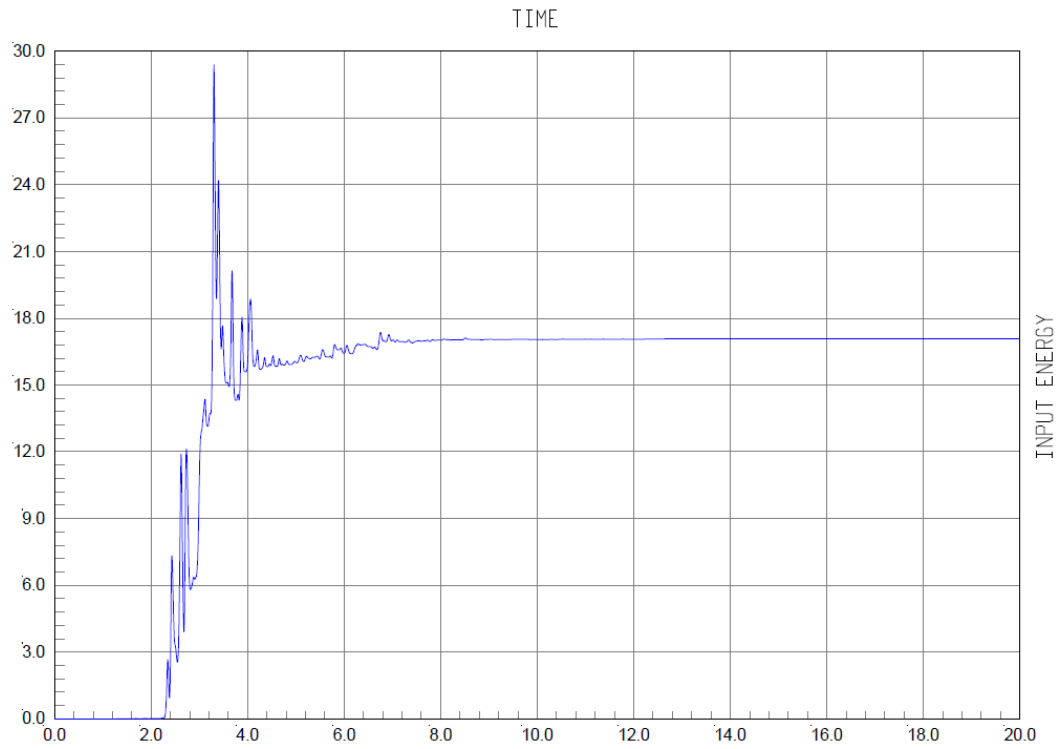


Figure 6-26 Input energy trend over time due to Kobe earthquake on base-isolated structure (N-m)

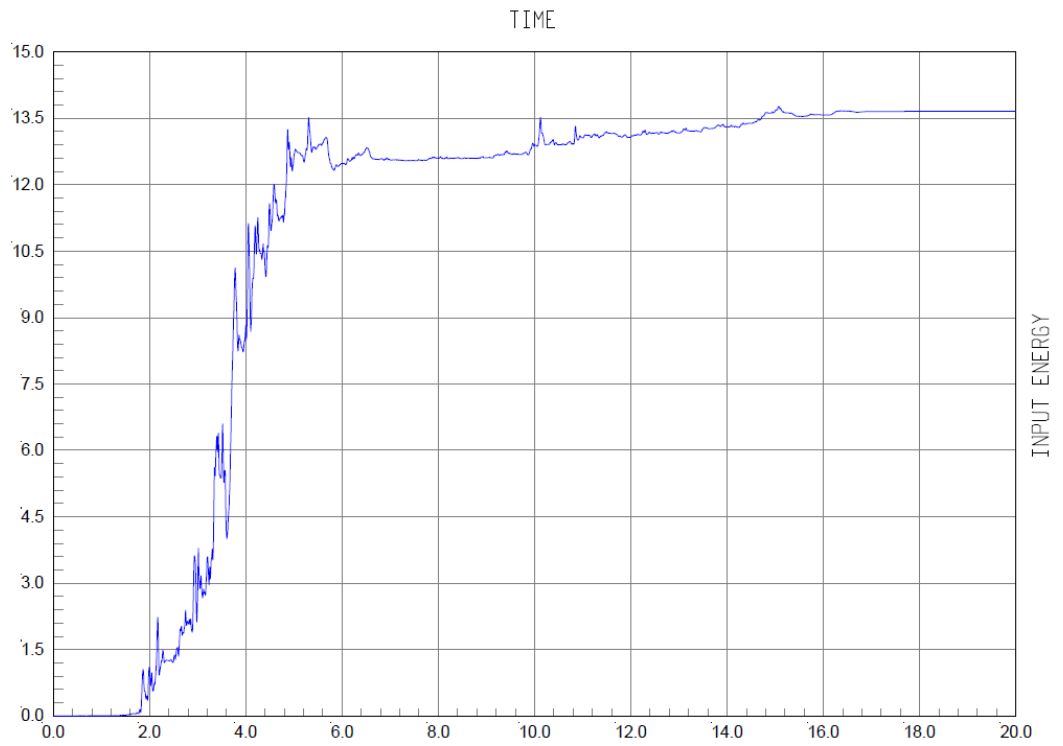


Figure 6-27 Input energy trend over time due to Manjil earthquake on base-isolated structure (N-m)

6.7 Conclusion

Numerical assessment of capability of the proposed isolation system was presented in this chapter. The ability of the new system to protect structural and non-structural elements from seismic hazards through its implementation on a structure were checked. It is found that the new isolation system is able to greatly reduce the structure accelerations, story drifts and base shears, while keeping acceptable displacement at base. The proposed isolation system is highly effective when both moderate and strong motion are considered.

It was clear from results that a larger period of vibration and a faster attenuation of acceleration amplitude accompany the isolated structure. Although, the best performance of the isolation system is obtained when strong motions are considered, the results confirmed that the efficiency of the present system against earthquake attacks does not highly depend on the type of input earthquake. It should be noted that, one of the drawbacks of current base-isolation systems is dependency on the input shocks characteristics.

7 Conclusion and future works

This chapter concludes the thesis with a summary of results, the main contributions and proposes topics that may be considered for future works.

7.1 Conclusion

Results from the experiments and numerical simulations reveal that the present isolation system is a very efficient tool for seismic protection of building structures under different earthquake features. The new isolation system exhibits a robust performance for a scaled model of a typical five-story building. The behaviour of the structure isolated by the new proposed system is relatively independent of the frequency content and the amplitude of base excitation.

As the core of the idea for the new proposed isolation system was to make use of air-bearing solutions, the air-bearing units were explicitly designed, analysed and optimised through numerical simulation and further investigated through experimental tests. The experimental tests on the air-bearing devices confirmed the best shape for the nozzles of bearing in order to handle larger loads.

The purpose of the experimental study on the scaled structure was to determine whether observations agree with or conflict with the predictions derived from the hypothesis established earlier and its subsequent analytical model. The experiments confirmed that

the isolation system is able to lengthen the fundamental period of the structure and add significant level of damping to the whole system (structure and its isolation). It was also concluded that the isolation system reduces the level of acceleration exerted to the structure subject to different applied impulse loadings. In addition, the isolation system provides the structure with a reduction in the level of story drifts which is a known cause of damages to the structures.

The computer investigation was conducted in order to simulate the behaviour of the structure with two different base configurations (fixed base and base isolated) and subject to different earthquakes; El-Centro 1940 as a moderate and short excitation, Kobe 1994 as a strong and near-field ground motion, and Manjil 1990 as a strong ground motion with long duration. The performance of the isolation system was confirmed appropriate in terms of lengthening the fundamental period of vibration of the structure, great attenuation of structural acceleration, significant reduction in story drifts and a reduction of input energy to the structure in all cases. This is a great achievement that the structure isolated by proposed isolation system is working quite independently from the characteristics of input earthquake. As discussed in the literature review, one of the drawbacks of current isolation systems is that they are not efficient in moderate earthquakes and their performance is highly dependent on the input earthquake characteristics; whereas, the new proposed system is able to protect a structure regardless of the characteristics of the ground motion.

Measurements in engineering research works are usually accompanied by estimation of their uncertainty. The value of the measured frequencies and periods by experiments concur with the values obtained from the analytical model and numerical simulations. There are only around 10% and 3% differences for fixed-base structure and base-isolated structure, respectively, between experiments and computer modelling. This stems from the uncertainty in the stiffness and damping characteristics of the structure and its isolation system. A small variation in stiffness produces quite a large difference in measures of dynamic parameters.

There are some limitations in computing equivalent damping values using experimental data which arises because linear behaviour for a dynamic system is normally assumed.

When the given dynamic system is behaving highly nonlinear, a substantial error could be introduced into the damping estimation. Nonetheless, it is routine to assume linear viscous damping in experimental data analysis.

7.2 Contributions

This research aimed to develop an innovative isolation system that is efficient and has some particular capabilities which are not offered by contemporary isolation systems. The proposed isolation system works as a semi-active isolation system which can be triggered by the signals received from metrological centres as an early warning. The isolation system, then, employs air-bearing solutions to decouple the super-structure from its base at the time of ground motion. The air-bearing system is accompanied by a re-centring mechanism such as rubber-bearings or friction pendulum for self-re-centring. As the horizontal stiffness at the base of a structure is reduced the fundamental period of the structure is shifted to a greater one and the accelerations exerted in the structure are reduced. Below is the list of features provided by the new system:

- Great decoupling system
- Lengthening the vibration period to the designer desire
- Involving a wide range of base stiffness
- Great level of energy dissipation
- Self-re-centring system
- Suitable for all range of earthquake from moderate to strong motions
- Improvement of damping mechanism

7.3 Future works

Further research beyond the scope of this study is recommended in relation to the present isolation system in the following area:

- Testing the scaled structure with and without the proposed isolation system on a shaking table in order to observe the behaviour of the structure and performance of the isolation system in practice.
- Checking the feasibility of the proposed isolation system for bridges isolation.
- Design and development of a large-scale prototype, for characterisation evaluations and experimental tests.
- Undertaking a cost analysis of the isolation system with respect to the savings in the use of materials and energy from production to construction and implementation.
- Checking the uplift response of the structure when isolated with the proposed isolation system and subjected to different kinds of earthquakes.
- Checking the influence of the proposed isolation system on torsional responses.
- Performing a comparative study on the proposed system against current isolation systems.
- Performing a numerical investigation on the proposed air-bearing with dynamic mesh generation.

Future works are not limited to the above mentioned activities and researchers interested in this area may define their own aims and objectives to fill the gap in knowledge.

8

References

Ab-Malek, K. & Kamaruddin, S., 2010. *Opportunities Of Manufacturing Engineering Rubber Products*. Buloh, Rubber research institute of Malaysia.

Aerogo, 2015. *moving heavy loads up to 5000 tons*. [Online]
Available at: <http://www.aerogo.com/heavy-load-moving/moving-heavy-loads-up-to-5000-tons/4>
[Accessed 10 08 2015].

Airfloat, 2015. *casestudy*. [Online]
Available at: <http://www.airfloat.com/casestudy/arena-seating/>
[Accessed 10 08 2015].

ANSYS, 2015. *ANSYS help*. Canonsburg: ANSYS.

Aris, R., 1989. *Vectors, Tensors and the Basic Equations of Fluid Mechanics*. Newyork: Dover Publications.

Avitabile, P., 2001. *Experimental Modal Analysis*, Lowell: University of Massachusetts Lowell.

Bailey, W. S., 1961. Gas Particle Flow in an Axisymmetric Nozzle. *ARS Journal*, 31(6), pp. 793-798.

Bernstein, A., Heiser, W. H. & Hevenor, C., 1967. Compound-Compressible Nozzle Flow. *Journal of Applied Mechanics*, 34(3), pp. 548-554.

Beychok, M., 2010. *De Laval nozzle*. [Online] Available at: http://en.citizendium.org/wiki/File:De_Laval_nozzle_2.png [Accessed 22 09 2015].

Boroschek, K. R., 2002. *Base Isolation in Hospitals*. Barbados, Seminar on Design of Health Facilities to Resist Natural Hazards .

Braga, F., 2001. *Seismic Isolation Using Slide and Rubber Bearings*. Assisi, Italy, s.n.

Brennan, D., 2001. *The numerical simulation of two phase flows in settling tanks*. London: Imperial College London.

Buchanan, A. et al., 2011. *Base Isolation and Damage Resistant Technologies for Improved Seismic Performance of Buildings*, Christchurch: University of Canterbury.

Buckle, I. G., 2000. *Passive Control of Structures for Seismic Loads*. s.l., s.n.

Butterworth, J., Lee, J. H. & Davidson, B., 2004. *Experimental Determination of Modal Damping from Full Scale Testing*. Vancouver, 13th Conference on Earthquake Engineering .

Castillo, J., 1991. Discrete Variational Grid Generation. In: J. Castillo, ed. *MATHEMATICAL ASPECTS OF NUMERICAL GRID GENERATION*. s.l.:SIAM.

Chopra, 2007. *Dynamics of Structures*. Third Edition ed. Upper Saddle River: Pearson Prentice Hall.

Clancy, L., 1975. *Aerodynamics*. New York: John Wiley & Sons Inc.

Clough, R. W. & Penzien, J., 2003. *DYNAMICS OF STRUCTURES*. 3rd ed. Berkeley: Computers & Structures.

Cooperstock, F., 2009. *General relativistic dynamics: extending Einstein's legacy throughout the universe*. Singapore: World Scientific.

De Silva, C. W., 2007. *Vibration Damping, Control, And Design*. Boca Raton: Taylor & Francis.

Deardorff, W., 1970. numerical study of three-dimensional turbulent channel flow at large Reynolds numbers. *Journal of Fluid Mechanics*, 41(2), p. 453-480.

Elarms, 2012. *Earthquake Alarm System*. [Online]

Available at: www.elarms.org

[Accessed 1st March 2012].

Eswaran, V. & Pope, S., 1988. Direct numerical simulations of the turbulent mixing of a passive scalar. *Physics of Fluids*, 31(March), pp. 506-520.

Eurocode8, 2011. *Design of structures for earthquake resistance Part 1*, s.l.: British standard.

Forni, M. & Martelli, A., 1998. Seismic isolation of civil buildings in europe. *Progress in Structural Engineering and Materials*, Volume 3(3), pp. 286-294.

Forni, M. & Martelli, A., 1998. Seismic isolation of civil buildings in europe. *Progress in Structural Engineering and Materials*, Volume 3(3), pp. 286-294.

Fujita, S., Minagawa, K., b, G. & HaruoShimosaka, 2011. Intelligent seismic isolation system using air bearings and earthquake early warning. *Soil Dynamics and Earthquake Engineering*, 31(2), p. 223-230.

GeoSIG, 2013. *AC-43 Force Balance Accelerometer*, Schlieren: GeoSIG.

GeoSIG, 2015. *GMSplus Measuring System*, Schlieren: GeoSIG.

Godfrey-Smith, P., 2003. *Theory and Reality: An introduction to the philosophy of science*. Chicago: University of Chicago Press.

Griffith, T., 2001. *The physics of everyday phenomena: a conceptual introduction to physics*. 3rd ed. Boston: McGraw-Hill.

Harris, F., 1978. On the use of windows for harmonic analysis with the discrete Fourier Transform. *Proc. IEEE*, 66(January), pp. 51-83.

Hendriks, F., 2001. *Shape optimization of pressurized air bearings*, Hawthorne: Rensselaer Polytechnic Institute.

Hibbeler, R. C., 2002. *Engineering Mechanics Dynamics*. 2nd ed. Singapore: Prentice Hall.

HOVAIR, 2013. *How does an air bearing work?*. [Online] Available at: <http://hovair.com/information-files/what-is-an-air-bearing-how-does-an-air-bearing-work.htm> [Accessed 01 06 2013].

Iqbal, A., 2006. *Soft First Story with Seismic Isolation System*. s.l., NZSEE Conference.

Ismail, M., 2009. *An Innovative Isolation Device for Aseismic Design*. PhD Thesis ed. Barcelona: Technical University of Catalonia.

Ismail, M., Rodellar, F. & Ikhoulane, 2010. An innovative isolation device for aseismic design. *Engineering Structures*, pp. 1168-1183.

Izumi, M., 1988. *State-of-the-art report: Base isolation and passive seismic response control*. Tokyo, s.n., pp. 385-396.

Izumi, M., 1988. *State-of-the-art report: Base isolation and passive seismic response control*. Tokyo, s.n., pp. 385-396.

Jangid, R. S., 1996. Optimum Damping in Non-linear Base Isolation System. *Journal of Sound and Vibration* , 189(4), pp. 477-487.

Jasak, H., 1996. *Error Analysis and Estimation for the Finite Volume Method with Applications to Fluid Flows*. London: Imperial College of Science, Technology and Medicine.

Jevons, W. S., 1958. *The Principles of Science: A Treatise on Logic and Scientific Method*. New York: Dover Publications.

Kani, N., Takayama, M. & Wada, A., 2006. *Performance of Seismically Isolated Buildings in Japan*. San Francisco, 8th U.S. National Conference on Earthquake Engineering .

Kelly, T. E., 2001. *Base Isolation of Structures*, Wellington: Holmes Consulting Group Ltd.

Kravchuk, N., Colquhoun, R. & Porbaha, A., 2008. *Development of a Friction Pendulum Bearing Base Isolation System for Earthquake Engineering Education*. Sacramento, American Society for Engineering Education Pacific Southwest Annual.

Kuramoto, H., 2006. Seismic Design Codes for Buildings in Japan. *Journal of Disaster Research*.

Marsico, M. R., 2008. *Seismic Isolation and Energy Dissipation: Theoretical Basis and Applications*. Napoli: Napoli Federico II university.

MATLAB help (2011) The MathWork Inc.

Mavriplis, D. J., 1996. Mesh generation and adaptivity for complex geometries and flows. In: R. Peyret, ed. *Handbook of computational fluid mechanics / edited by Roger Peyret*. 2 ed. London: Academic Press.

Monfared, H., Shirvani, A. & Nwaubani, S., 2013. An investigation into the seismic base isolation from practical perspective. *INTERNATIONAL JOURNAL OF CIVIL AND STRUCTURAL ENGINEERING*, 3(3), pp. 451- 463.

Mukai, T., 2006. *Analysis of Dynamic Characteristics of Air Bearing*, s.l.: NIPPON STEEL.

Naeim, F. & Kelly, J. M., 1999. *Design of seismic isolated structures: from theory to practice*. New York: John Wiley & Sons.

Naeim, F. & Kelly, J. M., 1999. *Design of seismic isolated structures: from theory to practice*. New York: John Wiley & Sons.

Naeim, F. & Kelly, J. M., 1999. *Design of seismic isolated structures: from theory to practice*. New York: John Wiley & Sons.

- Nakashima, M. & Chusilp, P., 2003. A Partial View of Japanese Post-Kobe Seismic Design and Construction Practices. *Earthquake Engineering and Engineering Seismology*, Vol. 4, No. 1.
- Newway, 2006. *Air Bearing Application and Design Guide*, Aston: New way air bearing.
- Ørsted, H. C., 1998. *Selected Scientific Works of Hans Christian Ørsted*. Princeton: Princeton University Press.
- Parducci, A., 2010. *SEISMIC ISOLATION: WHY, WHERE, WHEN*, San Francisco: esempi di Architettura.
- Precision, N. W., 2003. *Air Bearing Application and Design Guid*, Aston, PA: New Way Precision.
- Popper, K., 2002. *Conjectures and Refutations: The Growth of Scientific Knowledge*. Abingdon: Routledge Classics.
- Popper, K., 2002. *The Logic of Scientific Discovery*. London: Routledge Classics.
- Powell, J. W., 1970. *Design of Aerostatic Bearings*. s.l.:Machinery Publishing Ltd .
- Ramezanpour, A., 2009. *AUTHENTIC OPTIMISATION STUDY OF THE NOVEL COMPACT HEAT EXCHANGER*. 1st ed. s.l.:VDM Verlag.
- Ramirez, R., 1975. *The FFT: Fundamentals and concepts*, Beaverton: Tekronix.
- Renn, J.-C. & Hsiao, C.-H., 2004. Experimental and CFD study on the mass flow-rate characteristic of gas through orifice-type restrictor in aerostatic bearings. *Tribology International*, 37(4), pp. 309-315.
- Roussis, P. C. & Constantinou, M. C., 2006. Uplift-restraining Friction Pendulum seismic isolation system. *EARTHQUAKE ENGINEERING AND STRUCTURAL DYNAMICS*, 35(5), p. 577–593.
- Saiful-Islam, Jumaat, M. J. & Zamin, M., 2011. Seismic isolation in buildings to be a practical reality: Behavior of structure and installation technique. *Journal of Engineering and Technology Research*, Vol. 3(4),, pp. pp. 99-117.

Solving, 2015. *400t handling system for diesel engines*. [Online]
Available at: <http://www.solving.com/case-studies/400t-handling-system-for-diesel-engines>

[Accessed 10 08 2015].

Sterken, C., 2003. *Jean Baptiste Joseph Fourier*. San Francisco, Astronomical Society of the Pacific.

Symans, M. D., 2004. *Seismic Protective Systems*. s.l.:FEMA 451.

Tajirian, F. F., 1998. *Base Isolation Design for Civil Components and Civil Structures*. San Francisco, Structural Engineers World Congress.

Tiwari, P., Stein, A. & Lin, Y.-L., 2013. Dual-Solution and Choked Flow Treatment in a Streamline Curvature Throughflow Solver. *Journal of Turbomachinery*, 135(4), p. 041004.

USGS, 2015. *Earthquake Early Warning*. [Online]

Available at: <http://earthquake.usgs.gov/research/earlywarning/>

[Accessed 20 10 2015].

Walters, M., 2003. *THE SEISMIC RETROFIT OF THE OAKLAND CITY HALL*. San Francisco , SMIP03 Seminar on Utilization of Strong-Motion Data.

Wei, L. & Gang, B., 2010. Entrance Effect on Load Capacity of Orifice Compensated Aerostatic Bearing with Feeding Pocket. *CHINESE JOURNAL OF MECHANICAL ENGINEERING*, Volume 23.

Wilcox, D. C., 2006. *Turbulence Modeling for CFD*. 3rd ed. La Canada, California: DCW Industries, Inc.

Wilczek, F. & Devine, B., 2006. *Fantastic realities : 49 mind journeys and a trip to Stockholm*. New Jersey: World Scientific.

Wright, K. R. & Zegarra, A. V., 2000. *Machu Picchu: A Civil Engineering Marvel*. s.l.:ASCE Press.

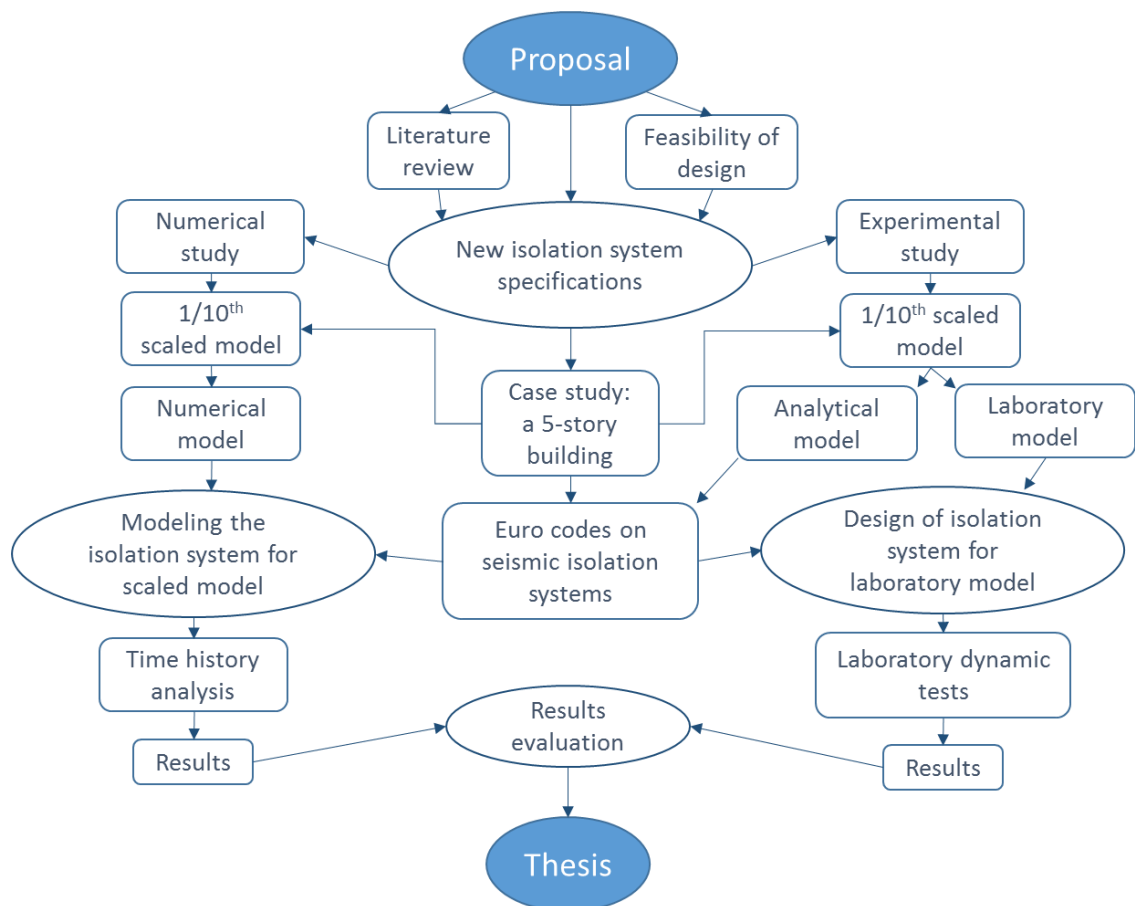
Wu, Y. M. & Samali, B., 2002. Shake Table Testing of a Base Isolated Model. *Engineering Structure*, 24(2002), pp. 1203-1215.

Zhou, F. L., Yang, Z., Liu, W. G. & Tan, P., 2004. *New Seismic Isolation System For Irregular Structure With The Largest Isolation Building Area In The World*. Vancouver, 13th World Conference on Earthquake Engineering.

Appendices

A.1 Research flowchart

Diagram below shows the research path from proposal to thesis.



A.2 BI projects around the world

Seismic base-isolation projects in U.S.A

Project	Purpose and location	Isolating system	Construction completed in year	Description
Foothill Communities Law and Justice Center (Naeim & Kelly, 1999)	Official building to be built, Rancho Cucamonga near Los Angeles	Isolation bearing, 98 High-damping natural rubbers	1985	The first base-isolated building in the United States and the first building in the world to use High-damping natural rubber, the four stories high with 170,000 ft ² area, designed to withstand an 8.3 magnitude earthquake.
Flight simulator manufacturing facility (Naeim & Kelly, 1999)	Official building to be built, Salt Lake city	Isolation bearing, 98 isolators, 50 of the bearings are lead plug and 48 plain elastomeric bearings	1988	The building is located very close to the Wastach Fault which has capability of generating 7.5 magnitude earthquakes, a four-story building with 116,000 ft ² area.
The M. L. King/C. R. Drew Diagnostic trauma center (Naeim & Kelly, 1999)	Hospital building to be built , Willowbrook, Los Angeles county	Isolation and Sliding bearings, 70 high-damping natural rubbers and 12 sliding bearings	1995	The largest isolation bearings fabricated in the United States at the time, a five stories building with 140,000 ft ² area.
AutoZone head quarter (Naeim & Kelly, 1999)	Official building to be built, Memphis	Isolation bearing, composed of 24 lead-plug rubber isolators and 19 high-damping	1995	A large office building, eight stories and 250,000 ft ² area, withstand a maximum seismic event of 9.0

		natural rubber isolators		magnitude, without the base isolation system, the building itself could withstand a magnitude 6.0 event.
Oakland City Hall (Walters, 2003)	Historical building to be retrofitted, Oakland	Isolation bearing, composed of 113 elastomeric bearings approximately half of which have lead cores	1995	The top of the 18-story building is 324 feet above street level which was completed in 1914, the first high-rise government building in the United States at the time.
U.S. Court of Appeals (Naeim & Kelly, 1999) (Kravchuk, et al., 2008)	Historical building to be retrofitted, San Francisco	Friction Pendulum System, 256 bearings	1996	A five-story building with 350,000 ft ² area. was built in 1905 on a steel gravity frame with unreinforced granite and brick masonry walls.
San Francisco City Hall (Naeim & Kelly, 1999)	Historical building to be retrofitted, San Francisco	Isolation bearing, composed of 530 lead-plug rubber bearings	1998	A five-story building with 300 ft high dome. The structural system is a steel frame which was designed in 1912.
San Francisco International Airport (International Terminal) (Kravchuk, et al., 2008)	Building to be built, San Francisco, California	Friction Pendulum System, 267 bearings	2000	The largest isolated building of the world, can resist a magnitude 8 earthquake.

Some seismic base-isolation projects in Japan

Project	Purpose and location	Isolating system	Construction completed in year	Description
Science University of Tokyo (Izumi, 1988)	Official building to be built, Tokyo	Double columns and dampers	1981	The first modern base-isolated building in Japan
Yachiyodai Unitika (Izumi, 1988)	Residential building to be built, Tokyo	Laminated rubber bearing and PC plate friction damper	1983	-
Oyles Technical center (Izumi, 1988)	Official Building to be built,	Laminated lead rubber bearing, 45 bearings	1987	-
West Japan Postal Computer Center (Naeim & Kelly, 1999)	Official building to be built, Sanda	120 elastomeric Isolators, additional steel and lead dampers	Before 1995	A six-story building, 506,000 ft ² area, has shown a very reasonable performance during the 1995 Kobe earthquake
C-1 Building	Computer center to be built, Fuchu City, Tokyo	68 Lead Rubber Bearing	1992	A seven-story building, with the area of 407,350 ft ²
Maiya Matsumoto hospital (Boroschek, 2002)	Hospital to be built, Kyoto	24 rubber bearings, 8 lead dampers and 14 steel bar dampers	1997	-
Kyorin University School of Medicine (Boroschek, 2002)	Hospital to be built, Shinkawa, Mitaka City, Tokyo	72 lead rubber bearings	2000	A seven-story building, one below ground, with maximum height of 40.30m
NS computer center (Kani, et al., 2006)	Official building to be built, Nagaoka City	-	2004	The first data center with seismic isolation

Some notable seismic base-isolation projects around the world

Project	Purpose and location	Isolating system	Construction completed in year	Description
New Fire Station and Headquarter of Napoli (Forni & Martelli, 1998)	Official building, Italy	Mechanical dissipaters and isolators	1981	The first base-isolated building in Italy
Union House Auckland (Naeim & Kelly, 1999)	Official building, Auckland, New Zealand	Sleeved-pile system	1984	A 12-story reinforced concrete building with additional damping system
Ancona SIP buildings (Marsico, 2008) (Naeim & Kelly, 1999) (Forni & Martelli, 1998)	Official building, Italy	Rubber bearings with recessed plate connections	1988-1992	The first base-isolated building in Italy with application of rubber bearings
Wellington Central Police Station (Naeim & Kelly, 1999)	Official building, Wellington, New Zealand	Sleeved-pile system	1991	A 10-story reinforced concrete building with additional lead-extrusion dampers for controlling purposes
National museum of New Zealand (Braga, 2001) (Naeim & Kelly, 1999)	Museum, Wellington, New Zealand	142 lead-rubber bearings, and 36 Teflon pads under the shear walls	1995	A five story building with 23m high
Department of Mathematics, University of Basilicata (Forni & Martelli, 1998)	Official Building, Italy	89 High-damping Rubber bearings	1995	Block 1-4 of Faculty of Agriculture also were built on 132 bearings in the same year
Museum (Zhou, et al., 2004)	Official building to be built, China	Rubber bearings	1996	A 13-story reinforced concrete building
New Zealand parliament House (Naeim & Kelly, 1999)	Historical building to be retrofitted, Wellington, New Zealand	More than 514 lead-rubber bearings	1996	The building was designed in 1911 and strengthened and refurbished between 1991 to 1996

Corinth Canal Bridges (Roussis & Constantinou, 2006)	Bridge to be built, Greece	Elastomeric and Flat sliding bearings	1997	One of the notable seismic-isolation in Greece
LNG Tanks, In-Chon (Tajirian, 1998)	Infrastructure, Korea	Steel-laminated rubber bearings	1997	An example of utilizing base- isolation system for infrastructures
Sanctuary of Siracusa (Marsico, 2008)	Temple to be retrofitted, Italy	New kind bearings namely “moon’s sickle”	2006	One of the notable retrofitting projects in Europe
Parand residential project (Ab-Malek & Kamaruddin, 2010)	Residential buildings to be built, Iran	More than 8,000 rubber bearings	Under construction	150 blocks of residential building of 8 and 12-storey high, this is the world’s largest application of seismic rubber bearings in a single project, 360rubber bearings had been installed until 2009

A.3 Roller bearing specifications

Part number 9101 was chosen and used with respect to space restrictions under the scaled structure and roller's load capacity.

HIGH CAPACITY RANGE - Maximum Precision www.omnitrack.co.uk

Low Friction	Speed	Temperature	Orientation	High Shock	Drain / Debris	User
1: 0,005	2 m/sec	-30 to 160 °C	ANY	Resistance	Channels ▼	Serviceable ▼

▼ = Not applicable on units with Ball Ø 12.7mm

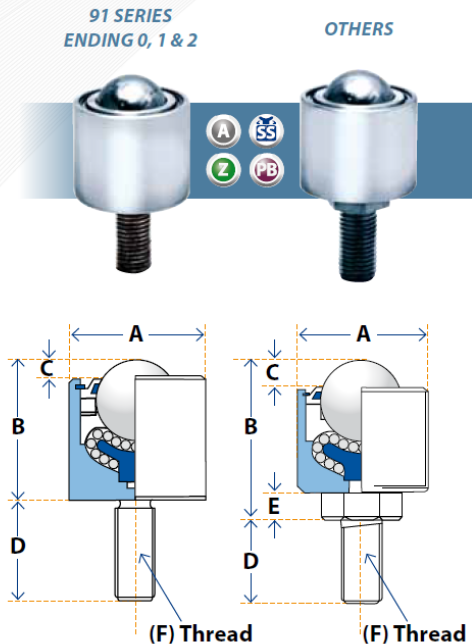
High Capacity "double recirculation" range offers maximum precision & smoothest performance. Machined from solid steel bar this innovative design provides the highest load capacity & longest service life available. User-serviceable with factory spares backup.

Standard Materials - high grade AISI 52100 chrome steel Balls & zinc plated carbon steel housing	Corrosion Resistance	Contaminated Environment	Temperature Low	Temperature High	Radiation Resistance	Delicate Surfaces
A = Stainless Steel Balls (AISI 440) but other materials as Standard	✓	✓	✓	✓	✓	
Z = 'Arduous Conditions' Stainless Steel (AISI440) = Internal parts & Balls. "Anti-Oxide" finish to outer housing – see page 2	✓✓	✓✓	✓✓	✓	✓	
SS = All parts Stainless Steel – outer housing AISI 304. Internal parts & Balls AISI 440	✓✓✓	✓✓✓	✓✓✓	✓✓✓	✓✓✓	
PB = Phenolic Resin main ball option available with 'Standard', 'Z' ('Arduous Conditions') & 'SS' (all Stainless Steel) material options – see Technical Reference on page 10 for load ratings						✓✓✓

91 Series - *THREADED STUD*

Part No	Load (kg)	Ball Ø mm	A	B	C	D	E	F
9100	46	12.7	20	19.1	3.8 *	16.1		M8 x 1.25
9101	46	12.7	20.6	19.1	3.8 *	28.7		M8 x 1.25
9102	46	12.7	20.6	19.1	3.8 *	28.7		5/16" UNF
9112	46	12.7	22.2	22.2	3.8 *	25.4		5/16" UNF
9120	225	25.4	44	48.3	5.6	25		M12 x 1.75
9123	225	25.4	44	47.3	5.6	25	6	M12 x 1.75
9124	225	25.4	44.5	47.3	7.1	25.4	6	1/2" UNF
9130	375	25.4	50	51.3	6.4	25		M12 x 1.75
9133	375	25.4	50	50.5	6.4	25	6	M12 x 1.75
9134	375	25.4	50.8	50.5	6.4	25.4	6	1/2" UNF
9135	375	25.4	50.8	42	6.4	60	10	1" UNF
9140	1100	38.1	60	73.5	12.7	40		M20 x 2.5
9143	1100	38.1	60	71.5	12.7	40	10	M20 x 2.5
9144	1100	38.1	60.3	71.5	12.7	38.1	10	3/4" UNF
9145	1100	38.1	60.3	60	12.7	75	6	1" UNF
9150	2200	50.8	100	105	14.3	54		M24 x 3.0
9153	2200	50.8	100	109	14.3	50	10.6	M24 x 3.0
9154	2200	50.8	101.6	109	14.3	50.8	10.6	1" UNF
9160	4550	76.2	160	145	21	57.2		1" UNF
9163	4550	76.2	160	145	21	100	15	M30 x 3.5

* further 1.5mm @ 16.2mm outside Ø
91 Series units omit drain/debris channel - contact us if required

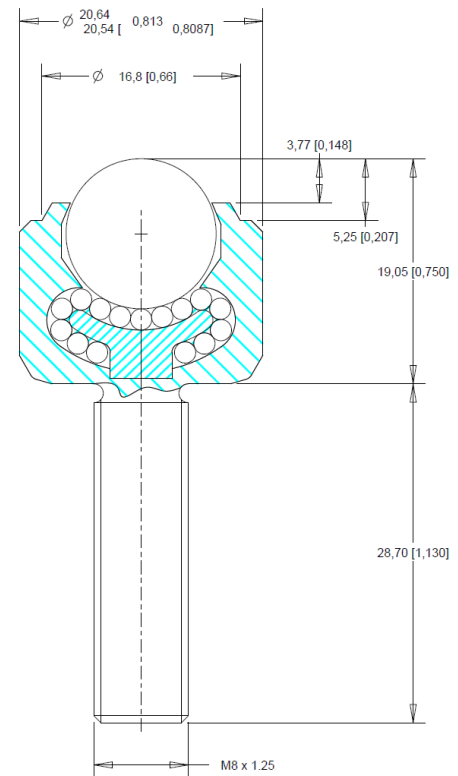


Available Material Options			
Part #	Load bearing internal materials	Ball Material	Casing material & finish
9101	AISI 52100	AISI 52100	AISI 1012 - Zinc plated
9101-A	AISI 52100	AISI 440	AISI 1015 - Zinc plated
9101-SS	AISI 440	AISI 440	AISI 304 - Natural

LOAD CAPACITY 46kg

<small>THIS DOCUMENT CONTAINS OMNITRACK LTD PROPRIETARY AND CONFIDENTIAL INFORMATION. IF IT IS LOANED FOR LIMITED PURPOSES ONLY AND REMAINS THE PROPERTY OF OMNITRACK LTD. IT MAY NOT BE REPRODUCED IN WHOLE OR PART OR DISCLOSED TO THIRD PARTIES WITHOUT THE PRIOR WRITTEN CONSENT OF OMNITRACK LTD. THIS DOCUMENT IS TO BE RETURNED TO OMNITRACK LTD UPON REQUEST AND IN ALL RESPECTS FOR PROTECTION OF THE INFORMATION CONTAINED HEREIN.</small>		
ALL DIMENSIONS SHOWN IN mm		
DRAWING No.		
9101		
		Omnitrack Ltd Station Road Industrial Estate, Woodchester, Gloucestershire, GL5 5EQ - UK Tel: +44 (0) 1453 873 345 Fax: +44 (0) 1453 878 500 info @ omnitrack.co.uk www.omnitrack.co.uk

Omnitrack Ltd
Station Road Industrial
Estate, Woodchester,
Gloucestershire,
GL5 5EQ - UK
Tel: +44 (0) 1453 873 345
Fax: +44 (0) 1453 878 500
info @ omnitrack.co.uk
www.omnitrack.co.uk



A.4 Modal analysis (fixed-base model)

M= structural mass matrix

K= structural lateral stiffness matrix

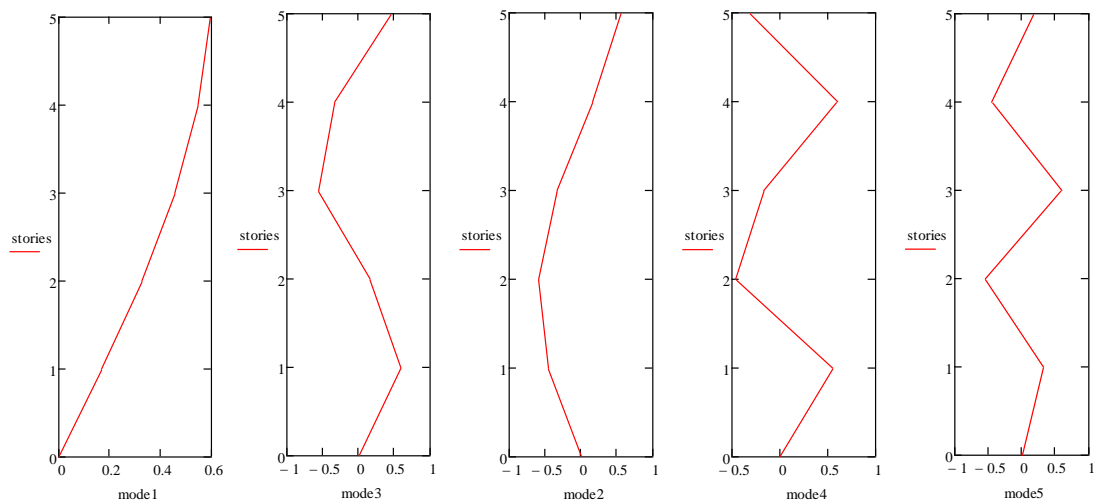
$$M := \begin{pmatrix} 40 & 0 & 0 & 0 & 0 \\ 0 & 40 & 0 & 0 & 0 \\ 0 & 0 & 40 & 0 & 0 \\ 0 & 0 & 0 & 40 & 0 \\ 0 & 0 & 0 & 0 & 40 \end{pmatrix} \quad K := \begin{pmatrix} 469400 & -469400 & 0 & 0 & 0 \\ -469400 & 938800 & -469400 & 0 & 0 \\ 0 & -469400 & 938800 & -469400 & 0 \\ 0 & 0 & -469400 & 938800 & -469400 \\ 0 & 0 & 0 & -469400 & 938800 \end{pmatrix}$$

$$M^{-1} = \begin{pmatrix} 0.025 & 0 & 0 & 0 & 0 \\ 0 & 0.025 & 0 & 0 & 0 \\ 0 & 0 & 0.025 & 0 & 0 \\ 0 & 0 & 0 & 0.025 & 0 \\ 0 & 0 & 0 & 0 & 0.025 \end{pmatrix} \quad M^T = \begin{pmatrix} 40 & 0 & 0 & 0 & 0 \\ 0 & 40 & 0 & 0 & 0 \\ 0 & 0 & 40 & 0 & 0 \\ 0 & 0 & 0 & 40 & 0 \\ 0 & 0 & 0 & 0 & 40 \end{pmatrix}$$

$$D := M^{-1} \cdot K = \begin{pmatrix} 1.173 \times 10^4 & -1.173 \times 10^4 & 0 & 0 & 0 \\ -1.173 \times 10^4 & 2.347 \times 10^4 & -1.173 \times 10^4 & 0 & 0 \\ 0 & -1.173 \times 10^4 & 2.347 \times 10^4 & -1.173 \times 10^4 & 0 \\ 0 & 0 & -1.173 \times 10^4 & 2.347 \times 10^4 & -1.173 \times 10^4 \\ 0 & 0 & 0 & -1.173 \times 10^4 & 2.347 \times 10^4 \end{pmatrix}$$

$$\text{eigenvals}(D) = \begin{pmatrix} 950.7 \\ 8.1 \times 10^3 \\ 2.013 \times 10^4 \\ 3.322 \times 10^4 \\ 4.321 \times 10^4 \end{pmatrix} \quad \Psi := \text{eigenvecs}[D, ("R")] = \begin{pmatrix} 0.597 & 0.549 & 0.456 & -0.326 & 0.17 \\ 0.549 & 0.17 & -0.326 & 0.597 & -0.456 \\ 0.456 & -0.326 & -0.549 & -0.17 & 0.597 \\ 0.326 & -0.597 & 0.17 & -0.456 & -0.549 \\ 0.17 & -0.456 & 0.597 & 0.549 & 0.326 \end{pmatrix}$$

$$\text{mode 1} := \begin{pmatrix} 0 \\ 0.17 \\ 0.326 \\ 0.456 \\ 0.549 \\ 0.597 \end{pmatrix} \quad \text{mode 2} := \begin{pmatrix} 0 \\ -0.456 \\ -0.597 \\ -0.326 \\ 0.17 \\ 0.549 \end{pmatrix} \quad \text{mode 3} := \begin{pmatrix} 0 \\ 0.597 \\ 0.17 \\ -0.549 \\ -0.326 \\ 0.456 \end{pmatrix} \quad \text{mode 4} := \begin{pmatrix} 0 \\ 0.549 \\ -0.456 \\ -0.17 \\ 0.597 \\ -0.326 \end{pmatrix} \quad \text{mode 5} := \begin{pmatrix} 0 \\ 0.326 \\ -0.549 \\ 0.597 \\ -0.456 \\ 0.17 \end{pmatrix}$$



$$\Psi = \begin{pmatrix} 0.597 & 0.549 & 0.456 & -0.326 & 0.17 \\ 0.549 & 0.17 & -0.326 & 0.597 & -0.456 \\ 0.456 & -0.326 & -0.549 & -0.17 & 0.597 \\ 0.326 & -0.597 & 0.17 & -0.456 & -0.549 \\ 0.17 & -0.456 & 0.597 & 0.549 & 0.326 \end{pmatrix} \quad \Psi^T = \begin{pmatrix} 0.597 & 0.549 & 0.456 & 0.326 & 0.17 \\ 0.549 & 0.17 & -0.326 & -0.597 & -0.456 \\ 0.456 & -0.326 & -0.549 & 0.17 & 0.597 \\ -0.326 & 0.597 & -0.17 & -0.456 & 0.549 \\ 0.17 & -0.456 & 0.597 & -0.549 & 0.326 \end{pmatrix}$$

$$\lambda := \text{eigenvals}(D) = \begin{pmatrix} 950.7 \\ 8.1 \times 10^3 \\ 2.013 \times 10^4 \\ 3.322 \times 10^4 \\ 4.321 \times 10^4 \end{pmatrix} \quad \lambda_i = \begin{array}{|c|} \hline 950.7 \\ \hline 8.1 \cdot 10^3 \\ \hline 2.013 \cdot 10^4 \\ \hline 3.322 \cdot 10^4 \\ \hline 4.321 \cdot 10^4 \\ \hline \end{array} \quad i := 1..5$$

$$\omega_i := \sqrt{\lambda_i} = \dots \quad \omega_i = \begin{array}{|c|} \hline 30.833 \\ \hline 90.002 \\ \hline 141.88 \\ \hline 182.263 \\ \hline 207.88 \\ \hline \end{array} \quad f_i := \frac{\omega_i}{2\pi} \quad f_i = \begin{array}{|c|} \hline 4.907 \\ \hline 14.324 \\ \hline 22.581 \\ \hline 29.008 \\ \hline 33.085 \\ \hline \end{array} \quad T_i := \frac{1}{f_i} \quad T_i = \begin{array}{|c|} \hline 0.204 \\ \hline 0.07 \\ \hline 0.044 \\ \hline 0.034 \\ \hline 0.03 \\ \hline \end{array}$$

$$\underline{\underline{m}} := \Psi^T M \cdot \Psi = \begin{pmatrix} 40 & 9.326 \times 10^{-15} & -3.553 \times 10^{-15} & -1.332 \times 10^{-15} & -1.066 \times 10^{-14} \\ 1.066 \times 10^{-14} & 40 & 3.553 \times 10^{-15} & 1.776 \times 10^{-15} & 1.599 \times 10^{-14} \\ -3.553 \times 10^{-15} & 0 & 40 & -1.243 \times 10^{-14} & 0 \\ 0 & 0 & -1.243 \times 10^{-14} & 40 & 6.217 \times 10^{-15} \\ -1.021 \times 10^{-14} & 1.599 \times 10^{-14} & 0 & 7.994 \times 10^{-15} & 40 \end{pmatrix}$$

$$i := 1..5$$

$$m_{i,i} =$$

40
40
40
40
40

$r :=$

1
1
1
1
1

$$\underline{\underline{L}} := \Psi^T M \cdot r = \begin{pmatrix} 83.882 \\ -26.409 \\ 13.919 \\ 7.751 \\ 3.541 \end{pmatrix}$$

$L_{i,1} =$

83.882
-26.409
13.919
7.751
3.541

$$\Gamma_i =$$

$\Gamma_i := \frac{L_{i,1}}{m_{i,i}} = ...$

2.097
-0.66
0.348
0.194
0.089

$$meff_i =$$

$meff_i := \frac{(L_{i,1})^2}{m_{i,i}} = ...$

175.906
17.435
4.843
1.502
0.314

 $mtotal := \sum meff = 200$

A.5 Modal analysis (base isolated)

M= structural mass matrix

K= structural lateral stiffness matrix

$$M := \begin{pmatrix} 40 & 0 & 0 & 0 & 0 & 0 \\ 0 & 40 & 0 & 0 & 0 & 0 \\ 0 & 0 & 40 & 0 & 0 & 0 \\ 0 & 0 & 0 & 40 & 0 & 0 \\ 0 & 0 & 0 & 0 & 40 & 0 \\ 0 & 0 & 0 & 0 & 0 & 40 \end{pmatrix} \quad K := \begin{pmatrix} 469400 & -469400 & 0 & 0 & 0 & 0 \\ -469400 & 938800 & -469400 & 0 & 0 & 0 \\ 0 & -469400 & 938800 & -469400 & 0 & 0 \\ 0 & 0 & -469400 & 938800 & -469400 & 0 \\ 0 & 0 & 0 & -469400 & 938800 & -469400 \\ 0 & 0 & 0 & 0 & -469400 & 483900 \end{pmatrix}$$

$$M^{-1} = \begin{pmatrix} 0.025 & 0 & 0 & 0 & 0 & 0 \\ 0 & 0.025 & 0 & 0 & 0 & 0 \\ 0 & 0 & 0.025 & 0 & 0 & 0 \\ 0 & 0 & 0 & 0.025 & 0 & 0 \\ 0 & 0 & 0 & 0 & 0.025 & 0 \\ 0 & 0 & 0 & 0 & 0 & 0.025 \end{pmatrix}$$

$$D := M^{-1} \cdot K = \begin{pmatrix} 1.173 \times 10^4 & -1.173 \times 10^4 & 0 & 0 & 0 & 0 \\ -1.173 \times 10^4 & 2.347 \times 10^4 & -1.173 \times 10^4 & 0 & 0 & 0 \\ 0 & -1.173 \times 10^4 & 2.347 \times 10^4 & -1.173 \times 10^4 & 0 & 0 \\ 0 & 0 & -1.173 \times 10^4 & 2.347 \times 10^4 & -1.173 \times 10^4 & 0 \\ 0 & 0 & 0 & -1.173 \times 10^4 & 2.347 \times 10^4 & -1.173 \times 10^4 \\ 0 & 0 & 0 & 0 & -1.173 \times 10^4 & 1.21 \times 10^4 \end{pmatrix}$$

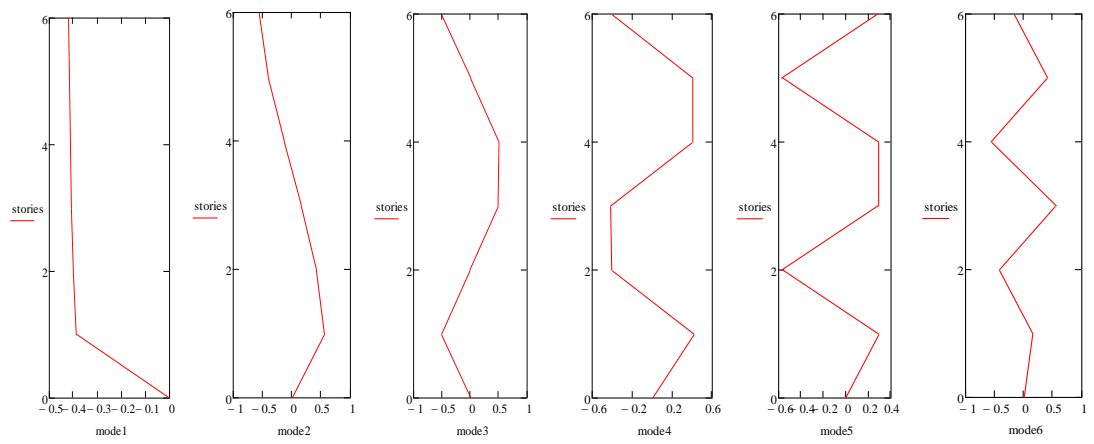
$$\text{eigenvals}(D) = \begin{pmatrix} 57.654 \\ 3.258 \times 10^3 \\ 1.183 \times 10^4 \\ 2.353 \times 10^4 \\ 3.524 \times 10^4 \\ 4.38 \times 10^4 \end{pmatrix}$$

$$\Psi := \text{eigenvecs}[\mathbf{D}, ("R")] = \begin{pmatrix} -0.42 & -0.552 & -0.498 & -0.407 & 0.288 & -0.149 \\ -0.418 & -0.399 & 3.891 \times 10^{-3} & 0.409 & -0.577 & 0.408 \\ -0.414 & -0.135 & 0.502 & 0.405 & 0.29 & -0.557 \\ -0.408 & 0.166 & 0.494 & -0.411 & 0.286 & 0.558 \\ -0.4 & 0.421 & -0.012 & -0.403 & -0.577 & -0.409 \\ -0.389 & 0.56 & -0.506 & 0.414 & 0.293 & 0.151 \end{pmatrix}$$

$$\Psi = \begin{pmatrix} -0.42 & -0.552 & -0.498 & -0.407 & 0.288 & -0.149 \\ -0.418 & -0.399 & 3.891 \times 10^{-3} & 0.409 & -0.577 & 0.408 \\ -0.414 & -0.135 & 0.502 & 0.405 & 0.29 & -0.557 \\ -0.408 & 0.166 & 0.494 & -0.411 & 0.286 & 0.558 \\ -0.4 & 0.421 & -0.012 & -0.403 & -0.577 & -0.409 \\ -0.389 & 0.56 & -0.506 & 0.414 & 0.293 & 0.151 \end{pmatrix}$$

$$\Psi^T = \begin{pmatrix} -0.42 & -0.418 & -0.414 & -0.408 & -0.4 & -0.389 \\ -0.552 & -0.399 & -0.135 & 0.166 & 0.421 & 0.56 \\ -0.498 & 3.891 \times 10^{-3} & 0.502 & 0.494 & -0.012 & -0.506 \\ -0.407 & 0.409 & 0.405 & -0.411 & -0.403 & 0.414 \\ 0.288 & -0.577 & 0.29 & 0.286 & -0.577 & 0.293 \\ -0.149 & 0.408 & -0.557 & 0.558 & -0.409 & 0.151 \end{pmatrix}$$

$$\begin{array}{l} \text{mode 1} := \begin{pmatrix} 0 \\ -0.389 \\ -0.4 \\ -0.408 \\ -0.414 \\ -0.418 \\ -0.42 \end{pmatrix} \text{mode 2} := \begin{pmatrix} 0 \\ 0.56 \\ 0.421 \\ 0.166 \\ -0.135 \\ -0.399 \\ -0.552 \end{pmatrix} \text{mode 3} := \begin{pmatrix} 0 \\ -0.506 \\ -0.012 \\ 0.494 \\ 0.502 \\ 0.004 \\ -0.498 \end{pmatrix} \text{mode 4} := \begin{pmatrix} 0 \\ 0.414 \\ -0.403 \\ -0.411 \\ 0.405 \\ 0.409 \\ -0.407 \end{pmatrix} \text{mode 5} := \begin{pmatrix} 0 \\ 0.293 \\ -0.577 \\ 0.286 \\ 0.29 \\ -0.577 \\ 0.288 \end{pmatrix} \text{mode 6} := \begin{pmatrix} 0 \\ 0.151 \\ -0.409 \\ 0.558 \\ -0.557 \\ 0.408 \\ -0.149 \end{pmatrix} \end{array}$$



i := 1..6

$$\lambda := \text{eigenvals}(D) = \begin{pmatrix} 57.654 \\ 3.258 \times 10^3 \\ 1.183 \times 10^4 \\ 2.353 \times 10^4 \\ 3.524 \times 10^4 \\ 4.38 \times 10^4 \end{pmatrix} \quad \lambda_i = \begin{array}{|c|} \hline 57.654 \\ \hline 3.258 \cdot 10^3 \\ \hline 1.183 \cdot 10^4 \\ \hline 2.353 \cdot 10^4 \\ \hline 3.524 \cdot 10^4 \\ \hline 4.38 \cdot 10^4 \\ \hline \end{array} \quad \omega_i = \begin{array}{|c|} \hline 7.593 \\ \hline 57.075 \\ \hline 108.75 \\ \hline 153.399 \\ \hline 187.712 \\ \hline 209.294 \\ \hline \end{array}$$

$$\omega_i := \sqrt{\lambda_i} = \dots$$

$$f_i = \begin{array}{|c|} \hline 1.208 \\ \hline 9.084 \\ \hline 17.308 \\ \hline 24.414 \\ \hline 29.875 \\ \hline 33.31 \\ \hline \end{array} \quad T_i = \begin{array}{|c|} \hline 0.827 \\ \hline 0.11 \\ \hline 0.058 \\ \hline 0.041 \\ \hline 0.033 \\ \hline 0.03 \\ \hline \end{array}$$

$$f_i := \frac{\omega_i}{2\pi} \quad T_i := \frac{1}{f_i}$$

$$\underline{\underline{m}} := \Psi^T M \cdot \Psi = \begin{pmatrix} 40 & 7.105 \times 10^{-15} & 8.882 \times 10^{-15} & -9.77 \times 10^{-15} & -1.776 \times 10^{-15} & -5.329 \times 10^{-15} \\ 3.553 \times 10^{-15} & 40 & 7.105 \times 10^{-15} & 0 & 4.441 \times 10^{-15} & 6.217 \times 10^{-15} \\ 6.217 \times 10^{-15} & 7.105 \times 10^{-15} & 40 & -5.329 \times 10^{-15} & -4.441 \times 10^{-15} & 3.553 \times 10^{-15} \\ -8.882 \times 10^{-15} & 0 & -8.882 \times 10^{-15} & 40 & 4.441 \times 10^{-15} & 0 \\ 0 & 1.776 \times 10^{-15} & -4.441 \times 10^{-15} & 1.776 \times 10^{-15} & 40 & 9.548 \times 10^{-15} \\ -7.55 \times 10^{-15} & 7.105 \times 10^{-15} & 3.553 \times 10^{-15} & 0 & 7.994 \times 10^{-15} & 40 \end{pmatrix}$$

$$i := 1..6$$

$$m_{i,i} =$$

40
40
40
40
40
40

$$r := \begin{pmatrix} 1 \\ 1 \\ 1 \\ 1 \\ 1 \\ 1 \\ 1 \end{pmatrix}$$

$$\underline{\underline{L}} := \Psi^T M \cdot r =$$

$$\begin{pmatrix} -97.946 \\ 2.491 \\ -0.62 \\ 0.255 \\ 0.12 \\ 0.05 \end{pmatrix}$$

$$L_{i,1} =$$

-97.946
2.491
-0.62
0.255
0.12
0.05

$$\Gamma_i =$$

-2.449
0.062
-0.015
$6.37 \cdot 10^{-3}$
$3.01 \cdot 10^{-3}$
$1.253 \cdot 10^{-3}$

$$\Gamma_i := \frac{L_{i,1}}{m_{i,i}} = \dots$$

$$meff_i =$$

239.833
0.155
$9.61 \cdot 10^{-3}$
$1.623 \cdot 10^{-3}$
$3.623 \cdot 10^{-4}$
$6.285 \cdot 10^{-5}$

$$meff_i := \frac{(L_{i,1})^2}{m_{i,i}} = \dots$$

$$m_{total} := \sum meff = 240$$

A.6 Air pump specifications

1- The air pump model used for producing pressurised air:





2- The air pump specifications according to its provider's manual:

	Net weight Kg.					
	HP 7,5 - kW 5,5	HP 10 - kW 7,5	HP 15 - kW 11	HP 15 - kW 11 (IVR)	HP 20 - kW 15	HP 20 [®] - kW 15 [®]
Weight (without / with) dryer	235 - 265	240 - 270	260 - 290	305 - 335	285 - 315	315 - 345
With air receiver 270 l. Weight	330	335	355	400	380	440
With air receiver 500 l. Weight	415	420	440	486	465	495

	HP 7,5 - kW 5,5			HP 10 - kW 7,5			HP 15 - kW 11		
	8 bar	10 bar	13 bar	8 bar	10 bar	13 bar	5 bar	7 bar	13 bar
Standard air capacity l/min.	820	670	520	1153	1000	810	1665	1435	1210
Max. pressure bar	8	10	13	8	10	13	8	10	13
Noise product. dB(A)	66						69		
Power HP - kW	7,5 - 5,5			10 - 7,5			15 - 11		
Oil operation timer setting °C	110								
Oil load l.	~ 5								

	HP 15 - kW 11 (IVR)				HP 20 - kW 15			HP 20 [®] - kW 15 [®]		
	6 bar	8,5 bar	9,5 bar	12,5 bar	8 bar	10 bar	13 bar	8 bar	10 bar	13 bar
Standard air capacity l/min.	1559	1535	1435	405	1985	1771	1480	2218	2020	1538
Max. pressure bar	5	7	9,5	12,5	8	10	13	8	10	13
Noise product. dB(A)	73				69			70		
Power HP - KW	15 - 11				20 - 15			20 - 15		
Oil operation timer setting °C	110									
Oil load l.	~ 5									

Type Dryer	Weight Kg.	Freon R 134a Kg.			Nominal Power W			Nominal Power W		Nominal Power W		bar MAX.
		50 Hz	60 Hz		50 Hz	60 Hz		50 Hz	60 Hz	50 Hz	60 Hz	
A 3	25	0,350			233			33		266		bar 13
A 4	27	0,480			302			60		362		bar 13

Reference conditions:
Ambient temperature 25 °C
Inlet air temperature 35 °C
Pressure 7 bar
Dew point in pressure 3 °C

Limit conditions:
Max. ambient temperature 43°C
Min. ambient temperature 5°C
Max. inlet air temperature 55°C
Max. working pressure 13 bar

A.7 GMSplus specifications and calibration

GeoSIG Ltd
Wiesenstrasse 39
8952 Schlieren
Switzerland

Tel: +41 44 810 21 50
Fax: +41 44 810 23 50
E-mail: info@geosig.com
Web: www.geosig.com

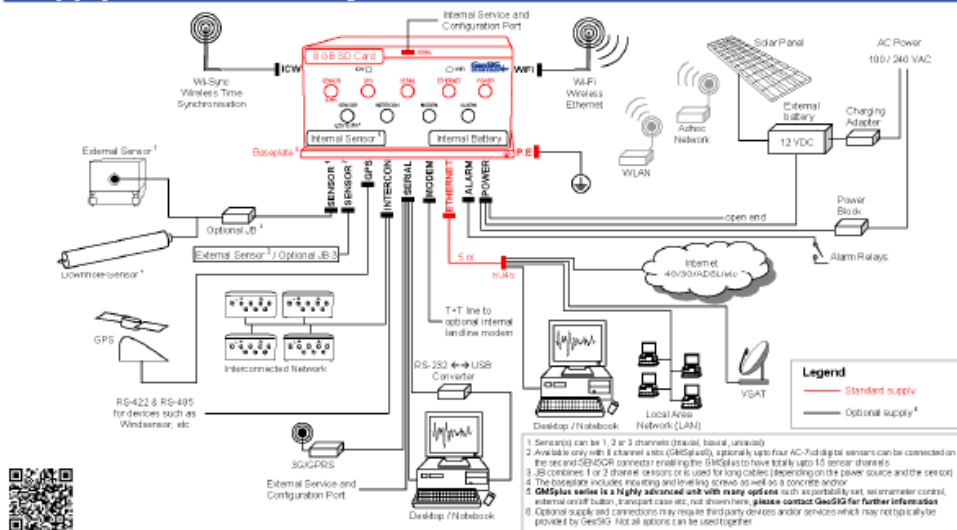


GMS^{plus} Measuring System

Features	Applications
<ul style="list-style-type: none"> Second generation of NetQuakes Recorder 3 or 6 channels, up to 1000 sps sampling rate up to 15 channels using digital sensors Low noise individual 24-bit $\Delta\Sigma$ ADC per channel Internal built-in and/or external sensors Wired Ethernet, Wi-Fi and Serial links Smart NTP timing, GPS time base, or time synchronisation via radio channel or cable Enhanced connectivity via landline modems, 3G cellular devices and satellite links Recording to SD or CF cards, up to 128 GByte USB interface for external storage and communication devices Continuous data recording to ringbuffers Flexible configuration of multiple triggers Simultaneous data streaming to several clients On board data processing and evaluation Rugged aluminium housing with levelling base plate for easy installation Configuration and status monitoring via Web Interface compatible with Smartphones Simple and secure communication over Internet with full remote management Internal battery, low power consumption Alarm output with up to 4 relays flexibly configurable for different types of events Easily configurable interconnected networks with common timing and triggering 	<ul style="list-style-type: none"> Broadband Seismic, Earthquake and Structural measuring and monitoring Real-time Seismology for Freefield and Urban Areas High Density Earthquake Monitoring Networks Shake / Hazard Mapping based on Instrumental Data Earthquake Early Warning[®] and Rapid Response Damage Estimation, Disaster Management Seismic Alarm and Safe Shutdown Ambient Vibration Testing (optionally fully wireless) Induced Vibration Monitoring and Notification Building Code Compliant Instrumentation



Supply and Connectivity



Specifications **GMS^{plus}**

Set-up and Configuration

An intuitive web interface is available for easy configuration with any web browser. Alternatively the configuration file in XML format can be edited on site through the instrument console, exchanged by replacing the memory card, remotely from a server or through SSH. Even if the configuration file can be manually edited at any time, a tool is provided to edit it securely.

Data Analysis

The GeoDAS software provides basic data evaluation in the field meeting the requirements of most scientific and engineering applications. Optionally GMSplus can perform certain analyses onboard.

Sensor

Various GeoSIG sensors as well as a number of other third party sensors can be housed internally or connected externally to the unit. In case of internal sensor, the levelling is done on the base plate of the GMSplus via its three levelling screws. The base plate is mounted using a single bolt during installation.

Digitizer

Channels:	3 or 6 optionally up to 15 using AC-7xd digital sensors
A/D conversion:	24 bit Δ -Σ converters Individual for each channel
DSP:	32 bit output word length
Dynamic range:	146 dB (per bin @ 1 Hz rel. full scale rms) 137 dB @ 50 sps
Sampling rate:	1000, 500, 250, 200, 100, 50 sps per channel
Max. bandwidth:	DC to 250 Hz
Anti Aliasing Filter:	Analog and digital FIR (finite impulse response)

CPU

Processor:	ARM 400 MHz
RAM:	64 MByte
Operating System:	GNU/Linux

Triggering

Several Trigger Sets can be defined in the instrument. Each set can be flexibly configured regarding the source of trigger, main and advanced trigger parameters, trigger processing and selected channels for storage. A voting logic based on the monitored channels can be defined.

Trigger Filter

Fully independent high-, low- or bandpass trigger filters can be configured.

Level Triggering

User adjustable threshold.

STA/LTA Triggering

User adjustable STA / LTA values and STA/LTA trigger and detrigger ratio.

Event Recording

Pre-event memory:	1 to 720 seconds, typical
Post-event duration:	1 to 7200 seconds, typical

Event Summary and Parameters

Content:	PGA, PGV, PGD, SA (at 0.3, 1, 3 Hz)
Transmission delay:	User defined from trigger time

Ring Buffer

Usage:	User can request an event from any period of the ring buffer by specifying the start time/date and the duration from the console or remotely from a server. Ringbuffer files with configurable duration which can be uploaded automatically to data server.
Method:	

Data Stream

Protocol/Compatibility:	GSBU, SeedLink, compatible to Earthworm
-------------------------	---

Storage Memory

Size and Type:	8 GByte Removable SD Card, Optionally Compact Flash Card higher capacity up to 128 GByte on request FAT32 or EXT4 formatted
Management:	Intelligent management of memory card capacity using policies as per file type and ring buffer capacity specification.
Recording format:	miniSEED with extended information encapsulated into blockette 2000
Estimated Capacity:	Sampling rate [sps] x 0.4 [MB / day / 3 channel] (example: 40 MByte / day / 3 channel @ 100 sps) typical, since the data is compressed, capacity depends on the context of the data.

Self Test

- Permanent self monitoring of hardware and software components without affecting their normal operation.
- User-configurable periodical state of health (SOH) report based on comprehensive test of instrument, which can be requested at any time.
- User-configurable periodical sensor test.

Time Base

Internal:	Intelligent Adaptive Real Time Clock (IARTC)
External:	NTP, optionally GPS, Wired or Wireless Interconnection
Standard TCXO accuracy:	±0.5 ppm (15 s/year) @ +25 °C ±2.5 ppm (75 s/year) @ -10 to +50 °C Optionally higher accuracy TCXO's available.
Accuracy after learn:	< ±0.5 ppm (15 s/year or 2 ms/h)
Accuracy with NTP:	< ±4 ms typical, assuming reasonable access to NTP servers

Power Supply

Input voltage:	12 - 18 VDC (optional 9 - 36 or 18 - 75 VDC) optional 90 - 260 VAC / 50 - 60 Hz to 15 VDC switched UL approved external power block
Power consumption:	130 mA @ 12 VDC for 3 channels 200 mA @ 12 VDC for 6 channels
Internal battery:	optional 7.2 Ah for > 24 h autonomy with Intelligent charger, higher autonomy is optionally available with external batteries

Indicators

Green:	Active Charge LED
Green:	Run/Stop LED
Yellow:	Event/Memory LED
Blue:	Network link/Traffic LED
Red:	Warning/Error LED

Communication

Configuration, Data Retrieval:	Via Ethernet, Wi-Fi, Serial line, Console, or directly via removable memory card. Fixed or Dynamic IP on Ethernet LAN and/or Internet connection with Ethernet interface optional OpenVPN
Network requirements:	Wi-Fi (b/g/n) network with WEP, WPA, WPA2 security and Enterprise Mode
Security:	GeoDAS proprietary protocol over SSL Checksum and software handshaking
Serial ports:	2 ports standard, + 3 ports optional
Baud rates:	Console: 115200 baud Serial Stream: 38400, 57600, 115200 baud

Alarm / Seismic Switch / Warning / Notification Option

Alarms:	3 Independent or 4 common relay contacts for trigger alarm and/or error SMS notification is optionally available
Alarm levels:	Configurable based on event triggers (NO or NC selectable during order)
Relay Hold-On:	1 to 60 seconds (User programmable)
Capacity:	The contacts are suitable for a low voltage control. In case large load must be switched then external relays should be implemented. 125 V / 250 mA

Interconnected Network Option

Wired or Wireless common time and trigger interconnection network, distributing GPS-grade time precision among several units is optionally available.

Modem Option

Internal or external modems of different types, including cellular 3G/4G modems, are optionally available.

Environment / Reliability

Operational temperature:	-20 to +70 °C*
Storage temperature:	-40 to +85 °C*
Humidity:	0 to 100 % RH (non condensing)
MTBF:	> 500'000 hours

Housing

Type:	Cast aluminium housing
Size:	296 x 175 x 140 mm (W x D x H)
Size with base plate:	296 x 225 x 156 mm (W x D x H)
Weight:	4.7 kg (optional < 4 kg) 0.3 kg internal sensor, 2.6 kg battery, 1.3 kg base plate, ask for other options
Protection:	IP65 (NEMA 4), optionally IP67 (NEMA 6)
Mounting:	Base plate with single bolt, surface mount. When base plate levelled and fixed, GMSplus can be replaced without re-leveling.

Easy Transport:

Optional portability accessories are available
to facilitate short term measurements.

GMSplus series are produced in different types to suit particular specifications or regulations. Specifications mentioned in this datasheet may be different among different types.

*: use of an internal battery may degrade this specification.

®: contact GeoSIG for the optional Earthquake Early Warning functionality.

101352_GS_Test_Record_GMSplus

Test Record GMSplus

Test Record	1351	Job	10975
S/N	101352	Test Procedure	GS_GMSplus_TestProcedure_V01

Customer	CH_GEOSIG_Ghadimzadh	Date	30.10.2014
		Tested by	GES

Model	GMSplus	101352	Option 1	GMS-WiFi	135409
Type	3 Ch		Option 2	AC-41-H ± 4 g	53756
Description	Recorder		Option 3	AC-41-H ± 4 g	53762
Main board	GS_IA18_S-MN/V6.H2	135169	Option 4	AC-41-H ± 4 g	53761
Conn. board	GS_IA18-CB/V10	135302	Option 5		
Input range	± 2 V DIFF		Option 6		
Sensor 1			Ext. Option 1		
Power	15 VDC		Ext. Option 2		
Predas	21.09.02		Ext. Option 3		
Armdas	21.09.02		MAC	8C:8E:76:00:3A:9B	
Linux	gms-linux-firmware-r96_20140711.gsfw		DSP	51.03.03	
			RTC	80.02.02	

Remarks: Mini Sensors X Only Wired**1. Test Equipment**

1.1. Test equipment is as per list and ready	<input checked="" type="checkbox"/> Ok
--	--

2. Visual Check

2.1. No defects found during visual check	<input checked="" type="checkbox"/> Ok
---	--

3. Configuration

3.1. Description	GMSplus - GeoSIG Ltd.
3.2. Memory	8GB
3.3. Station	GSGMS
3.4. Location	UK
3.5. Sampling rate	50 SPS
3.6. Units	cm/s ²
3.7. LSB value	0.000519753 cm/s ² /count
3.8. Pre event	5 s
3.9. Post event	20 s
3.10. Trigger level	300.000 cm/s ²
3.11. Alarms Trigger level	n/a

4. Sensor input test

4.1. AC input test	<input checked="" type="checkbox"/> Ok
4.2. DC input test	<input checked="" type="checkbox"/> Ok
4.3. Noise test	<input checked="" type="checkbox"/> Ok
4.4. Offset [counts]	<input checked="" type="checkbox"/> Ok

5. Real sensor test

5.1. Test pulse	<input type="checkbox"/> Ok	<input checked="" type="checkbox"/> n/a
5.2. Event X-Y-Z	<input type="checkbox"/> Ok	<input checked="" type="checkbox"/> n/a
5.3. Tilt	<input type="checkbox"/> Ok	<input checked="" type="checkbox"/> n/a
5.4. Over range	<input checked="" type="checkbox"/> Ok	<input type="checkbox"/> n/a

6. Options testing

6.1. GMS-Wi-Fi	<input type="checkbox"/> Ok	<input checked="" type="checkbox"/> n/a
6.2. GMS-GPS	<input type="checkbox"/> Ok	<input checked="" type="checkbox"/> n/a
6.3. GXX-3GM	<input type="checkbox"/> Ok	<input checked="" type="checkbox"/> n/a
6.4. ALC, Config:	<input type="checkbox"/> Ok	<input checked="" type="checkbox"/> n/a
6.5. GMS-Interconnection	<input type="checkbox"/> Ok	<input checked="" type="checkbox"/> n/a
6.6. Serial modem	<input type="checkbox"/> Ok	<input checked="" type="checkbox"/> n/a
6.7. Ethernet modem	<input type="checkbox"/> Ok	<input checked="" type="checkbox"/> n/a
6.8. Sensor junction box	<input checked="" type="checkbox"/> Ok	<input type="checkbox"/> n/a

7. Physical inspection

7.1. Housing	<input checked="" type="checkbox"/> Ok
7.2. Fixation and screws	<input checked="" type="checkbox"/> Ok
7.3. Cables and connectors	<input checked="" type="checkbox"/> Ok
7.4. Labels	<input checked="" type="checkbox"/> Ok
7.5. Cleanliness	<input checked="" type="checkbox"/> Ok

8. Configuration backup

8.1. Instrument configuration (*.xml)	<input checked="" type="checkbox"/> Ok
8.2. Software configuration (*.gsc)	<input checked="" type="checkbox"/> Ok
8.3. Test files archived	<input checked="" type="checkbox"/> Ok

Final Acceptance

All tests were executed according to the test procedure and all results were checked and are according to the specifications.

Tested by

GES

GES

on 30.10.2014

Approved by

THL

V.L.

on 30.10.2104

A.8 Accelerometer specifications and calibration

GeoSIG Ltd
Wiesenstrasse 39
8952 Schlieren
Switzerland
Tel: +41 44 810 21 50
Fax: +41 44 810 23 50
E-mail: info@geosig.com
Web: www.geosig.com



AC-43 / AC-42 / AC-41 Force Balance Accelerometer

Features

- ❑ Full Scale: ± 2 g (± 0.625 , 1, 4, 5 g optional)
- ❑ Bandwidth DC to 100 Hz
- ❑ MEMS Force Balance Accelerometer
- ❑ High accelerations measurement
- ❑ High shock survivability
- ❑ Large temperature range
- ❑ High lifetime stability
- ❑ Cost effective sensor
- ❑ Low power consumption
- ❑ Simple test and calibration
- ❑ Single Bolt Mounted Enclosure provides up to $\pm 10^\circ$ of Leveling Adjustment



Outline

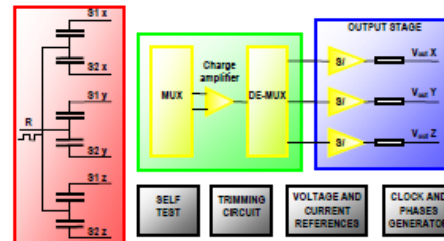
The AC-43 sensor package is a triaxial accelerometer designed for urban and industrial applications regarding strong motion earthquake survey and vibration monitoring as well as alarm and switch systems.

All these applications require rugged sensors with minimum maintenance and a simple method for periodic testing.

The AC-43 accelerometer is based on the modern MEMS (Micro Electro-Mechanical Systems) technology, consisting of sensing cells assembled in a way that optimizes their performances. This combined with the state of the art proprietary circuit design yields this cost effective and reliable accelerometer.

MEMS cells include linear accelerometer sensing elements which measure the capacitance variation in response to any movement or inclination and a factory trimmed interface chip that converts the capacitance variations into analog or digital signal proportional to the motion.

The DC response allows the sensor to be easily repaired, tilt tested or recalibrated in the field. With the help of the TEST LINE the AC-43 accelerometer can be completely tested assuring proper operation.



The AC-43 is typically housed in the standard GeoSIG sealed cast aluminium housing with dimensions of 195 x 112 x 96 mm. The housing also incorporates a single bolt mount with three levelling screws. Stainless steel packaging options are available.

The AC-4x accelerometer is directly compatible with the GeoSIG recorders. It is also designed to be mounted internally in standard GeoSIG recorders.



Specifications AC-43 / AC-42 / AC-41 Force Balance Accelerometer

General Characteristics

Application:

- Strong-Motion earthquake recording
- Vibration monitoring
- Alarm / Switch systems

Configurations:

AC-43 or AC-43i*:
AC-42-H or AC-42-Hi*:
AC-42-V or AC-42-Vi*:
AC-41-H or AC-41-Hi*:
AC-41-V or AC-41-Vi*:

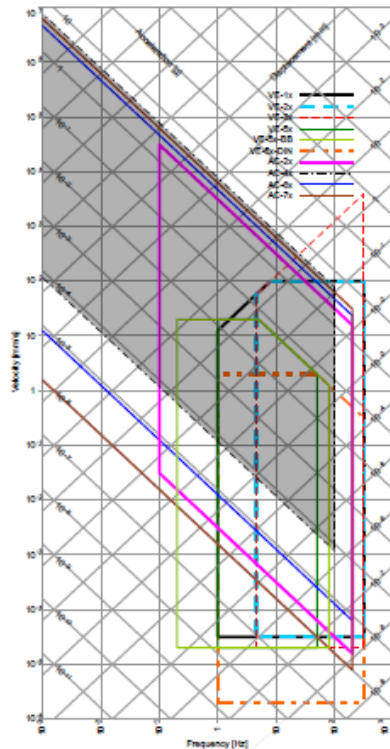
	Triaxial	Bi-axial	Uni-axial	Axes	Alignment**
■	■	■	■	X - Y - Z	H - H - V
■	■	■	■	X - Y	H - H
■	■	■	■	X (or Y) - Z	H - V
■	■	■	■	X (or Y)	H
■	■	■	■	Z	V

* I : Internal sensor ** H: Horizontal, V: Vertical

Full Scale Range: ± 2 g Std
Optional $\pm 0.625, \pm 1, \pm 4$ or ± 5 g

Sensor Element

Type: MEMS Force Balance Accelerometer
Dynamic Range: >95 dB
Noise: < 80 μg_{RMS}
Nonlinearity: < 0.3 % typ., < 0.6 % for vertical
Cross Axis Sensitivity: < 2 % typ.
Bandwidth: DC to 100 Hz
Span drift: 100 ppm/°C
Offset Drift: ± 0.8 mg / °C
Full Scale Output: 0 ± 10 V differential (20 Vpp)
optional 2.5 ± 2.5 V single-end (5 Vpp)
0 to 20 mA current loop
Measuring Range: See plot



Power

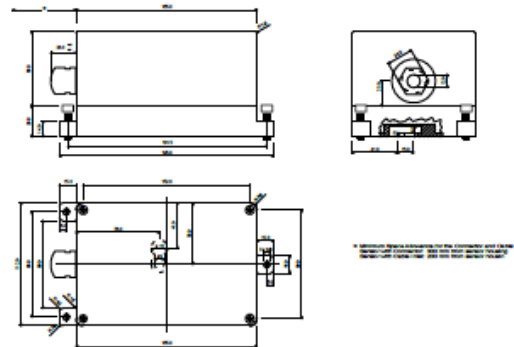
Supply Voltage: 7 to 15 VDC, single supply
optional, 7 to 30 VDC
Consumption: 9 mA @ 12 VDC
Connector: Metallic, Shielded, IP67, 12 pins, male
optional MIL, Bendix PT07A 14-19P
Mating: Binder / Coniners type RC
Overvoltage Protection: All pins are protected

Connector Pin Configuration

Pin 1-8: Signal output for axis X, Y, Z
Pin 7,8: Test Input
Pin 9-10: + 12 VDC power supply
Pin 11-12: Not used
Case: Shielded Ground

Environment/Housing

Housing Type: Cast aluminium
Sealed access cover
Housing Size: 195 x 112 x 96 mm
Weight: 2.0 kg
Index of Protection: IP 65
optional IP68
Temperature Range: - 40 to 85 °C (operating)
- 40 to 85 °C (non-operating)
Humidity: 0 to 100 % (non-condensing)
Orientation: Can be configured for mounting in any position.
Mounting: Single bolt, surface mount, adjustable within $\pm 10^\circ$



Standard AC-4x

Floor mounted, Full scale ± 2 g,
2 m cable with cable inlet and recorder
mating connector, concrete anchor bolt
and user manual on CD

Options

Cable & connector: Cable connector
Metallic, Shielded, IP67, 12 pins, male
optional MIL, Bendix PT07A 14-19P
Cable with shielded twisted pairs for any
length (including mating sensor
connector) with open end
Cables for connection to GeoSIG
recorder
Connector on user specification mounted
at cable end
Housing: Watertight IP 68 housing
Downhole housing (AC-4x-DH)
Stainless steel protective housing
As internal sensor
Mounting: Wall mounted

Test Record AC-41-H-Mini

Test Record	6895	Job	10975
S/N	53756	Test Procedure	GS_TP_GS_AC-43_calibration.V1.doc

Customer	CH_GEOSIG_Gadimzadeh
----------	----------------------

Model	AC-41-H-Mini	H	Option 1		
Main board	GS_AC43_SENSOR/V02	S/N 138828	Option 2		
Output range	2.5 ± 2.5 V		Option 3		
Full scale	±4 g		Option 4		
Description	Accelerometer		Option 5		
Mother S/N			Option 6		

Remarks: X channel only

1. Test equipment

1.1. Test equipment is as per list and ready	<input checked="" type="checkbox"/> OK
--	--

2. Visual check

2.1. No defects found during visual check	<input checked="" type="checkbox"/> OK
---	--

3. Configuration

3.1. Cell full scale	<input checked="" type="checkbox"/> ± 6 [g]
3.2. Power input range	<input checked="" type="checkbox"/> 7..15 [VDC]

4. Pre-test

4.1. Supply current	[mA]	< 80 [mA]	<input checked="" type="checkbox"/> OK
4.2. + 8.2 [VDC] supply	[VDC]	+8.2 ± 0.5 [VDC]	<input checked="" type="checkbox"/> OK
4.3. - 8.2 [VDC] supply	[VDC]	-8.2 ± 0.5 [VDC]	<input checked="" type="checkbox"/> OK
4.4. + 5 [VDC] supply	5.08 [VDC]	5 ± 0.1 [VDC]	<input checked="" type="checkbox"/> OK
4.5. + 2.5 [VDC] reference	2.544 [VDC]	2.5 ± 0.05 [VDC]	<input checked="" type="checkbox"/> OK
4.6. X offset pre adjustment		0 ± 100 [mV]	<input type="checkbox"/> N/A <input checked="" type="checkbox"/> OK
4.7. Y offset pre adjustment		0 ± 100 [mV]	<input type="checkbox"/> N/A <input checked="" type="checkbox"/> OK
4.8. Z offset pre adjustment		0 ± 100 [mV]	<input type="checkbox"/> N/A <input checked="" type="checkbox"/> OK
4.9. Sensor reacts to shaking			<input checked="" type="checkbox"/> OK
4.10. Level the sensor with spirit level			<input checked="" type="checkbox"/> OK

5. Calibration of X axis

5.1. Offset in standard position	0.0 [mV]	<input type="checkbox"/> N/A <input checked="" type="checkbox"/> OK
5.2. Output when + 1 [g] applied	0.624 [V]	<input type="checkbox"/> N/A <input checked="" type="checkbox"/> OK
5.3. Output when - 1 [g] applied	-0.626 [V]	<input type="checkbox"/> N/A <input checked="" type="checkbox"/> OK
5.4. Sensitivity: [(5.2) - (5.3)] / 2	0.625 [V/g]	<input type="checkbox"/> N/A <input checked="" type="checkbox"/> OK

6. Calibration of Y axis

6.1. Offset in standard position	0.0	[mV]	<input type="checkbox"/> N/A <input checked="" type="checkbox"/> OK
6.2. Output when + 1 [g] applied	0.626	[V]	<input type="checkbox"/> N/A <input checked="" type="checkbox"/> OK
6.3. Output when - 1 [g] applied	-0.624	[V]	<input type="checkbox"/> N/A <input checked="" type="checkbox"/> OK
6.4. Sensitivity: [(6.2) - (6.3)] / 2	0.625	[V/g]	<input type="checkbox"/> N/A <input checked="" type="checkbox"/> OK

7. Calibration of Z axis

7.1. Offset when flat	0.625	[mV]	<input type="checkbox"/> N/A <input checked="" type="checkbox"/> OK
7.2. Output when -2 [g] applied	-0.623	[V]	<input type="checkbox"/> N/A <input checked="" type="checkbox"/> OK
7.3. Calculate sensitivity: 5.0 [V/g] \pm 0.5 %	0.624	[V/g]	<input type="checkbox"/> N/A <input checked="" type="checkbox"/> OK

8. Offset measurement

8.1. X axis offset	0.1	[mV]	0 \pm 5	[mV]	<input type="checkbox"/> N/A <input checked="" type="checkbox"/> OK
8.2. Y axis offset	0.6	[mV]	0 \pm 5	[mV]	<input type="checkbox"/> N/A <input checked="" type="checkbox"/> OK
8.3. Z axis offset	0.3	[mV]	0 \pm 5	[mV]	<input type="checkbox"/> N/A <input checked="" type="checkbox"/> OK

9. Sensor test check

9.1. X axis pulse	137	[mV]	<input type="checkbox"/> N/A <input checked="" type="checkbox"/> OK
9.2. Y axis pulse	134	[mV]	<input type="checkbox"/> N/A <input checked="" type="checkbox"/> OK
9.3. Z axis pulse	208	[mV]	<input type="checkbox"/> N/A <input checked="" type="checkbox"/> OK

10. Over range check

10.1. X axis output	<input type="checkbox"/> N/A <input checked="" type="checkbox"/> OK
10.2. Y axis output	<input type="checkbox"/> N/A <input checked="" type="checkbox"/> OK
10.3. Z axis output	<input type="checkbox"/> N/A <input checked="" type="checkbox"/> OK

11. Polarity check

11.1. X axis polarity	<input type="checkbox"/> N/A <input checked="" type="checkbox"/> OK
11.2. Y axis polarity	<input type="checkbox"/> N/A <input checked="" type="checkbox"/> OK
11.3. Z axis polarity	<input type="checkbox"/> N/A <input checked="" type="checkbox"/> OK

12. Final acceptance

12.1. If everything is OK put green label with your initials on the PCB
12.2. All tests were executed according to the test procedure and all results were checked and are according to the specifications

System tested by: MID

DSS

On: 28.05.2014

Approved by: GES

GES

On: 30.10.2014

A.9 FFT algorithm and implementation

The functions $Y = \text{fft}(x)$ and $y = \text{ifft}(X)$ implement the transform and inverse transform pair given for vectors of length N by:

$$X(k) = \sum_{j=1}^N x(j) \omega_N^{(j-1)(k-1)}$$

$$x(j) = (1/N) \sum_{k=1}^N X(k) \omega_N^{-(j-1)(k-1)}$$

where

$$\omega_N = e^{(-2\pi i)/N}$$

is an N th root of unity.

$Y = \text{fft}(x)$ returns the discrete Fourier transform (DFT) of vector x , computed with a fast Fourier transform (FFT) algorithm.

$Y = \text{fft}(X,n)$ returns the n -point DFT. $\text{fft}(X)$ is equivalent to $\text{fft}(X, n)$ where n is the size of X in the first nonsingleton dimension. If the length of X is less than n , X is padded with trailing zeros to length n (MATLAB help, 2011).

MATLAB implementation code for FFT analysis:

```

Fs = 50; % Sampling frequency
T = 1/Fs; % Sample time
L = 1000; % Length of signal
t = (0:L-1)*T; % Time vector
NFFT = 2^nextpow2(L); % Next power of 2 from length of y
data1=transpose(xFBDISPL);
data1(isnan(data1))=[];
data2=transpose(xBIDISPL);
data2(isnan(data2))=[];
Y1= fft(data1,NFFT)/L;
Y2 = fft(data2,NFFT)/L;
f = Fs/2* linspace(0,1,NFFT/2+1);
% Plot single-sided amplitude spectrum.
plot(f,2*abs(Y1(1:NFFT/2+1)))
title('Single-Sided Amplitude Spectrum of y(t)')
xlabel('Frequency (Hz)')
ylabel('|Y(f)|')
hold on
plot(f,2*abs(Y2(1:NFFT/2+1)),'r')

```